Achilles tendon elasticity and deformation patterns in young and middle-aged adults evaluated using quantitative ultrasound approaches

By

Laura Chernak Slane

A dissertation submitted in partial fulfillment of

The requirements for the degree of

Doctor of Philosophy

(Biomedical Engineering)

at the

UNIVERSITY OF WISCONSIN-MADISON

2014

Date of final oral examination: April 25, 2014

The dissertation is approved by the following members of the Final Oral Committee:
Darryl G. Thelen, Professor, Biomedical Engineering, Mechanical Engineering
Bryan C. Heiderscheit, Professor, Orthopedics and Rehabilitation
Kenneth S. Lee, Associate Professor, Radiology
Tomy Varghese, Professor, Medical Physics
Ray Vanderby Jr., Professor, Orthopedics and Rehabilitation

ProQuest LLC.
789 East Eisenhower Parkway
P.O. Box 1346
Ann Arbor, MI 48106 - 1346

Acknowledgments

I would like to gratefully acknowledge the support, mentoring and friendship that I have been so fortunate to have throughout my doctoral work. I would like to acknowledge *Dr. Darryl Thelen*, for his mentoring, support and assistance throughout my entire doctoral experience. I would also like to recognize the members of my PhD committee, *Dr. Tomy Varghese, Dr. Bryan Heiderscheit, Dr. Ken Lee* and *Dr. Ray Vanderby Jr.*, all of whom have substantially contributed to my success.

I would also like the acknowledge the specific research collaborations that I have been fortunate to have with *David Bunger, Dr. Ryan DeWall, Alex Ehlers, Nathan Kleinhans, Tanner Marshall, and Daniel Volk.* I also appreciate the research assistance and mentoring that I have received from *Dr. Sarah Duenwald-Kuehl, Dr. Kayt Frisch, Dr. Amy Silder* and *Dr. Joseph Towles*, as well as the mentoring of my professional development from *Dr. Don Gillian-Daniel* and *Dr. Bob Mathieu.*

Finally, I would like to acknowledge my deepest appreciation for my labmates, friends, family and husband. I particularly thank the members of the UW Neuromuscular Biomechanics Lab, the Bone and Joint Biomechanics Lab, the Vanderby Lab Group and the Delta Community.

Funding Support

I also gratefully acknowledge the funding that I have received to support my dissertation research:

NIH National Institute on Aging. Ruth L. Kirschstein National Research Service Award F31AG043216

NIH R01 AR057201

American Society of Biomechanics, Grant-in-Aid Award

International Society of Biomechanics, Matching Dissertation Program

Vilas Research Travel Grant, the Graduate School, University of Wisconsin-Madison

Clinical and Translational Science Award (CTSA) program, previously through the National Center for Research Resources (NCRR) grant 1UL1RR025011, and now by the National Center for Advancing Translational Sciences (NCATS), grant 9U54TR000021.

Abstract

Tendon injuries can be debilitating, and injury incidence is linked with aging. The Achilles tendon complex is particularly susceptible to injury during middle-age (e.g. tendinopathy), though the effects of aging on tendon mechanics are poorly understood. In fact, recent *in vivo* studies aiming to measure the effects of aging on Achilles tendon stiffness have shown contradictory results. These inconsistencies may arise due to limitations in methodological approaches, which often focus on the evaluation of gross tissue motion and may mask complex deformation patterns. Thus, the purpose of this dissertation was to utilize innovative ultrasound approaches to quantify high resolution *in vivo* tendon deformations and muscle-tendon mechanical properties in young and middle-aged adults. Using ultrasound elastography, we observed complex deformation patterns within the Achilles tendon, with deep portions of the tendon observed to undergo significantly more displacement than superficial portions. These non-uniform deformation patterns persisted with altered loading conditions and knee flexion angles, and may reflect variable motion between the tendon fascicles arising from the soleus and gastrocnemius muscles. We also observed small, but significant, posture- and load-dependent changes in displacement magnitudes. Supersonic Shear Imaging was used separately to characterize stretch-dependent variations in shear wave speed along the Achilles tendon and aponeurosis. Tendon shear wave speed increased with passive stretch, likely reflecting its strain-stiffening behavior, and varied significantly along the tendon length, with the proximal tendon (i.e. gastrocnemius aponeurosis) exhibiting lower shear wave speeds than the distal tendon (i.e. free tendon). Performing the same tasks, middle-aged adults exhibited evidence of significantly more uniform tendon deformation patterns and an increase in tendon compliance. The results of this dissertation demonstrate that Achilles tendon mechanics are highly non-uniform and change

with age, highlighting the importance of using high resolution quantitative ultrasound techniques to assess spatial variations in tendon properties. Age-related changes in tendon mechanics were also observed to occur near regions prone to injury (e.g. the gastrocnemius aponeurosis). These observations suggest a link between the effects of aging on tendon mechanics and injury development, though future work will be critical to interpret these results in the context of injury and rehabilitation.

Table of Contents

List of Figures

List of Tables

Chapter 1: Introduction and Motivation

1.1 Clinical Relevance of Lower Limb Muscle-Tendon Injuries

Muscle-tendon injuries are prevalent among middle-aged and older adults (Alfredson and Lorentzon 2000; Houshian *et al.* 1998; Kannus *et al.* 1989; McKean *et al.* 2006; Nillius *et al.* 1976). These injuries can be chronic and may limit physical activity, often leading to a downward spiral of disuse atrophy. In addition to increased injury incidence, aging also affects the type and location of these injuries. For example, in the lower limb, Achilles tendon and plantarflexor muscle injuries are reported by middle-aged runners nearly twice as often as their younger counterparts (McKean *et al.* 2006). This suggests that there may be underlying age-related factors that affect the development of specific injuries.

The Achilles tendon is among the most common regions of injury in middle-aged adults. These injuries often present as tendinopathy, a painful condition characterized by localized degeneration of tendinous tissue (Maganaris *et al.* 2004; Sharma and Maffulli 2005). Achilles tendinopathies are commonly observed in individuals involved in activities that subject the tendon to repetitive loading (e.g. running) (Maffulli *et al.* 2003). In fact, the annual incidence of Achilles tendinopathy in runners is estimated to be between 7% and 9% (Kujala *et al.* 2005), with the lifetime risk estimated to be as high as 50% among elite male distance runners (Zafar *et al.* 2009). Because of the link between these injuries and repetitive loading scenarios (Almeida *et al.* 1999; Knobloch *et al.* 2008), tendinopathies are largely considered to develop due to tendon overuse or overloading.

Clinically, Achilles tendinopathies are challenging to treat (Sharma and Maffulli 2005). Common treatments include rest, nonsteroidal anti-inflammatory drugs, corticosteroids and surgery (Alfredson 2003). In recent years, there has been increasing interest in using eccentric exercises as a conservative treatment for tendinopathy. These exercises, which involve repeat eccentric loading of the injured tendon, have shown success in some individuals with mid-substance tendinopathies (Alfredson *et al.* 1998; Fahlstrom *et al.* 2003; Knobloch 2007; Maffulli and Longo 2008). The reported successful outcomes are counterintuitive to the understanding of injury development from tendon overloading. However, biochemical studies support these findings by showing evidence that shear loading may stimulate tendon cells, thereby promoting tendon healing (Fong *et al.* 2005; Maeda *et al.* 2011). Thus, it is likely that the link between tendon loading and injury is complex, warranting further investigation.

Muscle strains also occur frequently in middle-aged adults (McKean *et al.* 2006), and are common in the gastrocnemius muscle (Garrett 1990; Orchard 2001; Speer *et al.* 1993). These injuries can have long-term consequences including impaired performance and risk of re-injury (Garrett 1990; Kannus *et al.* 1989; Orchard 2001). Loading condition is closely linked with acute injury development, with injuries observed to occur most often during eccentric loading conditions (Garrett 1990).

These observations highlight the clinical relevance of two specific injuries that involve the Achilles tendon-triceps surae complex. Both injuries are observed to increase in incidence in middle-age suggesting that there may be underlying factors that are altered with age that contribute to injury development. Thus, there is a clinical need for a better understanding of the contributions of age-related changes in muscle-tendon mechanics to injury and rehabilitation.

1.2 Anatomy of the Achilles Tendon and Triceps Surae

Anatomically, the Achilles tendon is located in the lower leg and arises as the shared tendon of the muscles of the triceps surae: the medial gastrocnemius, the lateral gastrocnemius and the soleus (Figure 1.1). The tendon thus runs the length of the majority of the shank from the heel to the mid-portion of the calf muscle and comprises regions of free tendon and aponeurosis (i.e. internal tendon (Zajac 1989)).

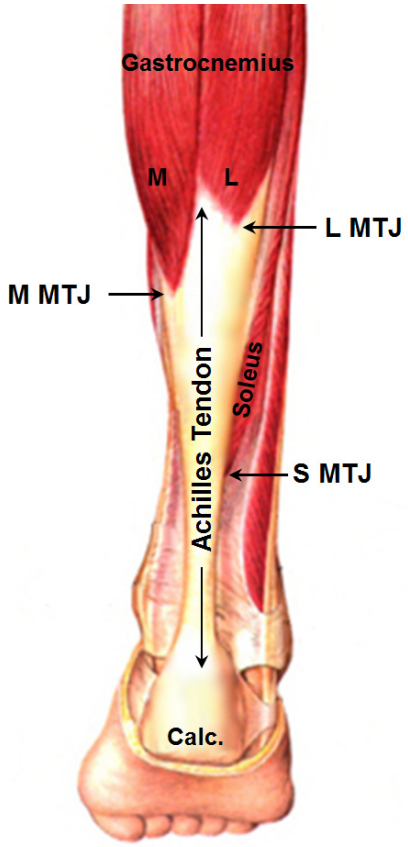

Figure 1.1 Achilles tendon anatomy. The Achilles tendon comprises fascicles arising from the soleus (S), medial (M) gastrocnemius and lateral (L) gastrocnemius. The insertions of the muscles onto the tendon are identified as muscle-tendon junctions (MTJ). *Adapted from public domain image* (Sobotta 1909).

Generally, the Achilles tendon can be considered to comprise three distinct sections: the Achilles free tendon, which spans from the distal calcaneus insertion to the soleus muscle tendon junction (S MTJ), the soleus aponeurosis, spanning from the soleus muscle-tendon junction to the gastrocnemius muscle-tendon junction (G MTJ), and the aponeuroses of the gastrocnemius muscle heads. These anatomical landmarks can be visualized with ultrasound (Figure 1.2).

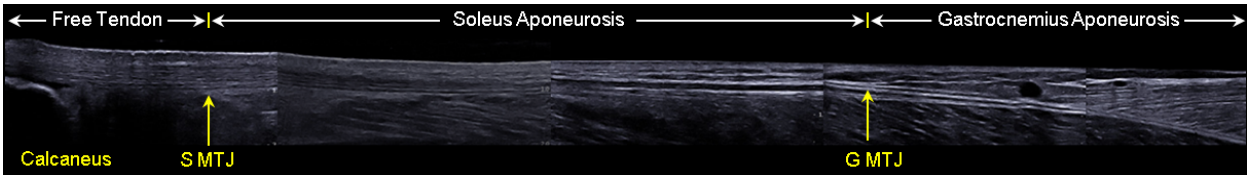

Figure 1.2 The Achilles tendon viewed with ultrasound. Anatomical landmarks are identified including the calcaneus bone, soleus muscle-tendon junction (S MTJ) and gastrocnemius muscle-tendon junction (G MTJ). This figure is a conglomeration of five ultrasound images, each 50 mm in width (with only a portion of the proximal image used), collected from a single subject.

Distally, the fascicles of the Achilles tendon are held together by a loose connective tissue known as the interfascicular matrix, and then inserts onto the calcaneus bone (Kim *et al.* 2011). Another important characteristic of the Achilles tendon is its helical twist (Cummins *et al.* 1946; Szaro *et al.* 2009; White 1943) which causes the relative positioning of tendon fascicles to vary along the Achilles length. Thus, in the mid-substance of the free Achilles tendon, the fascicles from the medial gastrocnemius are typically located in the superficial portion of the tendon, and fascicles from the soleus are primarily in the mid and deep portions of the tendon (Cummins *et al.* 1946; Szaro *et al.* 2009). There is evidence, however, of significant individual variation in normal tendon anatomy (Blitz and Eliot 2007; Cummins *et al.* 1946; O'Brien 1984), cautioning a generalization of Achilles tendon anatomy.

1.3 Relative Strains of the Achilles Tendon and Aponeuroses

Although tendons have traditionally been assumed to undergo uniform axial deformation during use, there is increased evidence of heterogeneous deformations during *in vivo* tendon loading. For example, a classic study by Lieber *et al.* measured significantly higher strains in the aponeurosis of the frog semitendinosus when compared with its tendon (Lieber *et al.* 1991). This result has inspired a variety of *in vivo* human studies, though the results are inconsistent. For example, an *in vivo* study found significantly higher strains in the human Achilles tendon than the gastrocnemius aponeurosis (Magnusson *et al.* 2003), yet another found no differences in strain between these two regions (Muramatsu *et al.* 2002). These contrasting results highlight a lack of clarity that exists in the literature with regards to tendon and aponeurosis mechanical properties.

There is also increasing evidence that tendon deformation and elasticity may vary within even smaller regions of the tendon, both along its length (DeWall *et al.* 2014; Finni *et al.* 2003) and within its cross-section (Arndt *et al.* 2012). In addition, *in vitro* experiments have shown evidence of complex tendon deformations facilitated by tendon fascicle sliding (Haraldsson *et al.* 2008; Komolafe and Doehring 2010; Screen *et al.* 2004), and likely modulated by the interfascicular matrix (Thorpe *et al.* 2012). These studies, paired with the independent loading that arises from the soleus and gastrocnemius muscles (Arndt *et al.* 1998; Ivanenko *et al.* 2004; Winter and Yack 1987), demonstrate the likelihood of the development of non-uniform deformations in the free Achilles tendon.

Clinically, specific regions of the Achilles tendon are more susceptible to certain injuries, suggesting that there may be a relationship between specific deformation patterns and injury. For example, Achilles tendinopathy most commonly occurs in the tendon mid-portion (roughly 3-6

cm proximal to the calcaneus insertion) (Astrom and Rausing 1995). In contrast, gastrocnemius muscle strain injuries develop most commonly in muscle tissue near the muscle-tendon junction (Garrett 1990; Kirkendall and Garrett 2002; Speer *et al.* 1993). The reasons for injury development in specific locations are not well understood, and only highlight the need for a better understanding of high resolution muscle-tendon mechanics

1.4 Aging and the Muscle-Tendon Unit

Although age-related increases in muscle-tendon injury incidence have been observed (Alfredson and Lorentzon 2000; Kannus *et al.* 1989; McKean *et al.* 2006), the link between aging and injury is not clear. Prior studies have investigated the effects of aging on skeletal muscle, and found that aging is correlated with a decrease in muscle strength (Porter *et al.* 1995), decrease in muscle cross-sectional area (Porter *et al.* 1995; Sipila and Suominen 1991), and an increase in non-contractile muscle content (Kent-Braun *et al.* 2000; Sipila and Suominen 1991). In tendon, comparative studies have observed aging to lead to specific changes including decreased collagen fibril diameter (Nakagawa *et al.* 1994), decreased collagen crimp angle (Patterson-Kane *et al.* 1997; Tuite *et al.* 1997), and changes in collagen type III content (Birch *et al.* 1999), though effects may vary based on the tendon's primary function (Birch *et al.* 1999; Thorpe *et al.* 2012; Thorpe *et al.* 2013). It is generally believed that these effects lead to an increase in tendon compliance, which progress with age following maturation, resulting in altered tendinous tissue even in middle-age. Biomechanical studies on isolated tendon specimens have supported this supposition with a variety of studies reporting an age-related decrease in the tendon elastic modulus following maturation (Blevins *et al.* 1994; Vogel 1980, 1983). However, recent *in vivo* studies, using similar techniques (see Chapter 2) have produced conflicting results, with some

studies finding aging correlated with Achilles tendon compliance increasing (Narici and Maganaris 2006; Onambele *et al.* 2006; Stenroth *et al.* 2012), decreasing (Kubo *et al.* 2007), or not changing (Karamanidis and Arampatzis 2005). The reasons for these inconsistent results are challenging to understand, but may arise in part due to the low resolution that these gross measurements have for evaluating variation along the tendon length, which prior studies have measured to be significant (DeWall *et al.* 2014; Finni *et al.* 2003). *In vitro* evidence of a reduction in fascicle sliding with age (Thorpe *et al.* 2013), further emphasizes the need for tools that are capable of measuring higher resolution deformation patterns.

1.5 Goal of Dissertation Research

The overall goal of this dissertation, therefore, is to evaluate high resolution muscle-tendon deformation patterns and elasticity in healthy adults, to gain insight into the effects of aging on these mechanics, and to interpret the results in the context of injury incidence and rehabilitation. To achieve these aims, we have utilized two quantitative ultrasound approaches: ultrasound elastography and shear wave elastography (see Chapter 2).

1.6 Overview of Dissertation Organization

The remainder of this dissertation is organized into an overview of quantitative ultrasound approaches (Chapter 2), the development and validation of a custom 2D elastography approach (Chapters 3 and 4), and the use of this approach in investigating non-uniform deformations of the Achilles free tendon in healthy young (Chapter 5) and middle-aged (Chapter 6) adults. I then use shear wave elastography to evaluate spatial variation in tendon elasticity with age (Chapter 7), and the effects of activation and posture changes on young adult muscle shear wave speeds

(Chapter 8). This dissertation is concluded with a summary of the contributions of this research and an overview of ongoing and intended future work (Chapter 9).

Chapter 2: Quantitative Ultrasound Approaches

Ultrasound has become a ubiquitous tool for evaluating soft-tissue mechanics and pathology. This imaging modality is well-suited for biomechanical studies due to its clinical relevance, safety, and general accessibility. In this chapter, I would provide an overview of a variety of ultrasound approaches that can be used to obtain quantitative information about underlying tissue mechanics or material properties (i.e. quantitative ultrasound approaches).

In the late 1990s and early 2000s, Maganaris and Paul introduced a new method for noninvasively quantifying *in vivo* muscle-tendon mechanics using ultrasound (Maganaris 2003; Maganaris and Paul 1999, 2000), which has gained significant use in the field of biomechanics. The typical approach is to collect ultrasound B-Mode images while a subject performs a task, such as isometric plantarflexion. The displacement of an anatomical landmark, often the gastrocnemius muscle-tendon junction, can then be manually tracked in the ultrasound images throughout the entire trial. By measuring, or assuming, the movement at the calcaneus insertion, tendon end-point displacements, and thus, average strains can then be computed. Adaptations of this method have been applied to estimate relative displacement and stretch across the tendon and aponeurosis (Arampatzis *et al.* 2005; Magnusson *et al.* 2001; Magnusson *et al.* 2003; Muramatsu *et al.* 2002). This landmark-tracking approach has provided insights into the effects of gender (Kubo *et al.* 2003), injury (Child *et al.* 2010), training (Karamanidis and Arampatzis 2005; Kubo *et al.* 2002; Rosager *et al.* 2002) and aging (Karamanidis and Arampatzis 2005; Kubo *et al.* 2007; Onambele *et al.* 2006) on tendon strain, stiffness and elastic modulus.

Although this technique has gained significant use, there remain fundamental limitations. For example, in many studies, there are assumptions made concerning the displacement of the

calcaneus, which may significantly underestimate tendon elongation by up to 35% (Maganaris 2005). Additionally, the methodology greatly simplifies the relationship between tendon, aponeurosis and muscle fibers by assuming all structures behave in series and thus experience the same loading (Epstein *et al.* 2006). The method is also limited to providing estimates of average strain across long portions of the tendon, which may have insufficient resolution for characterizing the localized strains where injuries are most often observed. Thus, in order to advance our understanding of the links between loading, injury, aging and rehabilitation, it is essential that we pursue additional approaches for evaluating high resolution muscle-tendon deformations and strains.

2.1 Ultrasound Speckle Tracking

The term "elastography" was first coined in 1991 (Ophir *et al.* 1991), and has come to describe a wide variety of methods of evaluating tissue stiffness using ultrasound among a variety of other methods. In a typical, quasi-static approach, the phase information inherent in ultrasound radiofrequency (RF) data is used to track the displacement of speckle patterns collected from tissue in undeformed and deformed states (Varghese 2009) (Figure 2.1). The spatial differentiation of displacement data then enables the estimate of strain variations within tissue (O'Donnell *et al.* 1994). Although this technique has been successful in evaluating pathological changes in breast, liver and thyroid tissues (Inoue *et al.* 2010; Itoh *et al.* 2006; Lyshchik *et al.* 2005; Zhi *et al.* 2007), there are significant challenges to applying elastography to tendinous tissue.

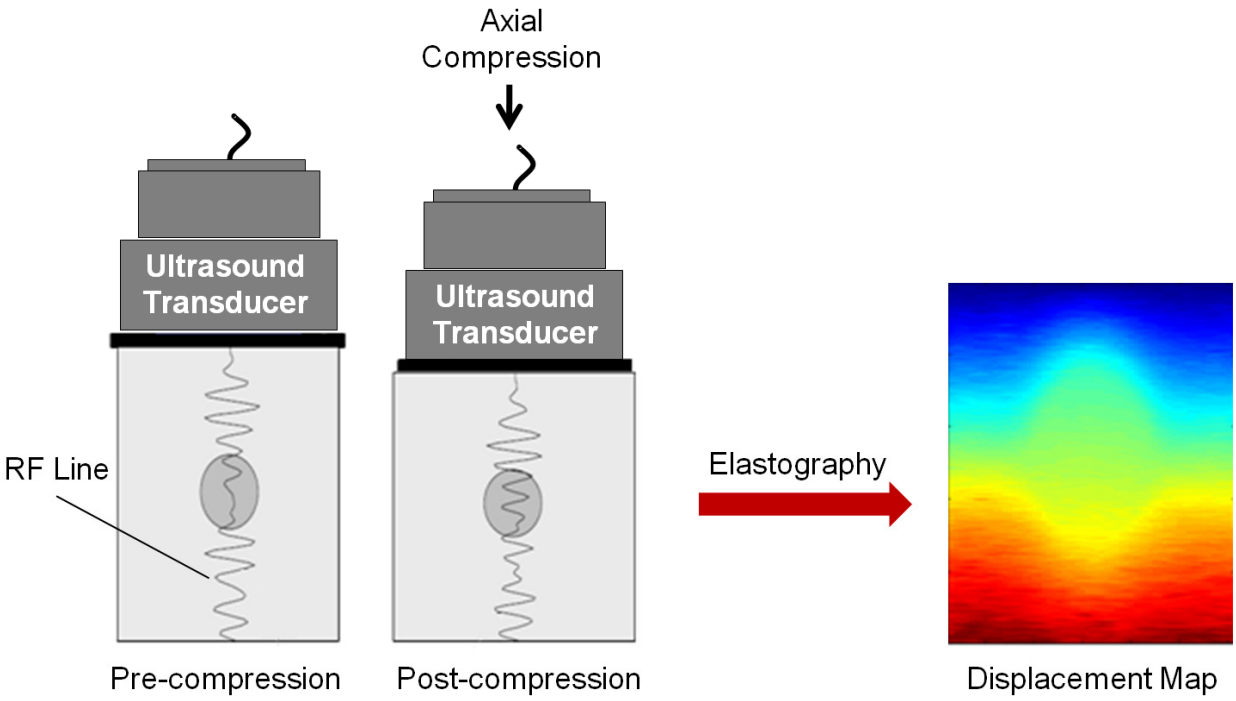

Figure 2.1 Traditional ultrasound elastography approach.
Image adapted from (Ultrasonix 2010).

For example, although a few studies have used this classic quasi-static approach to evaluate tendon deformation (De Zordo *et al.* 2009; Drakonaki *et al.* 2009), the results are challenging to interpret because of the limited relevance to functional loading scenarios. Tracking displacements during physiological tendon loading can be challenging, however, because the primary direction of tissue motion is parallel to the surface of the skin, which has inherently worse resolution in ultrasound (Bohs and Trahey 1991; Lopata *et al.* 2009; Ophir *et al.* 1999). Tracking is further complicated by the transversely isotropic structure of tendon that creates a highly organized speckle pattern that differs substantially from the tissues on which early elastography was focused (Varghese and Ophir 1997). Thus, although the principles of elastography are relevant to consider as a methodological approach to evaluating tendon deformation, significant adaptation is necessary for tendon applications. A major goal and

outcome of this dissertation was thus the development of a custom elastography approach for evaluating high resolution tendon deformation with loading (Chapters 3-6).

2.2 Supersonic Shear Imaging

A second approach for evaluating tissue mechanical properties that I will describe in this dissertation is known as Supersonic Shear Imaging. Although introduced relatively recently, this approach has evolved from a variety of earlier ultrasound approaches. Following the introduction of manual compression quasi-static approaches (see 2.1 Ultrasound), a variety of alternative methods for inducing tissue deformation emerged, with the goal of linking the resulting deformation with tissue elasticity. For example, early studies used low-frequency mechanical vibrators to induce tissue displacements (Lerner *et al.* 1990; Wells and Liang 2011), with advances involving the focusing of an ultrasound beam within tissue in the approaches of shear wave elasticity imaging (SWEI) (Sarvazyan *et al.* 1998) and acoustic radiation force impulse (ARFI) (Nightingale *et al.* 2002). In SWEI and ARFI correlation-based techniques are then used to estimate displacements and evaluate local viscoelastic properties of the tissue. However, the mechanical displacements within the tissue are dependent upon specific parameters of the input displacement including the beam geometry and tissue absorption coefficient, and cannot be linked directly with the tissue viscoelastic parameters (Bercoff *et al.* 2004).

Supersonic Shear Imaging (SSI) thus developed in recent years to overcome this challenge, while building upon the prior advances for evaluating soft tissue elasticity. Like prior techniques, SSI uses acoustic radiation force to induce transient shear waves in tissue of interest. However, in this approach, a unique shear source is created that moves faster than shear waves by successively focusing the pushing beam at different depths within this tissue. This approach then

creates two quasi-planar shear wave fronts that propagate in opposite directions (Bercoff *et al.* 2004). These wave fronts can then tracked using ultra-high frame-rate planar ultrasound (5000 – 20,000 frames/sec), and the shear wave propagation speed can be computed (Figure 2.2). Although prior iterations of this approach may have been limited by frame rate capabilities of the machine, at high shear wave propagation speeds, the maximum measureable wave speed becomes limited by the physical limitations of the time for sound waves to travel through tissue and return to the transducer (see Appendix A).

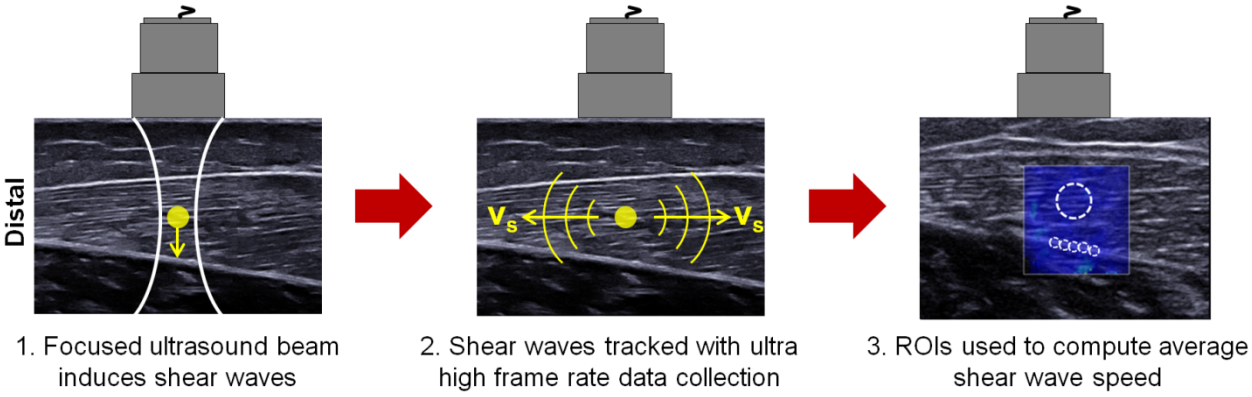

Figure 2.2 Overview of shear wave elastography approach.(Bercoff *et al.* 2004)

Shear wave speed (*SWS*) is an important tissue mechanical property that can be directly linked to shear elastic modulus (μ) in media that are purely elastic and have a known density (ρ):

$$\mu = \rho \cdot SWS^2 \tag{2.1}$$

This equation can be used in viscoelastic materials if the dispersion induced by viscosity is considered negligible (Bercoff *et al.* 2004). By also assuming isotropy, the shear modulus can then be related to tissue Young's modulus (E):

$$E \approx 3 \cdot \mu \tag{2.2}$$

However, because tendon is transversely anisotropic (Kuo *et al.* 2001), the assumptions required for Equation 2.2 do not hold (Royer *et al.* 2011), and thus in this dissertation I chose to report shear wave speeds in place of elastic modulus.

SWE initially gained success in detecting pathological changes in stiffness in a variety of soft tissues, such as the breast (Athanasiou *et al.* 2010), liver (Bavu *et al.* 2011), and thyroid (Sebag *et al.* 2010). Like traditional elastography, there are specific challenges to applying this approach to muscle-tendon tissue. These challenges relate to the fibrous structure of muscle and tendon and the high stiffness of tendon (Table 2.1). A recent surge in interest in musculoskeletal SWE have demonstrated promising results as to the success of applying SWE in muscle (Gennisson *et al.* 2005; Gennisson *et al.* 2010; Hug *et al.* 2013; Nordez and Hug 2010), and tendinous tissue (Brum *et al.* 2014; Hug *et al.* 2013).

Table 2.1 Resting elastic modulus measured using SWE in a variety of healthy tissues (n = 127). *Values from (Arda et al. 2011).*

Tissue	Elastic Modulus (kPa)
Achilles tendon	51.5 ± 25.1
Supraspinatus muscle	31.2 ± 13.0
Renal pelvis	23.6 ± 5.4
Gastrocnemius muscle	11.1 ± 4.1
Thyroid	11.0 ± 3.1
Submandibular glands	10.9 ± 3.1
Parotid glands	10.4 ± 3.5
Masseter muscle	10.4 ± 3.7
Renal cortex	5.0 ± 2.9
Pancreas	4.8 ± 3.0
Spleen	2.9 ± 1.8

The use of SWE in muscle and tendon imaging are described in more detail in Chapters 7 and 8.

2.3 Acoustoelasticity

A third quantitative ultrasound technique that has found use in evaluating tendon mechanics is known as acoustoelasticity. This technique is based on the principle that the acoustic properties of a material are altered when the material is subjected to loading or deformation (Hughes and Kelly 1953). In fact, in nearly incompressible materials (e.g. tendon), changes in reflected wave amplitude can be directly related to the mechanical behavior of the material in terms of strain-dependent stiffness and stress (Kobayashi and Vanderby 2005, 2006). In ultrasound B-Mode images, the brightness of the grayscale image is derived from the amplitude of the reflected sound wave. Thus, acoustoelastic approaches measure the brightness of B-Mode images, often referred to as ultrasound echo intensity, as a method for evaluating tissue stiffness.

In recent years, a variety of studies have investigated the potential of using acoustoelastic approaches to evaluate strain and stiffness in *ex vivo* tendon. For example, it has been shown that ultrasound echo intensity is almost linearly related with tendon strain (Duenwald *et al.* 2011), and has the sensitivity to capture time- and strain-history dependent changes in tendon mechanical properties (Duenwald-Kuehl *et al.* 2012a). Echo intensity has also been shown to be capable of measuring tissue stiffness changes due to damage (Duenwald-Kuehl *et al.* 2012b) and healing (Chamberlain *et al.* 2013).

Although *in vivo* use of this approach is still in its infancy, it has shown significant potential in *in vivo* canine tendons (Ellison *et al.* 2013), and has many exciting advantages over other approaches. One of these advantages is that the technique can quantify stiffness information directly from the brightness information captured in traditional B-Mode images. Thus,

quantitative mechanical characterization of tendon could seamlessly be integrated into the clinical setting. Although acoustoelasticity is not further investigated in this dissertation work, the promising studies that have been published in recent years suggest that this is an important ultrasound technique to consider for future *in vivo* studies aiming to measure tendon deformation and strain.

Chapter 3: Tendon Motion and Strain Patterns evaluated with Two-Dimensional Ultrasound Elastography[1]

3.1 Introduction

Tendon injuries can be both chronic and debilitating. Tendinopathy, for example, is a painful overuse injury in which a localized region of tendinous tissue has degenerated (Maganaris *et al.* 2004; Sharma and Maffulli 2005). Clinically, tendinopathies are challenging to resolve, which is due, in part, to the inconsistent response of patients to treatment protocols (Sharma and Maffulli 2005). Thus, new imaging techniques are needed to elucidate the implications of localized tendon damage on function, and to quantitatively assess the effects of tissue repair or regeneration as a measure of treatment efficacy (Fleming and Beynnon 2004). The development and use of new ultrasound analysis techniques can contribute to this goal by providing noninvasive assessments of tissue mechanics.

Ultrasound has become a ubiquitous tool in biomechanics for measuring tendon motion and strain in response to active muscle contractions. The most common method involves the collection and analysis of cine B-Mode images of a tendon during loading and/or movement of the joint. The motion of an anatomical landmark(s) (e.g. the muscle-tendon junction) can be tracked across successive images to estimate average tendon strain (Maganaris 2003; Maganaris and Paul 1999; Maganaris and Paul 2002; Peixinho *et al.* 2008). Prior studies using this method have provided fundamental insights into the relative stretch across the tendon, aponeurosis and muscle fascicles during *in vivo* loading conditions (Arampatzis *et al.* 2005; Arndt *et al.* 1998; Finni *et al.* 2003; Magnusson *et al.* 2003; Muramatsu *et al.* 2001). However, the anatomical

[1] Chernak LA, Thelen DG (2012). *Journal of Biomechanics* 45(15): 2618-2623.

feature tracking technique does not provide information on strain distributions, and therefore cannot assess the effect that tissue damage may have on localized tissue deformation.

Ultrasound elastography is an innovative technique for non-invasively assessing strain distributions within biological tissues. In standard elastography, ultrasound radiofrequency (RF) data are collected from a tissue in undeformed and deformed states (Varghese 2009). The phase information inherent in the RF data can be used to accurately track the displacement of speckle patterns within the tissue along the ultrasound beam direction (Ophir *et al.* 1991). Spatial differentiation of displacement data is used to estimate the strain variations within the tissue (O'Donnell *et al.* 1994). Elastography has proven effective for detecting anomalies in soft tissues such as the breast, liver and thyroid, with deformation induced via simple manual compression of the tissue with the transducer (Inoue *et al.* 2010; Itoh *et al.* 2006; Lyshchik *et al.* 2005; Zhi *et al.* 2007). A few prior studies have assessed tendon deformation using this standard elastographic approach (De Zordo *et al.* 2009; Drakonaki *et al.* 2009). However, manual compression does not provide insights into how tendinous tissue will deform with active muscle loading, and thus likely does not represent the deformation patterns relevant to injury and rehabilitation.

A major challenge in elastographic imaging of normal tendon loading is that the primary direction of tissue motion is parallel to the surface of the skin, and therefore perpendicular to the ultrasound beam direction. Accurate 2D motion tracking is required to ensure that strains are computed for each tissue region as the tendon is translating within the image window. This can be difficult because the lateral resolution of ultrasound RF data is substantially lower than the along-beam resolution (Bohs and Trahey 1991; Lopata *et al.* 2009; Ophir *et al.* 1999). A second challenge is that tendon can undergo large motion and deformation with muscle contraction, requiring that care must be taken to ensure that the tissue remains within the imaging plane and

that accumulated motion is tracked over time. The purpose of this study, therefore, was to assess the capacity to use cine imaging and recent advances in 2D elastography (Chen *et al.* 2004; Ebbini 2006; Huang and O'Donnell 2010; Jiang and Hall 2009; Lubinski *et al.* 1999) to evaluate tendon tissue motion and strain patterns under well-controlled axial loading conditions. We chose to use an *ex vivo* model such that applied force and displacement information could be directly compared to motion and strain data obtained using elastography. The results show a strong correlation between external and image-derived measures of tissue motion, suggesting that elastography shows promise as a tool for noninvasively assessing the relationship between tendon deformation and injury.

3.2 Methods

We performed mechanical testing on four porcine flexor tendons using a servo hydraulic mechanical test system (Bionix858; MTS, Minneapolis, MN) with a custom bath (Figure 3.1). The tendons were dissected from six-month old porcine specimens that were sacrificed for an unrelated study. The bony end of the tendon was secured in a metal block which was then loaded in a fixed grip. The insertion site was left intact at the distal end and embedded in lightweight filler (Evercoat, Cincinnati, OH). Tendons were kept hydrated with a phosphate buffered saline (PBS) solution during preparation. The specimens were wrapped in a PBS soaked towel and placed in a freezer in the time between dissection and testing. Tendons were fully thawed prior to mechanical testing. Prior evaluations of patellar tendon have suggested that there is little measureable effect on tendon mechanical properties following eight free-thaw cycles (Jung *et al.* 2011). The insertion end of the tendon was then secured in a grip on the test machine crosshead that was attached to a 50 lb load cell (Eaton Corporation, Cleveland, OH), and testing was

performed in a PBS solution filled bath. A 10 MHz, 38 mm wide linear array transducer (L14-5W/38, Ultrasonix Corporation, Richmond, BC, Canada) was secured in a holder and submerged in the bath such that RF data were provided from the midsection of the tendon. The transducer was aligned in the direction of the tendon fibers, and placed along the center axis of the tendon such that data were collected through the depth of the tendon from a longitudinal cross-section. Crosshead displacement and load cell data were simultaneously recorded with the ultrasound RF data.

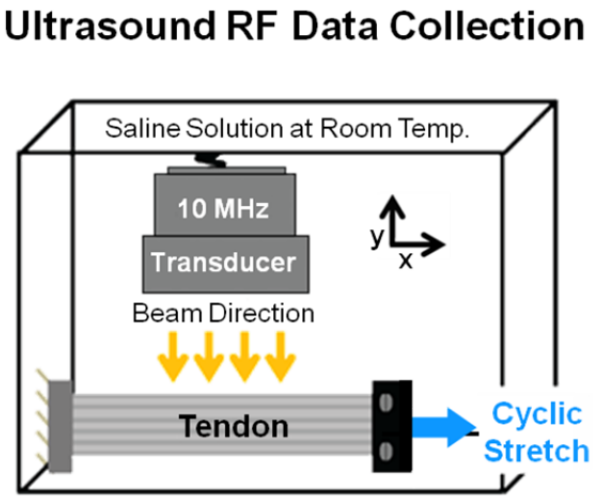

Figure 3.1 Overview of experimental setup. Ultrasound RF data were collected from a longitudinal cross-section of the tendon during cyclic stretch.

Tendons were initially stretched to the point of onset of force development. The tendons were then pre-conditioned with cyclic stretch to 2% strain for ten cycles. Following a seven minute rest period, the tendons were sinusoidally stretched at 0.5 Hz to 4% peak strain for ten consecutive cycles. Ultrasonic RF data were collected at 40 MHz over the final three cycles of motion. Three trials were performed for each specimen, with seven minutes of rest between cycles, such that data from a total of nine loading cycles were collected for each specimen. RF

data were collected at a frame rate of 63 frames per second over a 38 x 30 mm image window. The image resolution was 128 x 1560, which provided a pixel size of 0.297 x 0.019 mm. It is notable that the beam direction resolution was substantially greater than the resolution in the direction perpendicular to the beam. Calipers were used to measure the two major diameters of the tendon cross-section prior to loading, and the cross-sectional area was computed by assuming that the tendon had an elliptical profile (Arruda *et al.* 2006).

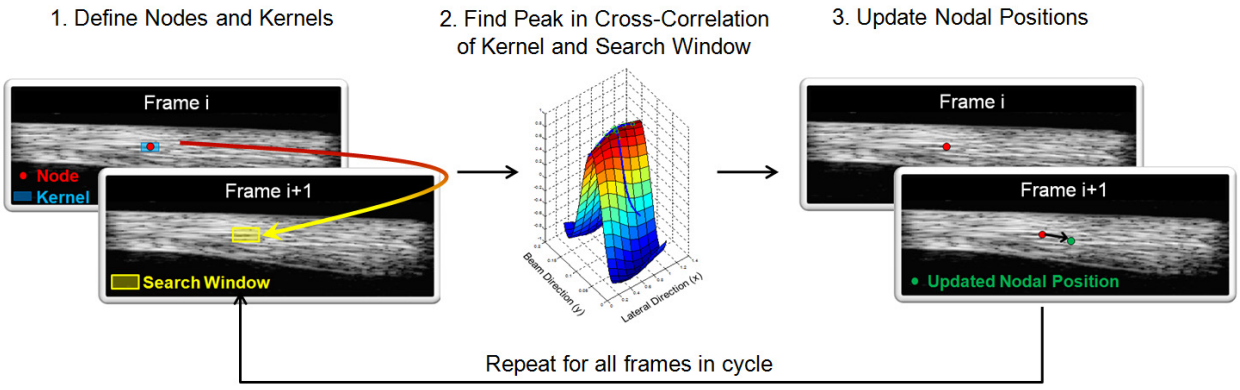

Figure 3.2 Frame-to-frame tissue speckle tracking was performed by first defining nodes in Frame i and then centering kernels (2 x 1 mm) around the nodes (only one node is shown for illustrative purposes). Cross-correlations are then computed between the kernel and a search window (2.8 x 1.4 mm) in Frame i+1. The sharp peak in cross-correlation function in the beam direction results from the phase information in RF data. The sub-pixel nodal displacements that maximize the correlation were found by fitting a 2D quartic spline to the correlation function near the nominal peak. The nodal positions are then updated (note: the displacement vector is exaggerated for illustrative purposes) and the process is repeated for all frames within a loading cycle.

A 2D ultrasound elastography algorithm was used to track tissue motion throughout each loading cycle (Figure 3.2). To determine the tendon slack length, we measured the tendon length at the frame for which the applied force first exceeded 5% of the peak tendon force. Tissue motion was then tracked until the frame at which the applied force dropped below 5% peak force. The RF images, force and displacement data for this time period were extracted. At each

frame, cubic spline interpolation was used to upsample the RF data by a factor of 4 and 2 in the along-fiber (x) and along-beam (y) directions, respectively (Table 3.1Table 3.1) (Parker *et al.* 1983). Upsampling was performed to increase the spatial density of the correlation functions that were used to track tissue motion (Konofagou and Ophir 1998). We then created a B-Mode image of the unloaded tendon, and manually placed a grid of nodes along ~25 mm regions in the mid-tendon portion (Figure 3.3). The nodes were positioned every 1.0 and 0.5 mm along the x and y directions, and kernels (2 x 1 mm) were centered on the nodes. The nodes were positioned purposefully to ensure that the kernels used to estimate nodal displacements remained within the boundaries of the tendon throughout the loading cycle.

Table 3.1 Parameters used for 2D elastographic tracking of tissue motion.

	Along-fiber (x)	**Along-beam(y)**
Node Spacing	1 mm	0.5 mm
Kernel size:	2 mm	1 mm
Search window:	2.8 mm	1.4 mm
RF upsample rate:	4	2
Sub-pixel estimation	2D Quartic Spline	
Correlation threshold:	0.7	
Spatial smoothing:	Median filter (3 x 3 nodes)	

Frame-to-frame displacements were computed using a 2D normalized cross-correlation technique. Specifically, RF data within a kernel centered at the current node location were cross-correlated with RF data in a search region (2.8 x 1.4 mm) at the same location in the subsequent frame. The gross kernel displacements were first computed by finding the position that maximized the 2D correlation function. Sub-pixel displacements were then computed by fitting a 2D quartic spline to a 5 x 5 matrix of normalized correlations centered at the gross displacement

value (Azar *et al.* 2010). A correlation threshold of $r = 0.7$ was used to discriminate valid displacement information (Farron *et al.* 2009; Korstanje *et al.* 2009; Korstanje *et al.* 2010). Frame-to-frame displacements were median filtered (3 x 3 nodes) (Thitaikumar *et al.* 2008), and node positions were then updated by subsequently adding on the filtered displacements. These steps were repeated for all frames in a loading cycle to obtain the cumulative 2D displacement of each node. Motion tracking was also performed in the reverse direction by starting at the last frame and incrementing toward the first frame. A weighted average of the forward and backward nodal trajectories was then computed such that the final nodal trajectories were ensured to be cyclic in nature (Pelc *et al.* 1995).

Tissue strains in the y-direction (e_{yy}) were computed by numerically differentiating (3 point finite difference) the nodal y-displacement data relative to the initial nodal positions, and using a small strain approximation (Figure 3.3b). The apparent Poisson's ratio was computed by taking the ratio of the negative transverse (e_{yy}) over the applied along-fiber (e_{xx}) strain from the final 50% of the loading phase (Smith *et al.* 1999). The change in transverse tendon width between the relaxed and stretched states was separately assessed via visual analysis of the B-Mode images (Iwanuma *et al.* 2011). To do this, tendon width was measured at five locations along the tendon based on the center of the region of interest. The average transverse strain of the entire ROI was then computed based on the change in width at the five locations normalized to the unloaded tendon width. Analysis using both strain measurement techniques was repeated three times for each loading cycle to evaluate repeatability.

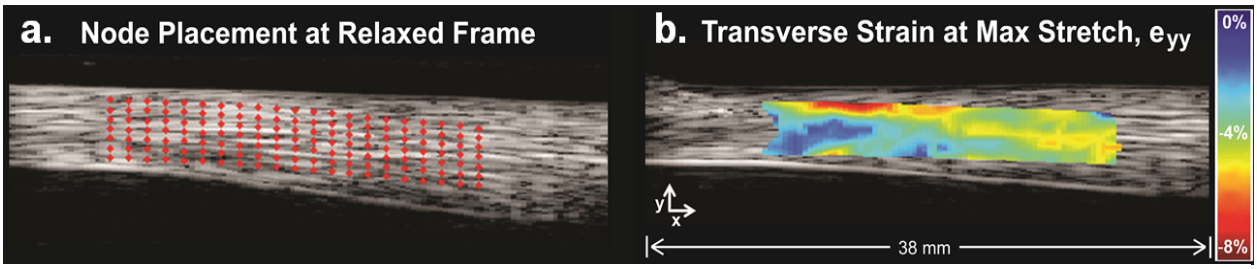

Figure 3.3 Nodal displacements and strains. (a) Grid of nodes was placed along tendon fascicle direction in relaxed frame. (b) Computed transverse tissue strains at most stretched position.

3.3 Results

The average elastographic nodal displacements along the tendon fascicle direction (x) agreed well with the prescribed crosshead displacements. Force-displacement curves derived from both measures demonstrated similar nonlinear strain-stiffening behavior (Figure 3.4a). The along-fiber and crosshead displacements were highly linearly correlated, with average r^2 values greater than 0.98 (Figure 3.4b). The ratio of along-fiber to crosshead displacement differed between specimens, but was extremely repeatable within the nine cycles for each specimen.

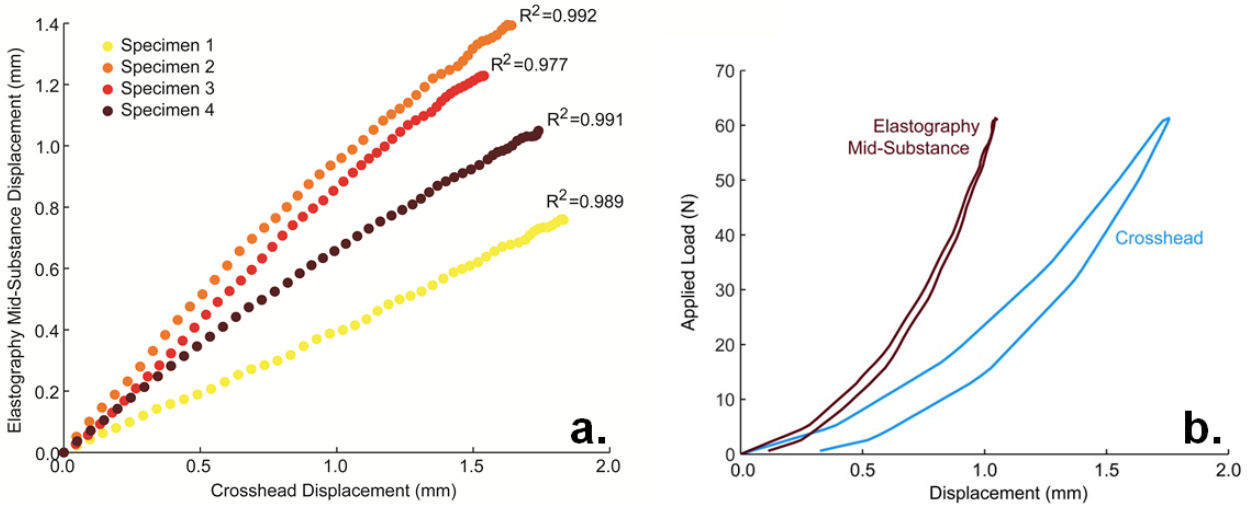

Figure 3.4 Load-displacement results. (a) Displacement of the mid-substance tendon measured with elastography exhibited similar strain-stiffening behavior as the applied crosshead displacement. (b) Crosshead and elastography displacement data were highly correlated over the entire loading range.

The average transverse strains at the most stretched frame varied between specimens, ranging from -2.5 to -8.5%. Average transverse strain magnitudes were comparable to measures of tendon width change, but exhibited substantially less variability across loading cycles (Figure 3.5).

At low strains, the average transverse strain magnitude within the ROI increased at a faster rate than the applied strain (Figure 3.6a). The apparent Poisson's ratios computed using strains from the last half of the loading cycle ranged from 0.8 to 1.64 (Figure 3.6b). Within a specimen, the coefficient of variation for the apparent Poisson's ratio ranged from 2.5-25% across nine repeat loading cycles.

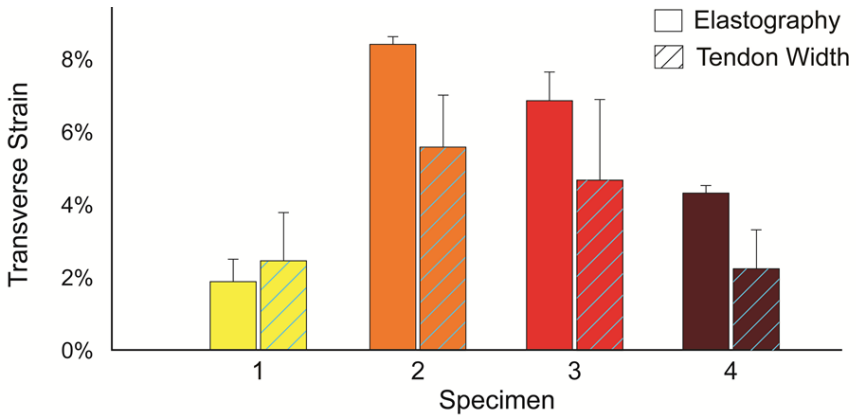

Figure 3.5 Peak transverse strains. Peak transverse strains computed via elastography and ascertained via visual analysis of B-Mode images. Strains were calculated three times for each of the nine repeat loading cycles (+ 1 standard deviation. shown). The two strain measures show similar results with more consistency for strains computed with elastography.

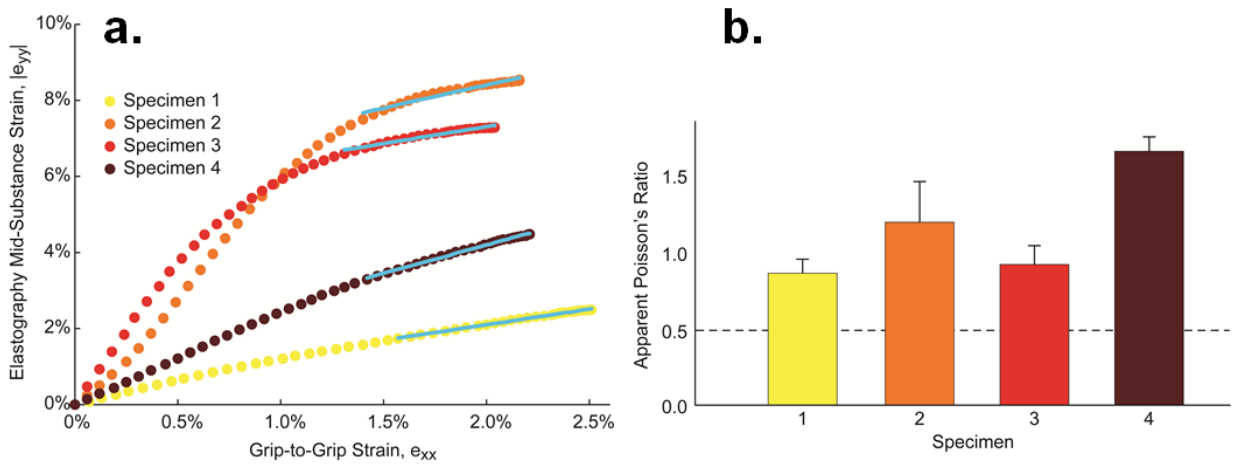

Figure 3.6 Comparison of strain results. (a) Average transverse strains ($|e_{yy}|$) increase faster than grip-to-grip strain (e_{xx}) at low loads, before settling in a more linear relationship. (b) Each specimen exhibited a Poisson's ratio that exceeded the incompressibility limit for isotropic materials (0.5).

3.4 Discussion

This study was undertaken to evaluate the use of 2D elastography to assess tendon tissue motion and deformation with axial loading. We found that along-fiber displacement curves obtained via elastography correlated highly with the applied crosshead displacement, which is expected if the deformation pattern along the tendon axis is relatively invariant with loading. The elastographic transverse strain magnitudes differed between specimens, but all specimens exhibited a monotonic increase with the applied grip-to-grip strains (Figure 3.6a). The apparent Poisson's ratio estimates exceeded 0.5 for all the tendon specimens, a phenomenon that has been previously been observed using other techniques (Cheng and Screen 2007; Lynch *et al.* 2003; Vergari *et al.* 2011). All elastographic measures of displacement and strain were relatively consistent between repeat loading cycles of a specimen. Hence, we believe that RF elastography is a promising new approach for noninvasively measuring tissue motion and deformation under axial loading conditions.

Ultrasound is often used in biomechanics to measure average *in vivo* tendon motion and stretch with loading. This is commonly accomplished by collecting ultrasound B-Mode images during a musculotendon contraction, and then retrospectively tracking the motion of an anatomical landmark at one end of the tendon (e.g. a muscle tendon junction) in the images. The motion at the other end of the tendon is then estimated based on assumptions made about motion (Maganaris 2003; Maganaris and Paul 1999; Maganaris and Paul 2002; Peixinho *et al.* 2008) or is tracked using a second transducer (Arndt *et al.* 2006). The difference in displacements between the two ends of the tendon provides an estimate of average tendon stretch (Arndt *et al.* 2006; Kongsgaard *et al.* 2011; Maganaris 2003; Maganaris and Paul 1999; Maganaris and Paul 2002; Peixinho *et al.* 2008). The complex temporal relationship between average tendon and muscle fascicle stretch has been elucidated using such techniques (Fukunaga *et al.* 2002). However, this anatomical feature tracking approach can only provide an estimate of average strain and thus cannot distinguish strain variations within the tissue that are considered relevant to localized tendon injuries (Maganaris *et al.* 2004; Sharma and Maffulli 2005).

Ultrasound elastography is an automated imaging based tool for characterizing spatial variations in tissue motion and strain. Fundamental to elastography is the use of RF data, which allows one to use small shifts in the phase of the reflected sound wave to ascertain the motion of speckles along the ultrasound beam direction (Varghese 2009). In fact, a recent theoretical study showed that elastographic motion estimates obtained using RF data resulted in more accurate displacement measures that what can be obtained using B-Mode images (Lopata *et al.* 2009). To assess this effect in our data, we computed the full width half maximum (FWHM) of the autocorrelation of the region of interest within the tendon for all images. Correlations obtained with RF data exhibited a sharper peak than those obtained from the B-Mode data, with the

average FWHM found to be 0.12 mm and 0.45 mm respectively. FWHM was substantially larger (2.7 mm) in the direction perpendicular to the ultrasound beam, which is related to the difference in spacing between the RF lines (0.296 mm) and the samples along the beam direction (0.019 mm). Although lateral motion tracking is less precise, the importance of 2D motion tracking has increasingly been recognized, and previous studies have used a variety of techniques to attain 2D elastographic tracking including plane strain assumptions (Lubinski *et al.* 1996; Righetti *et al.* 2003), synthetic phase (Chen *et al.* 2004; Huang and O'Donnell 2010) and 2D cross-correlation techniques (Ebbini 2006; Kaluzynski *et al.* 2001; Trahey *et al.* 1987). We chose to use the 2D normalized cross-correlation function with quartic spline interpolation, because it has been shown to result in substantially lower bias errors than using lower-order polynomial or cosine fits to the correlation function (Azar *et al.* 2010). An inherent advantage of the elastographic technique is that it is capable of estimating strain variations within the image window, which obviates the need for multiple transducers or making assumptions about motion outside the image window.

The apparent Poisson's ratios found in this study ranged from 0.82 to 1.64. These values are comparable to literature estimates of Poisson's ratio ranging from 0.55 to 2.98 for tendon (Cheng and Screen 2007; Lynch *et al.* 2003; Vergari *et al.* 2011) found using other methods, and is consistent with the findings for other transversely isotropic materials (Lempriere 1968). An apparent Poisson's ratio greater than 0.5 exceeds the incompressibility limit for isotropic materials, and reflects volume loss with stretch (Lanir *et al.* 1988). Physiologically, it is possible that this volume loss could arise from the exudation of fluid during stretch. A recent micromechanical tendon model investigated this issue and found that the apparent Poisson's ratio can greatly exceed the incompressibility limit, and its value is heavily dependent on the helical

pitch and crimp angles of the fibers (Reese *et al.* 2010). In addition, the helical organization of tendon fibrils result in a load dependent Poisson's ratio, with the highest values for strains below ~1.5% (Reese *et al.* 2010). Similarly, we found the transverse strains increased faster than the applied strains at low loads, before settling to a more constant ratio at higher loads (Figure 3.6a). The strong dependence of Poisson's ratio on specific structural features may explain the variation between specimens that have been noted in other studies (Cheng and Screen 2007; Lynch *et al.* 2003; Vergari *et al.* 2011), as well as in the current study. The elastographic transverse strain patterns were non-uniform across the tendon, but highly consistent between repeat loading cycles and generally consistent with tendon width measures as ascertained from the B-Mode images (Figure 3.5). Non-uniform strain patterns have also been observed when using optical markers to track surface strains (Cheng and Screen 2007), and could reflect variations in morphological structure as well as experimental factors such as specimen mounting and gripping.

As with other ultrasound approaches, we were only able to track tissue motion that occurred within the image window. We sought to minimize potential out-of-plane motion by fixing the transducer in space to continuously capture images from a cross-section of the tendon along the direction of the tendon fibers. We also collected RF data at a frame rate of 63 frames per second such that frame-to-frame motion was relatively low. The small frame-to-frame displacements increased the potential to keep scatterers in view, which decreases the effect of out-of-plane motion and therefore enhances the ability to accurately track motion (Ophir *et al.* 1999). The normalized cross-correlations of kernels were quite high ($r = 0.99$), reflecting a small amount of decorrelation was occurring between successive frames. A lower frame rate (33.5 Hz) was considered by skipping a frame in the tracking process. This reduced the correlations slightly ($r =$

0.98), but did not appreciably affect the cumulative tracking results. We note that there is no inherent limitation to using incremental elastographic techniques for tracking small deformations. However, it becomes more challenging to keep the region of interest within the image window if the tissue undergoes large rigid body motion or extremely large deformation, which are more likely to occur if the technique is used to track muscle tissue and aponeurosis motion. Therefore, in future studies, it will be important to assess the effects of out-of-plane motion on elastographic strain measures along and transverse to the sound beam, an issue which may be well suited for investigation with an ultrasound phantom.

In conclusion, we have demonstrated the potential to use 2D ultrasound elastography to quantitatively assess tendon tissue motion and strains with loading that are consistent with experimental measures and previous studies. The approach provides regional strain information that could prove relevant for quantitatively assessing tissue strain patterns following injury and clinical treatment.

Chapter 4: The use of 2D Ultrasound Elastography for measuring Tendon Motion and Strain[2]

4.1 Introduction

Quantitative ultrasound imaging techniques have emerged for characterizing *in vivo* tendon motion and deformation. The most common approach involves manually tracking the relative motion of a muscle-tendon junction across cine B-Mode images, and then using that information to compute average tissue strain (Maganaris and Paul, 1999; Maganaris and Paul, 2002; Magnusson et al., 2001; Peixinho et al., 2008). When coupled with force measurements, such methods have been used to assess the effects of training (Maganaris, 2003) and aging (Karamanidis and Arampatzis, 2005) on tendon elasticity. More recent work has shown progress in developing automated methods for tracking motion of the muscle-tendon junction (Gerus et al., 2011, Stenroth et al., 2012) and free tendon (Arndt et al., 2012). Although there is mounting evidence that micro tendon deformations are non-uniform (Cheng and Screen, 2007, Arndt et al., 2012) and dependent on fiber organization (Thorpe et al., 2013), it remains challenging to track spatial variations in tendon deformation with ultrasound. Thus, it would be advantageous if tendon displacement and strain patterns could be assessed within an ultrasound image window to provide more localized measures of tissue deformation.

Ultrasound elastography is an approach that uses correlation based tracking of successive ultrasound images to estimate tissue deformation (Ophir et al., 1991), with the phase information in ultrasound radiofrequency (RF) data enabling high resolution tracking of tissue motion along the beam direction (Bohs and Trahey, 1991; Lopata et al., 2009; Ophir et al., 1999). Although

[2] Slane LC, Thelen DG (2014). *Journal of Biomechanics* 47: 750-754.

tissue deformation in elastography is often achieved via manual compression (De Zordo et al., 2010; De Zordo et al., 2009), we have been interested in adapting elastography principles to track tendon deformation under loading conditions that are more physiologically relevant (Chernak and Thelen, 2012). Adapting elastography for tracking tendon can be challenging due to a variety of factors, including the lower resolution of ultrasound data in a direction transverse to the sound beam (Ophir et al., 1999) and the complex architectural features of tendon. Recent advances in 2D elastographic tracking methods have emerged (Chen et al., 2004; Ebbini, 2006; Huang and O'Donnell, 2010) that may be capable of addressing these challenges. The purpose of this study, therefore, was to investigate the fidelity of a 2D elastography method for evaluating motion and strain of tendon-shaped phantoms and *ex vivo* tendon specimens subjected to axial loading. Motion and strain data from elastography were compared with surface motion and strain measures obtained using digital image correlation (DIC) (Sutton et al., 1983). We also compared elastographic estimates obtained with RF and B-Mode data to better understand the potential advantages of using RF data to enhance tissue tracking.

4.2 Methods

Tendon-shaped phantom specimens and *ex vivo* porcine flexor tendons were tested using an identical protocol (Figure 4.1). Phantoms (12.7 x 14.3 x 101.6 mm) were created from polyvinyl chloride-plastisol (Spirou et al., 2005) with randomly dispersed glass beads (30-50 μm diameter) used as ultrasound scatter particles (Insana et al., 1990). Porcine flexor tendons were dissected with the distal bone intact, wrapped in a saline-soaked gauze pad, and frozen until one hour prior to testing. An oil-based paint speckle pattern was applied to each specimen surface to enable DIC tracking. The specimens were submerged in a saline solution bath (9g NaCL per L of water),

with the ends fixed in custom grips (Cheung and Zhang, 2006) of a materials testing machine (Criterion 43, MTS Systems Corporation, Eden Prairie, MN). Specimens were preconditioned with cyclic stretch (0.5 Hz) to 2% strain for ten cycles, followed by three trials of cyclic loading (0.5 Hz) to 4% strain for ten cycles. Prior to each test, specimens were given seven minutes of rest, preloaded to 10 N, and the grip-to-grip length (mean: 84.6 ± 2.9 mm) was measured.

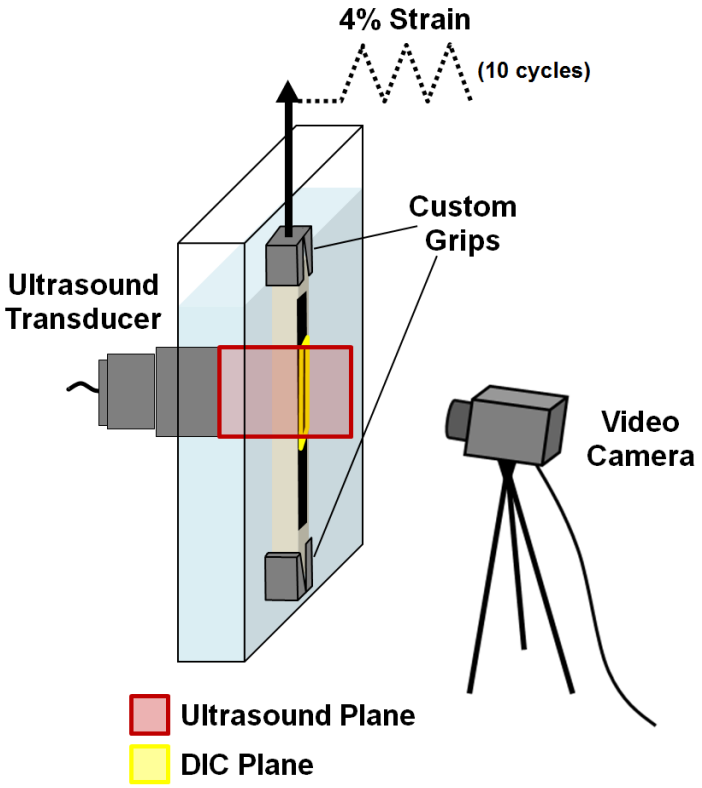

Figure 4.1 Overview of data collection methods. The specimen is mounted in custom grips and cyclically stretched to 4% strain. The ultrasound transducer is positioned to collect cine RF data from a fixed longitudinal cross-section of the specimen. A video camera was positioned to simultaneously collect surface images of the same tendon region.

A linear array ultrasound transducer (L14-5/38, Ultrasonix Corporation, Richmond, BC, Canada) was positioned to collect RF data in a fixed image plane (35 x 38 mm, 128 x 1824 pixels, 56 frames/sec). Video images (2048 x 2448 pixels, Vic-Snap, Correlated Solutions, Inc.,

Columbia, SC) were collected simultaneously such that the specimen and transducer were in view. For DIC analysis, a region of interest (ROI; Phantom: ~38 x 12 mm; Tendon: 38 x ~4 mm) was manually defined to align with the center of the transducer from an unstretched frame of data. Data were tracked (Vic-2D Version 2009, Correlated Solutions, Inc., Columbia, SC) using a seed point defined near the stationary grip (Vic-2D parameters, subset: 40, step size: 5), with the results used to compute strains. For each trial, we reviewed the DIC tracking results, load cell information and ultrasound images to ensure that out-of-plane motion was small, there was no evidence of slip and tendon fascicles remained in view throughout loading. All three phantoms and eight of the twelve porcine flexor tendons achieved these criteria and were included in the subsequent analysis.

Ultrasound data were evaluated using a custom 2D elastography method that has been described previously (Chernak and Thelen, 2012). Briefly, the RF data were up-sampled by a factor of 2 and 4 in the along-fiber (x) and transverse (y) directions (Parker et al., 1983) to increase the spatial density of correlation functions (Konofagou and Ophir, 1998). An ROI was defined within the specimen (Phantom: ~28.3 x 7.7 mm; Tendon: ~26.1 x 3.9 mm). Kernels (2 x 0.8 mm) were centered at nodes positioned every 1.0 and 0.4 mm along the x and y directions, respectively (Figure 4.2). The peak of a 2D normalized cross-correlation function was used to estimate frame-to-frame (incremental) kernel displacements. Sub-pixel displacements were defined as the maximum of a quartic surface spline fit of the correlations (Azar et al., 2010). Incremental displacements (du, dv) were median filtered (3 x 3 nodes) (Thitaikumar et al., 2008), and fitted with low-order polynomials to regularize the displacements (Pan et al., 2009). The along-fiber incremental displacements, du, were assumed to vary as a quadratic function of the nodal positions, x and y:

$$du = A_1x^2 + A_2y^2 + A_3xy + A_4x + A_5y + A_6 \tag{4.1}$$

The higher resolution along-beam incremental displacements, *dv*, were assumed to vary quadratically along each row of nodes at a fixed initial *x* position along the specimen:

$$dv = B_1y^2 + B_2y + B_3 \tag{4.2}$$

Polynomial parameters A_i and B_i were computed using a least squares fit to the experimental data. Nodal displacements, *u* and *v*, were updated at each frame by adding on the incremental displacements. Nodal tracking was repeated in the reverse direction and a weighted average of the nodal displacement trajectories from the forward and backward tracking results was computed (Pelc, 1995). Along-fiber strain $e_{x,i}$, at a node *i*, was estimated using a small strain assumption between nodes along the fascicles:

$$e_{x,i} = \frac{u_{i+1} - u_{i-1}}{x_{0,i+1} - x_{0,i-1}} \tag{4.3}$$

where x_0 represent the nodal positions in a relaxed frame, *u* represent nodal translations in the *x* direction and *i+1* and *i-1* refer to nodes to either side of the node of interest. Elastographic analysis was repeated on B-Mode image data generated from the RF data using a log compression and Hilbert transform:

$$B\text{-}Mode = 20 \cdot \log_{10}\left(abs\left(Hilbert(RF)\right)\right) \tag{4.4}$$

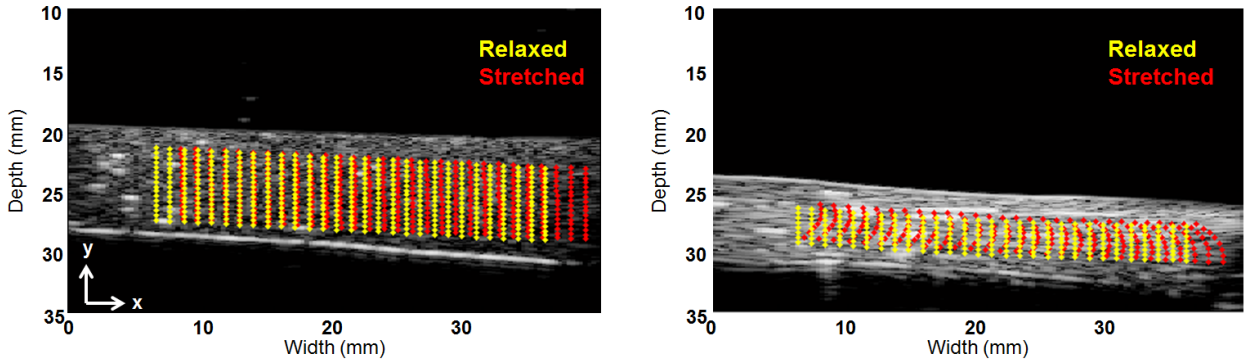

Figure 4.2 Nodal positions during relaxed and stretched frames of a sample phantom and tendon specimen. As this example shows, the phantoms tended to undergo more uniform deformation than the tendon.

We quantitatively compared the displacements and strains obtained using DIC and elastographic analyses by computing the correlation between trajectories over a loading cycle. We also performed paired t-tests to assess differences in estimates of peak strains between methods.

4.3 Results

Phantom Tracking: There was very good agreement ($R^2 > 0.97$) between DIC and RF elastographic estimates of phantom displacement (Figure 4.3a; Figure 4.4a) and strain (Figure 4.5a) trajectories (Table 4.1). Peak phantom strain (DIC: $e_x = 3.5 \pm 0.2\%$; RF: $e_x = 3.7 \pm 0.1\%$) was also comparable between methods (Figure 4.5a). However, elastographic tracking with B-Mode images resulted in an under-prediction of motion (Figure 4.3a, Figure 4.4a) and significant ($p < 0.05$) under-prediction ($1.9 \pm 0.8\%$) of peak strain.

Tendon Tracking: The tendon displacement trajectories computed with RF elastography were highly correlated with the DIC measurements ($R^2 > 0.92$; Figure 4.3b, Figure 4.4b). Both the DIC and elastographic strain estimates exhibited nonlinear strain-stiffening behavior with loading, with reasonably strong correlations ($R^2 = 0.77$; Figure 4.5b) and comparable estimates of peak tendon strain (DIC: $e_x = 2.6 \pm 1.4\%$; RF: $e_x = 2.2 \pm 1.3\%$). Elastographic tendon strain computed with B-Mode images tended to be lower ($e_x = 1.5 \pm 1.0\%$) than those obtained with DIC and RF data.

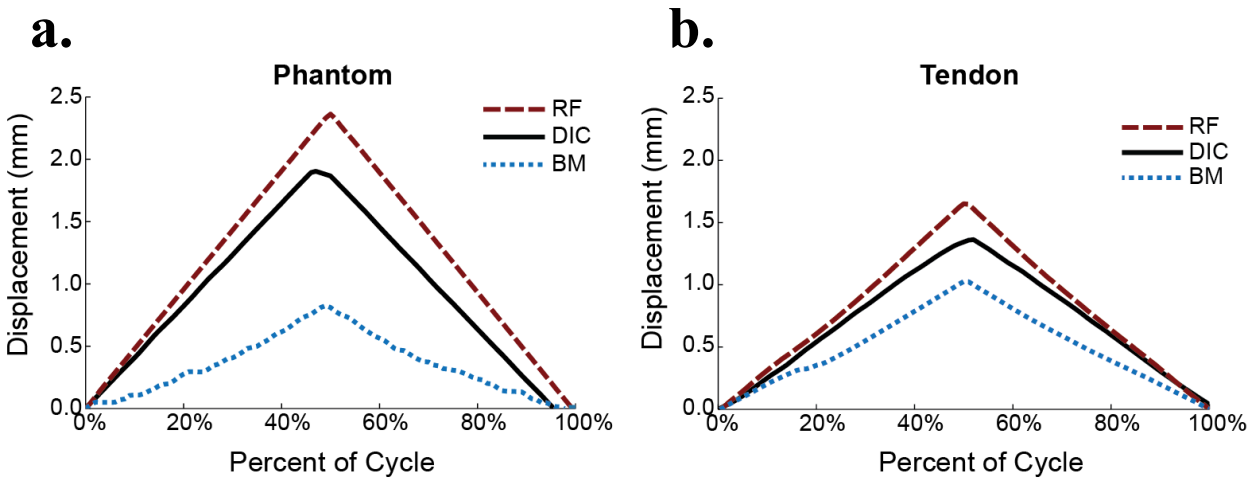

Figure 4.3 Sample displacement trajectories estimated using digital image correlation (DIC) analysis of the video data and 2D elastographic analysis of ultrasound data (RF). Elastographic tracking using B-Mode (BM) images tended to under-estimate motion, as was most evident in the phantom specimens.

4.4 Discussion

This study demonstrates that 2D elastography methods can produce reasonably accurate displacement and strain estimates arising from axial loading of tendon. The notable benefit of this technique is that all analysis is based on data contained within the transducer image window, which obviates the need for using multiple transducers or pre-assuming motion that is out of view. Furthermore, images of spatial variations in tissue motion (Figure 4.2) may provide new

insights into the complex deformation patterns of functionally loaded tendon (Arndt et al., 2012; Finni et al., 2003; Magnusson et al., 2003; Muramatsu et al., 2001).

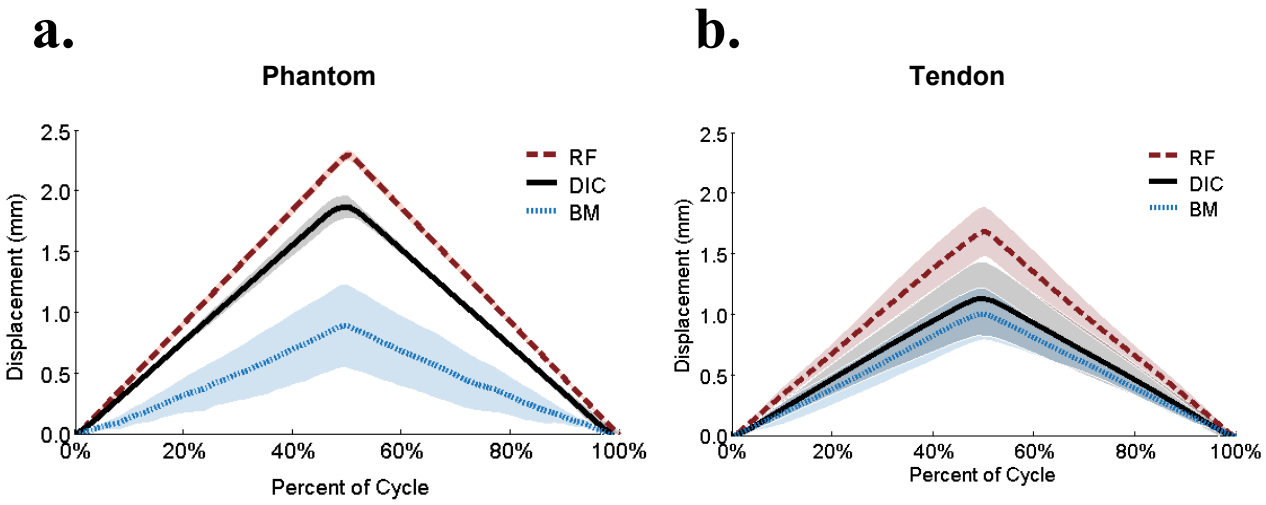

Figure 4.4 Average displacements (± standard deviation) for a) phantom (n = 3) and b) tendon (n = 8) specimens. The RF and DIC match more closely than the BM for the phantom specimens.

Two-dimensional elastographic tracking (Chen et al., 2004; Ebbini, 2006; Huang and O'Donnell, 2010; Lubinski et al., 1999) remains challenging due to limitations in lateral resolution and the potential for out-of-plane motion to obscure 2D displacement estimates. In this *ex vivo* study, we were able to visually ensure that an imaging plane could be defined that aligned with the primary plane of motion. Extending the approach to *in vivo* studies will require better understanding of the sensitivity of tissue displacement estimates to variations in tendon orientation. To address resolution issues, we used quartic spline fits of the correlation function to obtain sub-pixel motion estimates (Azar et al., 2010) and low-order polynomial fits to regularize displacement and strain estimates (Pan et al., 2009). We note that this regularization approach does diminish one's ability to resolve subtle variations in tissue deformation. Thus, it will be

important to consider more sophisticated regularization approaches when using the elastographic approach for assessing motion in tendons with localized damage.

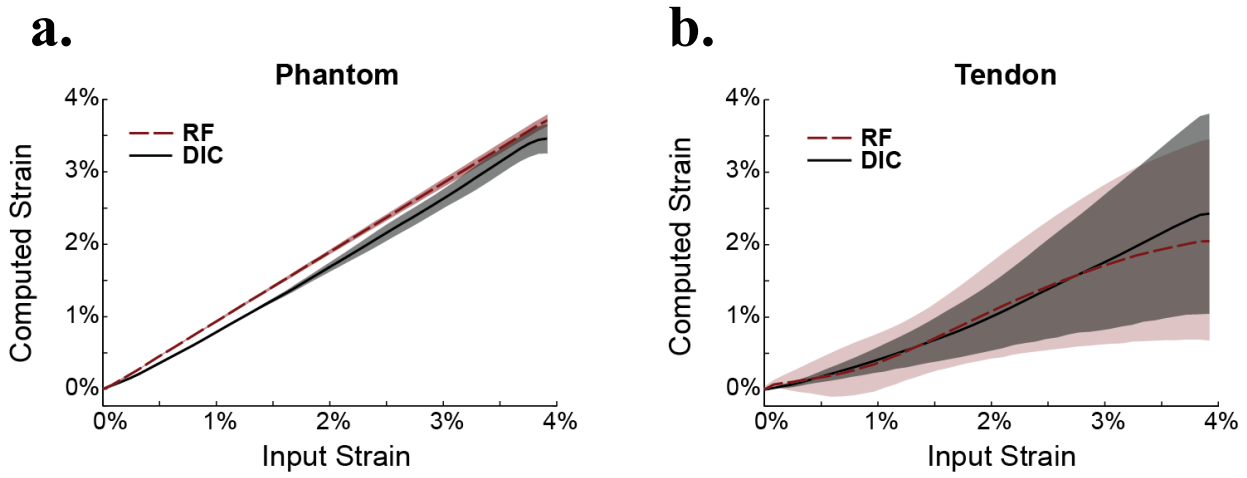

Figure 4.5 Average strain trajectories (shaded curve is ± standard deviation) computed with DIC and for both the phantom and tendon specimens. Mid-substance strains were less than the grip-to-grip strain (plotted along the x-axis), with larger differences observed in the tendon specimens.

Our results suggest that tracking is enhanced using RF data rather than B-Mode images. Elastographic analysis of B-Mode data tended to result in an under-prediction of motion and strain in both the phantom and flexor tendons (Figure 4.6). Although prior studies have used RF data to assess tendon deformation with compression (Brown et al., 2013; Korstanje et al., 2009; Korstanje et al., 2010), we believe this is the first study to demonstrate the benefit of using RF signals to track tendon motion under axial loading. The difference in tracking accuracy is likely attributable to the greater precision achieved by using the phase information inherent in RF data to track fine displacements (Lopata et al., 2009). We note that B-Mode images were generating using a simple Hilbert transformation, which may not reflect the B-Mode processing methods of commercial ultrasound systems.

Table 4.1 Comparison of displacement and strain estimates. The average (± 1 standard deviation) correlation (Pearson's R^2) between DIC and elastographic estimates of displacement and strain trajectories. Elastographic tracking of tendon deformation was highly correlated with DIC measures when using either the RF or B-Mode (BM) ultrasound data. However in the tendons, elastographic tracking with RF data produced trajectories that were more consistent with DIC estimates than B-Mode based tracking.

		Phantom	**Tendon**
Disp.	RF	0.992 ± 0.006	0.975 ± 0.027
	BM	0.976 ± 0.019	0.921 ± 0.161
Strain	RF	0.992 ± 0.001	0.765 ± 0.262
	BM	0.972 ± 0.014	0.634 ± 0.307

Both the DIC and elastography methods in this study consistently predicted maximum mid-substance tendon strains that were less than the grip-to-grip strain. This phenomenon is well-documented in the literature (Haraldsson et al., 2005), and is likely due to higher strains arising near the site of tissue clamping. Although the test setup (Figure 4.1) allowed us to directly compare displacements and strains of the same region of the specimen for both methods, it is important to note the different imaging planes of the surface DIC measures and the ultrasound cross-sectional information. This difference could have contributed to some of the variability in motion and strain between methods (Figure 4.3-5).

In summary, this study demonstrates the fidelity of a 2D elastography tracking method for measuring displacement and strain using ultrasound RF data collected during axial tendon loading. The approach may be extendible to *in vivo* use on humans, which would allow for quantitative analysis of tendon deformation in both normal and pathological states.

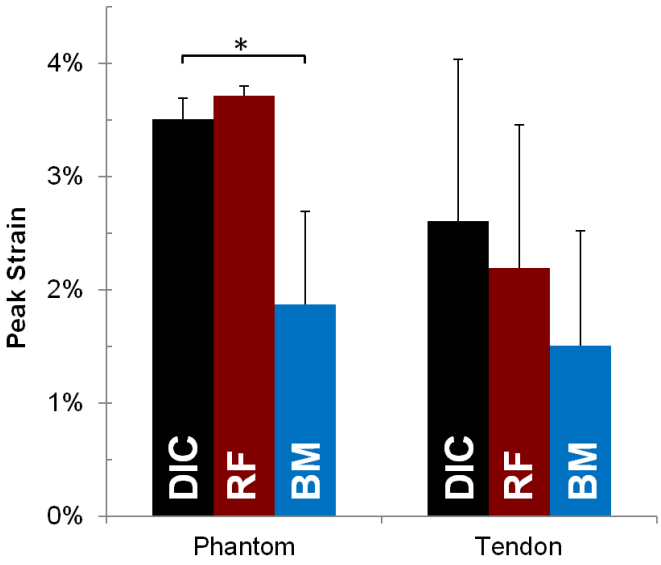

Figure 4.6 The average (+ 1 standard deviation) peak strain estimates obtained using DIC and elastographic analysis of RF and B-Mode (BM) image data. Average mid-substance phantom strains were significantly less than the strains computed using DIC analysis of video data (*$p < 0.05$).

Chapter 5: Non-uniform Displacements within the Achilles Tendon observed during Passive and Eccentric Loading[3]

5.1 Introduction

The frequency and type of tendon loading is an important determinant of injury potential and mechanobiological responses. For example, Achilles tendinopathies are most commonly observed in individuals involved in activities that subject the tendon to repetitive loading (e.g. running) (Maffulli et al., 2003). It has been hypothesized that this repetitive loading gives rise to the localized fibrillar damage and tissue degeneration that develops in tendinopathies (Riley, 2008). However, somewhat paradoxically, exercises involving repeat eccentric loading of the injured tendon have proven effective in treating some individuals with mid-substance tendinopathies (Alfredson, 2003; Fahlstrom et al., 2003; Maffulli et al., 2008). Although the underlying mechanism of this conservative treatment is not well understood, it is believed that the shear loading induced via eccentric exercises may stimulate the tenocytes to induce anabolic responses (Fong et al., 2005; Maeda et al., 2011). These observations highlight the importance of understanding tissue deformation patterns that arise from different *in vivo* loading paradigms.

There is increasing recognition that architectural features can give rise to complex deformation patterns within tendons. For example, micromechanical studies have demonstrated that tendon tissue stretch likely involves a combination of fascicle stretch and interfascicle sliding (Thorpe et al., 2013; Thorpe et al., 2012). These observations are highly relevant to the Achilles tendon, which consists of distinct fascicles arising from the soleus, medial

[3] Slane LC, Thelen DG (2014). *Journal of Biomechanics, in review*.

gastrocnemius and lateral gastrocnemius muscles (Szaro et al., 2009). Distally, the architecture of the Achilles tendon is characterized by a helical twist which causes the relative positioning of these fascicles to vary along the Achilles length. In the mid-substance of the free Achilles tendon, the fascicles from the medial gastrocnemius are located in the superficial portion of the tendon, while fascicles from the soleus are primarily in the mid and deep portion of the tendon (Szaro et al., 2009). This complex architecture, paired with independent loading from the soleus and gastrocnemius muscles (Arndt et al., 1999; Ivanenko et al., 2004; Winter and Yack, 1987), contribute to the potential for development of non-uniform deformation in the free Achilles tendon.

Quantitative ultrasound techniques have recently emerged that allow for the assessment of *in vivo* behavior of the Achilles tendon. For example, prior studies have used ultrasound-based manual tracking of anatomical landmarks to show that different amounts of strain are taken up by the free tendon and aponeurosis (Arampatzis et al., 2005; Magnusson et al., 2001; Magnusson et al., 2003; Muramatsu et al., 2001). Along-tendon non-uniform deformation could arise from variations in loading along the aponeurosis (Finni et al., 2003) as well as spatially varying tendinous tissue stiffness (DeWall et al., 2014). However, much less is known about spatial variations in tendon deformation across the tendon thickness. A prior study using ultrasound speckle tracking discovered variations in tissue displacement between the superficial, mid and deep layers of the Achilles tendon during passive stretch (Arndt et al., 2012), which suggested the existence of differential stretch in tendon fascicles that originate in the soleus and gastrocnemius muscles. It is likely that such behavior could vary with active muscle loading and limb posture, given that knee flexion shortens gastrocnemius muscle-tendon operating lengths.

Indeed, prior studies have shown that gastrocnemius contributions to ankle plantarflexor strength are greatly reduced in flexed knee postures (Arampatzis et al., 2006; Cresswell et al., 1995).

The goal of this study was to use ultrasound elastography (Chernak and Thelen, 2012; Slane and Thelen, 2014) to measure Achilles tendon displacement patterns under both passive and eccentric loading conditions in two knee postures. We hypothesized that eccentric loading would induce more non-uniform tendon motion than observed under passive stretch. We also hypothesized that knee posture would alter relative tendon tissue motion between the soleus and gastrocnemius portions of the Achilles tendon, due to a posture-induced change in loading sharing between gastrocnemius and soleus fascicles. When the knee is flexed, and the gastrocnemius is less stretched, we expected to observe an increase in displacement in the portion of the tendon comprising fascicles originating in the gastrocnemius muscle.

5.2 Methods

Nine healthy young (5F/4M; 24 ± 1 years) adults with no history of Achilles tendon injury were recruited for this study. Written consent was obtained from each subject as per our Institutional Review Board requirements prior to testing. Subjects were first asked to walk at a comfortable pace for six minutes to pre-condition the plantarflexor muscle-tendon units (Hawkins et al., 2009). Subjects were then positioned prone on an examination table with their foot secured in a rotating footplate whose axis was aligned with the ankle (Figure 5.1). The footplate was coupled via a stiff belt and gear-train to an inertial load that induced eccentric plantarflexor loading with ankle dorsiflexion. Loads were recorded using two load cells (LCM300 Futek, Irvine, CA) mounted on the belts of the loading assembly and recorded at 1000 Hz. Ankle angle was simultaneously recorded using an encoder mounted on the footplate rotation shaft. Load cell and

encoder data were subsequently used in post-hoc analyses to compute the internal sagittal ankle moment (Appendix B).

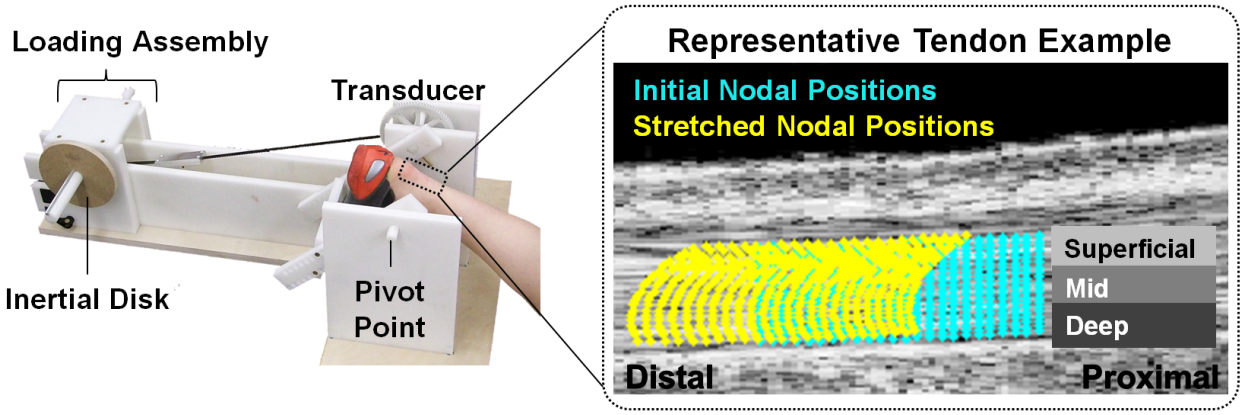

Figure 5.1 An overview of the experimental setup and image analysis. Inertial disks were used to induce eccentric plantarflexor contractions when moving from a plantarflexed to dorsiflexed position. An ultrasound transducer placed over the distal Achilles tendon was used to collect RF data throughout the cyclic trials. In post-hoc analysis, initial nodal positions were defined within the tendon from an image collected in the most plantarflexed position. Two-dimensional elastography was then used to track the subsequent motion of nodes located in superficial, mid and deep portions of the tendon.

Subjects performed eccentric and passive ankle trials at fixed knee flexion angles of 30 deg and 90 deg, referred to as extended and flexed knee postures, respectively. In eccentric trials, subjects were asked to cyclically dorsi- and plantarflex their ankle between 0 and 30 at a rate of 0.5 Hz and angular velocity of 30 deg/sec. A metronome was used to guide the cyclic rate, and subjects were provided real-time angular feedback to maintain the desired range of motion. Inertial disks on the loading device induced ankle plantarflexor moments, with the peak load of ~30 Nm defined to occur when the subject was in their most dorsiflexed position. For both knee angles, passive trials were also conducted in which a researcher guided the ankle through the same range of motion at the same cyclic rate and angular velocity as in the eccentric loading

trials. Trial order was randomized, and subjects were given one minute of practice with each loading condition prior to data collection.

Rectangular ultrasound standoff pads (178 x 127 mm, 16 mm thick) were created by heating a commercial pad (Aquaflex, Parker Laboratories, Fairfield, NJ) and letting it settle in a mold. The standoff pad was placed over the Achilles tendon and secured with an elastic ankle brace. A 10 MHz linear array transducer (L14-5/38, Ultrasonix Corporation, Richmond, BC) was then manually positioned to image the Achilles tendon, with the inferior edge of the transducer positioned just superior to the superior edge of the calcaneus (Figure 5.1b). For each test condition, three eight-second trials of cine ultrasound radiofrequency (RF) data were collected of the Achilles tendon at 70 frames/sec.

Tissue displacements were computed retrospectively from the RF data. Tissue tracking was performed using a 2D cross-correlation based elastography technique that has been described previously (Chernak and Thelen, 2012), and validated in phantom and *ex vivo* experiments (Chernak and Thelen, 2012; Slane and Thelen, 2014). Briefly, ankle angle data were used to define each cycle of motion, with the most plantarflexed position designated as the cycle start. To ensure that only tendinous tissue was included, a region of interest (ROI) was manually defined within an image of the Achilles tendon from the most plantarflexed position. A grid of nodes was then positioned (spaced: 0.5 x 0.2 mm) within the ROI (8.1 x 2.3 mm). Frame-to-frame nodal motion was assessed by finding the displacements that maximized the cross-correlation of rectangular kernels (2 mm x 1 mm) centered at the nodes in each pair of successive frames. Nodal displacements were regularized using a 2^{nd} order surface fit (Slane and Thelen, 2014). Nodal tracking was repeated in the reverse direction and a weighted average of the nodal

displacement trajectories from the forward and backward tracking results was computed (Pelc, 1995).

Displacement profiles for each trial were computed by averaging the along-fiber nodal displacements into twelve bins across the thickness of the tendon. For each bin, we computed the displacement when moving from the most plantarflexed to most dorsiflexed angle. For statistical comparison, we then further averaged the nodal displacements into three equally sized depths of the tendon: superficial, mid and deep. A repeated measures ANOVA was then used to evaluate the effects of loading condition (passive, eccentric) and depth (superficial, mid, deep) on the absolute displacement along the tendon fiber direction. To evaluate loading effects on non-uniformity, we computed the difference between regional displacements (superficial, mid, deep) and the displacement of the whole ROI. A repeated measures ANOVA was used to evaluate the effects of loading condition and depth on the differential displacements. Tukey Post-hoc analysis ($p < 0.05$) was used to test primary hypotheses.

5.3 Results

Achilles tendon thickness averaged 4.5 (± 0.5) mm for the 9 subjects tested. There were no significant differences in ankle angular excursion (25.6 ± 1.7 deg) between the passive motion and eccentric loading conditions (Figure 5.2a). In the eccentric condition, the device induced a peak ankle plantarflexor moment (33.6 ± 8.3 Nm) in a nearly fully dorsiflexed posture (Figure 5.2b). No significant difference in peak ankle moment was observed between eccentric loading tasks performed in extended and flexed knee postures. However, peak ankle moment did occur slightly and significantly earlier in the loading cycle for the flexed knee case (Extended: 57 ± 3% of cycle, Flexed: 52 ± 4% of cycle, $p = 0.007$).

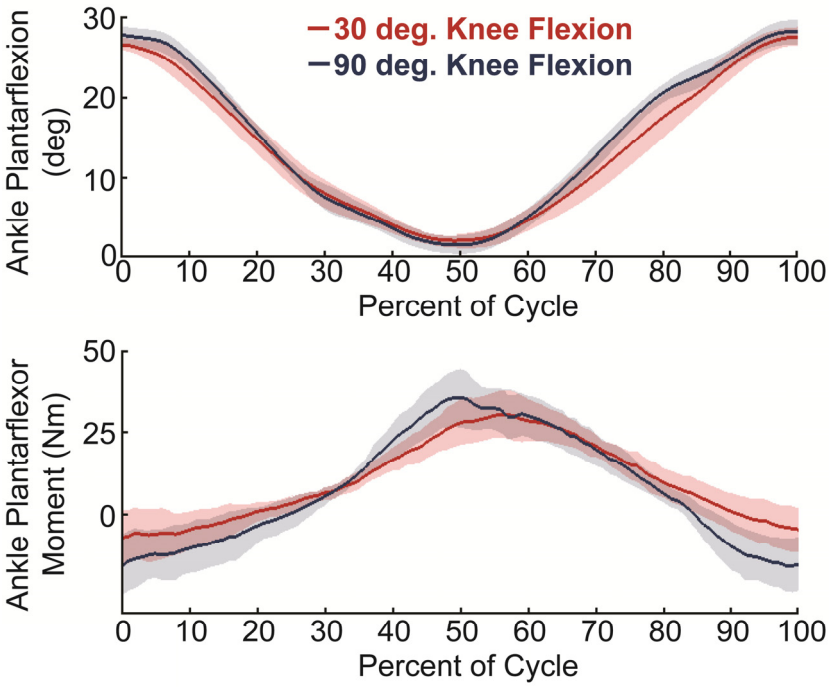

Figure 5.2 Average temporal patterns of the plantarflexion angle and internal ankle moment (±1 standard deviation) over an eccentric task motion cycle, with 0% corresponding to the most plantarflexed position. Ankle range of motion and peak ankle moments were not significantly different when performed with 30 and 90 deg of knee flexion.

Non-uniform tissue displacement patterns were observed across the tendon thickness, with the greatest displacement observed in the deeper tissue for all four test conditions (Figure 5.3). Knee angle had a significant effect on the magnitude of tissue displacements observed, with greater tissue displacement ($p < 0.002$) observed in the more extended knee posture for both loading conditions in the mid and deep portions of the tendon (Figure 5.4). In the extended knee posture, significantly greater displacements were measured in the passive loading condition than in eccentric loading condition at all depths ($p < 0.0002$). In the extended knee posture, significantly greater passive displacements were only observed in the mid and deep portions of the tendon ($p < 0.0002$). There were depth dependent significant ($p < 0.03$) differences in the relative tissue displacements between the superficial and mid layers for all four tasks (Figure

5.5). Differences between the mid and deep tissue displacements were only significant under the passive flexed condition ($p < 0.05$).

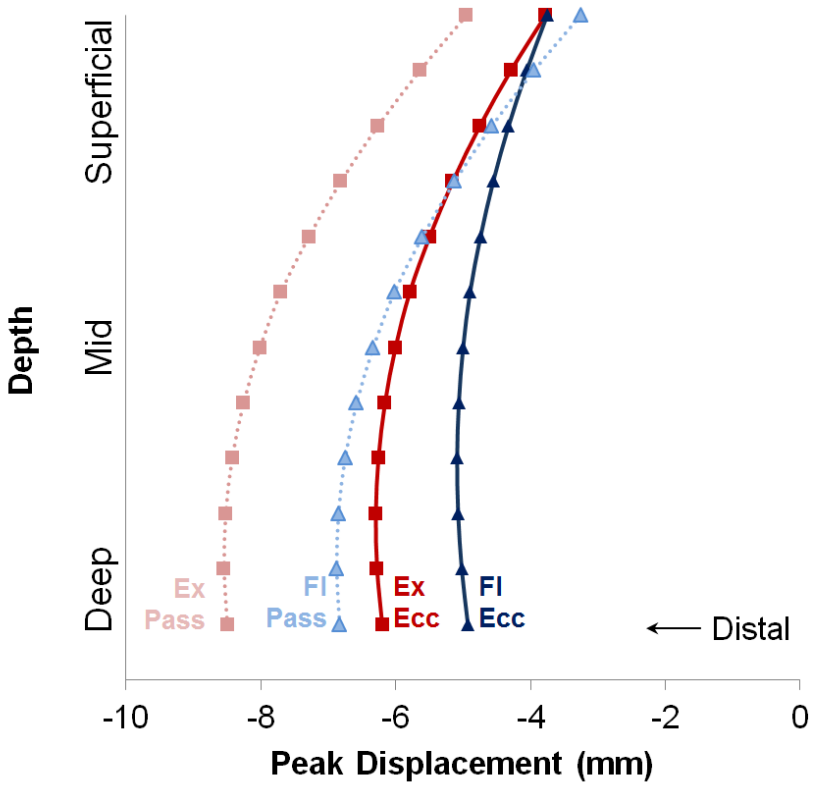

Figure 5.3 The average (across 9 subjects) peak nodal displacements (negative corresponds with distal) at different tissue depths for passive and eccentric loading tasks. Larger tissue displacements were observed when the knee was extended (Ex; 30 deg) compared with when the knee was flexed (Fl; 90 deg).

5.4 Discussion

Our data suggest that the Achilles tendon undergoes non-uniform displacement during both passive and eccentric plantarflexor loading. Specifically, we consistently observed greater displacement in the mid and deep tendon relative to the more superficial tendon when dorsiflexion the ankle. Similar patterns were previously observed with passive dorsiflexion (Arndt et al., 2012) and may reflect the tendon undergoing shear deformation and variable stretch

over the tendon cross-section. Such behavior may be relevant to consider when assessing both injury factors and mechanobiological stimuli.

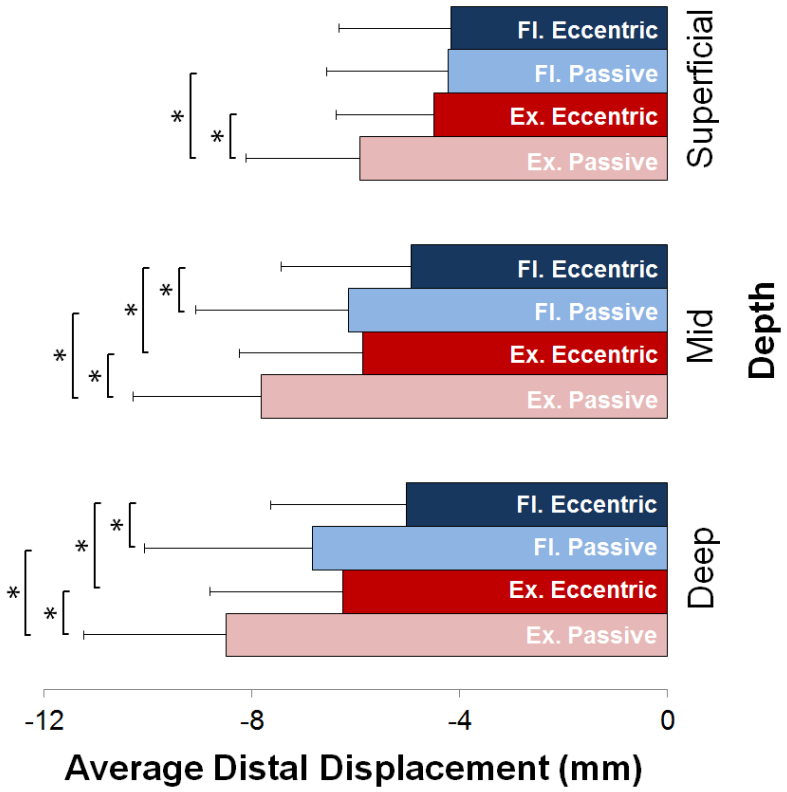

Figure 5.4 Average (+1 standard deviation) peak tissue displacements (negative corresponds with distal) when moving from plantarflexed to dorsiflexed positions. Knee posture significantly affected tissue displacements in superficial, mid and deep layers, whereas loading only significantly affected the mid and deep tissue displacements in a flexed knee posture. *$p < 0.05$.

Contrary to our first hypothesis, we did not consistently observe an increase in the non-uniformity of tendon motion with eccentric loading relative to passive loading. This hypothesis was based on the idea that eccentric loading may generate greater tissue shear stress and fluid flow that stimulates tenocytes to induce anabolic responses (Grigg et al., 2009). Such ideas are based on mechanobiological studies that have demonstrated the importance of tissue loading for promoting tissue homeostasis and repair responses (Fong et al., 2005; Maeda et al., 2011) and the clinical observation that eccentric activities are sometimes effective at conservatively treating

patients with Achilles tendinopathy (Alfredson, 2003; Fahlstrom et al., 2003; Maffulli et al., 2008). However, it should be noted that the eccentric exercises commonly performed for Achilles tendinopathy involve considerably larger loading than used in this study. Thus, further study is needed to determine how load magnitude may affect tissue displacement patterns.

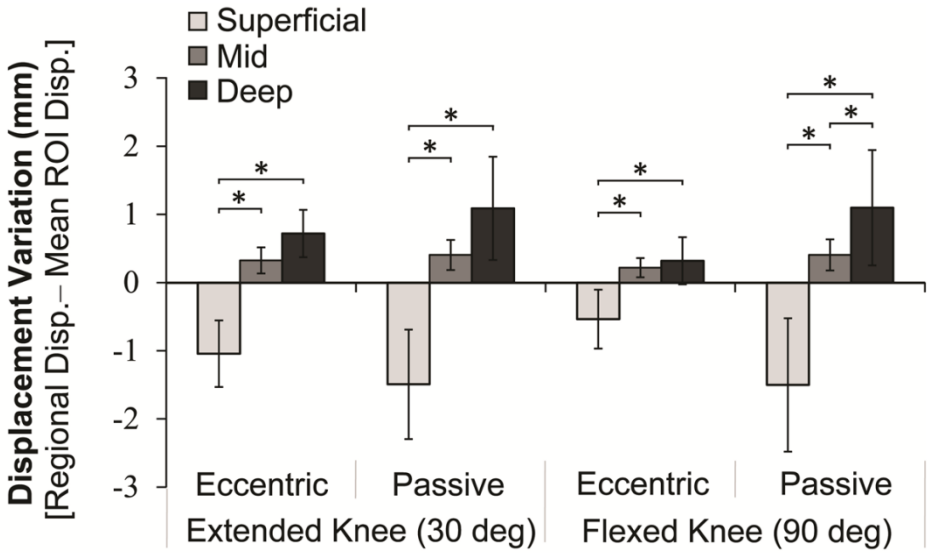

Figure 5.5 Variations in superficial, mid and deep tissue displacements, relative to the average ROI displacements for each condition, were observed. Depth dependent differences in differential tissue motion are evident for each of the tasks, though differences between the mid and deep layers are only significant in the passive flexed knee trial. *$p < 0.05$.

We did observe a significant effect of knee angle on tendon tissue motion (Figure 5.4), however this effect contrasted with our hypothesis. We hypothesized that knee flexion would lead to an increase in displacement, at least in the portion of the tendon comprising fascicles that originate in the gastrocnemius muscle due to the decreased stretch on the gastrocnemius muscle. In contrast, we consistently measured greater tissue displacement in extended knee postures under both passive and eccentric loading conditions. Greater displacement would imply that the portion of the tendon distal to the ROI is undergoing less stretch with dorsiflexion when the knee

is extended. This posture effect could result from the more stretched gastrocnemius inducing a preload that stiffens the Achilles tendon, and thereby reducing the additional stretch that arises with dorsiflexion. We observed knee flexion to affect motion in all three tissue layers. Although biomechanically, knee flexion only affects the muscle-tendon length of the biarticular gastrocnemius, a change in gastrocnemius muscle length can alter the relative load sharing across the triceps surae (Cresswell et al., 1995). Indeed, there is evidence of a posture dependent change in load sharing in our data. When the knee was flexed, eccentric loading significantly altered motion in the mid and deep portions of the tendon but not in the superficial tendon (Figure 5.4). This may reflect preferential loading of the soleus in a flexed knee posture, since the shortened gastrocnemius is at a length poorly tuned for force generation (Arampatzis et al., 2006; Cresswell et al., 1995). Greater soleus loading would potentially increase the distal stretch of the mid and deep fascicles of the Achilles tendon, thereby contributing to the observed reduction in displacement with eccentric loading.

There is ample anatomical evidence of the intricate hierarchical structure of the tendon that likely affects internal deformations. Distinct fascicles arise from the medial gastrocnemius, lateral gastrocnemius and soleus. These fascicles intertwine and undergo approximately a 90 deg helical twist distally (White, 1943). We imaged the free Achilles tendon, with the distal edge of our image located slightly proximal to the superior calcaneus. The ROI was centered on the tendon and positioned proximally to allow for the distal translation to remain within the image during dorsiflexion. Anatomically at this position, superficial displacements of the ROI would primarily reflect the portions of the tendon arising from the medial gastrocnemius, while the mid and deeper displacements of the ROI would most likely reflect fascicles arising from the soleus (Szaro et al., 2009). Lateral gastrocnemius tendon fascicles do twist and appear in deeper layers

in the most distal portion of the Achilles tendon, but likely were not a major component of the ROI at the level of the tendon we tracked. Therefore, the non-uniform motion that we observed may reflect relative sliding between the tendon fascicles originating in the medial gastrocnemius and soleus. This explanation would be consistent with recent *in vitro* tendon studies that have suggested that interfascicle sliding is an important component of tendon micromechanical behavior (Thorpe et al., 2013; Thorpe et al., 2012).

It was somewhat surprising that we observed less motion in the superficial Achilles tendon relative to the mid and deep tendon. The moment arm about the ankle would be larger for the superficially positioned fascicles of the medial gastrocnemius and thus could be expected to undergo greater displacement with dorsiflexion. However, there are a couple of potential explanations for our observations. First, it is possible that the tendon fascicles originating in the medial gastrocnemius are more compliant, resulting in greater stretch distal to the ROI and thus less displacement within the image window. Indeed, the longer length of the distal gastrocnemius tendon relative to the soleus distal tendon (Cummins et al., 1946) may result in it having lower compliance. Alternatively, it is possible that there is a component of twist to the motion of the gastrocnemius fascicles during dorsiflexion that is not captured in our two-dimensional tracking technique. In this case, the motion we measure would not be purely a function of dorsiflexion and tendon stretch. However, regardless of the underlying factors, it is likely that the non-uniform motion that we observe is arising from the architectural fascicle structure of the Achilles tendon.

There are a few limitations in this study to consider. An important component of this study was the evaluation of non-uniform tendon motion under distinct loading conditions and limb postures. To maintain a consistent ankle excursion across different tasks, visual biofeedback of

ankle angle was used to guide task performance. This method was effective at controlling ankle angle excursions, with no significant differences measured between conditions. However, we did measure a slight change in the timing of eccentric loading patterns (Figure 5.2). Our analyses were defined based on the time of peak dorsiflexion; such that the small change in load timing could have contributed to some of the posture effects occurred in the eccentric loading paradigm. The fact that we observed similar posture effects under both passive and eccentric loading conditions (Figure 5.3) would suggest this was not a major factor.

A second challenge is the use of 2D ultrasound imaging to capture motion from a 3D structure. This is a limitation that is present in many studies that have used 2D ultrasound to characterize Achilles tendon motion and deformation with loading (Arampatzis et al., 2005; Arndt et al., 2012; Maganaris, 2003; Magnusson et al., 2003; Muramatsu et al., 2001). We have previously performed extensive validation studies of our elastographic tracking technique on *ex vivo* tendon loading paradigms and found that displacement estimates are highly correlated ($R^2 > 0.92$) with displacements obtained by tracking markers on the tissue surface (Slane and Thelen, 2014). Thus, while we are unable to capture the out-of-plane motion that can arise from tendon twist, we are fairly confident in the capacity of this method to track motion within the image plane.

In summary, this study provides evidence of depth dependent tissue displacements across the Achilles tendon cross-section under both passive and eccentric loading conditions. We observed knee angle to play a significant role in altering tendon tissue motion, with greater tendon tissue displacements measured when the knee was extended. Eccentric loading was also observed to alter mid and deep Achilles tendon tissue displacements in a flexed knee posture, but not in the extended posture. These spatial and posture dependent motion patterns suggest that the Achilles

tendon undergoes non-uniform deformation under *in vivo* loading conditions. Such behavior could reflect relative sliding between the distinct tendon fascicle that arise from the gastrocnemius and soleus muscles.

Chapter 6: Achilles Tendon Displacements Patterns measured in Middle-Aged Adults[4]

6.1 Introduction

Achilles tendinopathies are common and increase in prevalence in middle-aged adults (Kvist 1991). For example, the annual incidence of Achilles tendinopathy in runners is estimated to be between 7% and 9% (Kujala *et al.* 2005), with middle-aged adults reporting nearly twice as many Achilles tendon injuries than their younger counterparts (McKean *et al.* 2006). It remains unclear why middle-age results in increased susceptibility to Achilles tendon damage. A recent hypothesis suggests that aging may alter the relative amount of sliding and stretch between tendon fascicles (Thorpe *et al.* 2013). Such changes could alter both injury susceptibility at the collagen fiber level, and the mechanobiological responses of the tissues (Arnoczky *et al.* 2007). Thus, an improved understanding of age-related changes in tendon deformation is relevant for both understanding the causes of tendinopathy, and for objectively designing conservative treatment exercise programs. For example, repeat eccentric loading has shown some success in treating Achilles tendinopathies (Alfredson *et al.* 1998; Fahlstrom *et al.* 2003; Maffulli and Longo 2008), but it remains challenging to predict who will benefit a priori.

There is increasing evidence that the Achilles tendon undergoes complex, non-uniform deformation patterns *in vivo*. This may be relevant to consider in the context of injury and rehabilitation, with biochemical studies demonstrating that shear loading may promote tendon healing (Fong *et al.* 2005; Maeda *et al.* 2011). Various studies have demonstrated that the Achilles free tendon and gastrocnemius aponeurosis are subjected to different amounts of stretch

[4] Slane LC, Thelen DG. Manuscript in preparation for submission to *Physics in Medicine and Biology*.

during loading (Magnusson *et al.* 2003; Muramatsu *et al.* 2001). There is also evidence of mechanical heterogeneity along the length of the Achilles (DeWall *et al.* 2014; Finni *et al.* 2003) and within its cross-section (Arndt *et al.* 2012; Slane and Thelen 2014a). Such spatial variations in tendon behavior could contribute to the tendency for Achilles tendinopathies to emerge at specific locations. For example, Achilles tendinopathy most commonly occurs in the tendon mid-portion (roughly 3-6 cm proximal to the calcaneus insertion) (Astrom and Rausing 1995).

The effects of aging on *in vivo* Achilles tendon behavior remain inconclusive. Comparative studies have observed specific microstructural changes that occur with age that include changes in collagen type III content (Birch *et al.* 1999), decreased collagen fibril diameters (Nakagawa *et al.* 1994) and decreased collagen crimp angle (Patterson-Kane *et al.* 1997; Tuite *et al.* 1997). It is generally thought that these microstructural changes will lead to an increase in tendon compliance with old age, as has been observed *in vitro* (Blevins *et al.* 1994; Vogel 1980, 1983). The specific effects on tendon compliance in middle-age are less well studied, and it is unclear how these mechanical changes progress with age. In humans, a few recent studies have aimed to evaluate the effects of aging on gross tendon strain and stiffness, but most have focused on only young and older adults, and even these have published conflicting results (Karamanidis and Arampatzis 2005; Kubo *et al.* 2007; Narici *et al.* 2005; Onambele *et al.* 2006; Stenroth *et al.* 2012). This lack of conclusive evidence may arise from a methodological limitation that focuses on the computation of changes in average tendon strains over a large portion of the lower limb, and may mask spatial variations.

Thus, the purpose of this study is to utilize a recently developed ultrasound-based soft tissue tracking technique to evaluate middle-aged Achilles tendon displacement patterns. We were interested in evaluating how displacement patterns differ along the cross-section of the tendon,

change with loading condition (passive stretch vs. eccentric loading), and differ from the patterns observed in young adults. We previously observed non-uniformity in tendon displacements in young adults, with deep tissue undergoing more displacement than superficial tissue (Slane and Thelen 2014a). We hypothesized that middle-aged adults would exhibit similar patterns of non-uniformity as young adults, with evidence of an increase in tendon compliance, and more uniformity in *in vivo* tendon deformation.

6.2 Methods

Nine healthy young adults (24.1 ± 1.4 years; 4 M, 5 F), and nine healthy middle-aged adults (49 ± 3.1 years; 4 M, 5 F) were recruited for this study (Table 6.1). Subjects had no history of prior Achilles tendon injury and provided written consent to participate. To precondition the plantarflexor muscle-tendon units, subjects first walked at a comfortable pace for six minutes (Hawkins *et al.* 2009). Subjects were then asked to lie prone on an examination table, with their knee extended (~30 deg flexion). The right foot of each subject was secured in the footplate of a custom loading device as described previously (Slane and Thelen 2014a). Briefly, the device was designed to induce eccentric plantarflexor loading with ankle dorsiflexion. Loading assembly force and ankle angle were measured at 1000 Hz using two load cells (LCM300 Futek, Irvine, CA) and a mounted encoder, respectively (Appendix B).

Data were collected during eccentric trials in which subjects dorsi- and plantarflexed their ankles cyclically between 0 and 25 deg of plantarflexion. Real-time angular feedback and a metronome were used to guide subjects through the range of motion at the desired cyclic rate (0.5 Hz). Passive trials were also collected in which a researcher guided the ankle through the

same range of motion at the same cyclic rate. Trial order was randomized and subjects were given one minute of practice prior to eccentric trials to gain familiarity with the testing setup.

Table 6.1 Comparison of subject populations.

	Young adults	Middle-aged adults
Age:	24.1 ± 1.4 years	49.0 ± 3.1 years
Subjects:	4 M, 5 F	4 M, 5 F
Height:	70.5 ± 5.5 inches	67.3 ± 5.7 inches
Tendon thickness:	4.5 ± 0.5 mm	4.8 ± 0.7 mm
Total exercise per week:	10.2 ± 4.5 hours	9.0 ± 5.4 hours
Passive ankle range of motion*:	25.2 ± 1.7 deg	22.7 ± 1.4 deg
Eccentric ankle range of motion:	25.6 ± 1.7 deg	26.1 ± 1.3 deg
Eccentric ankle plantarflexor moment:	30.1 ± 7.4 Nm	33.5 ± 2.9 Nm
Frame of peak ankle plantarflexor moment*:	57.0 ± 3.0	52.6 ± 3.7

*$p < 0.05$

Ultrasound radiofrequency (RF) data were collected from the distal Achilles tendon, with the distal edge of the probe positioned just proximal to the superior edge of the calcaneus. RF data were collected using a 10 MHz linear array transducer (L14-5/38, Ultrasonix Corporation, Richmond, BC) at 70 frames/sec. Custom rectangular standoff pads (Slane and Thelen 2014a) were secured within an elastic ankle brace to enhance collections.

Tissue displacements were then computed from the RF data using a 2D cross-correlation based method that has been described previously (Chernak and Thelen 2012; Slane and Thelen 2014b). Each cycle of motion was defined based on the ankle angle such that the start of each cycle corresponded with the most plantarflexed posture. Nodes were defined in the initial frame of each cycle and tracked throughout motion. Depth dependent displacement profiles were computed from the frame at the most dorsiflexed posture by averaging the along-fiber nodal displacements into twelve bins across the thickness of the tendon. To statistically evaluate depth

dependent effects, we further binned the data into three equally sized portions of the tendon: superficial, mid and deep. The displacement profile width was computed as the difference between the maximum and minimum aspects of the displacement profile (Figure 6.1). The displacement profile width was then divided by the average displacement (i.e. normalized displacement profile width) as a measure of relative non-uniformity in tendon displacement.

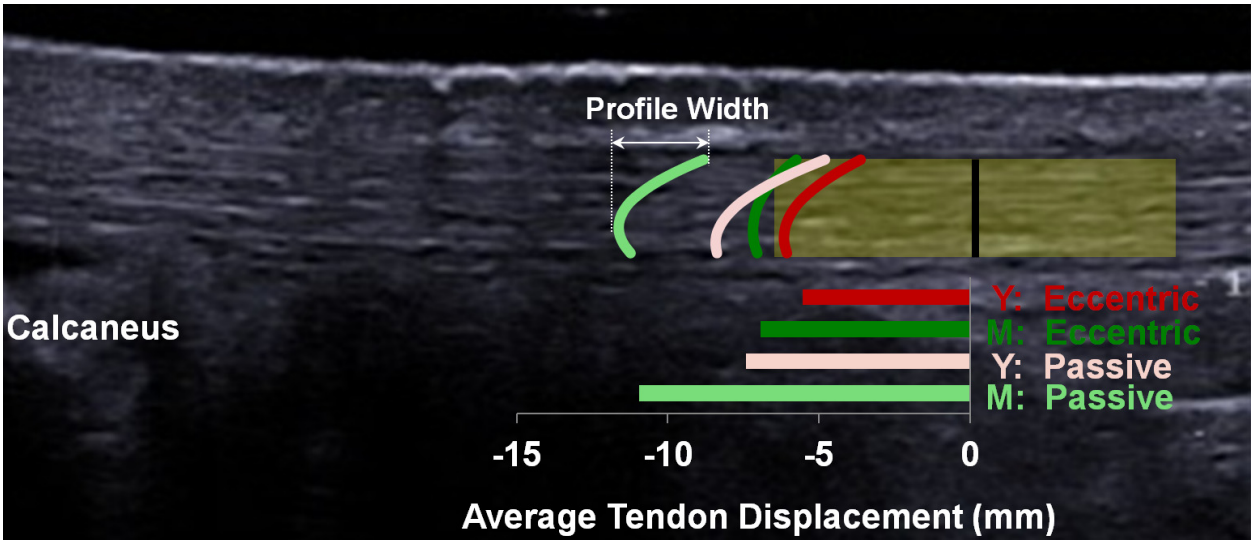

Figure 6.1 Ultrasound data were collected from the distal Achilles tendon**.** During post-hoc analysis, a region of interest (ROI) was defined (representative sample shown in yellow) within the tendon from a B-Mode image collected in the most plantarflexed posture. Nodes displaced distally for all motions, with significantly greater average displacement observed in passive loading than in eccentric loading for both young (Y; $p = 0.049$) and middle-aged (M; $p = 0.0002$) adults. Average passive displacement was also significantly greater for middle-aged adults than young adults ($p = 0.0002$). The width of the displacement profile was computed as the difference between maximum and minimum aspects of the displacement profile.

A general linear model (Statistica, StatSoft Inc., Tulsa, OK) was used to evaluate the effects of age group (young, middle-aged) and loading condition (passive, eccentric) on regional average displacements (superficial, mid and deep). General linear models were also used to evaluate the effects of age (young, middle-aged) and loading condition (passive, eccentric) on average ROI

displacement and normalized displacement profile width. The difference in average ROI displacement between passive and eccentric loading conditions was evaluated in a general linear model testing age (young, middle-aged) and tendon region (superficial, mid, deep). All significant interactions were followed up by Tukey post-hoc analysis ($p < 0.05$).

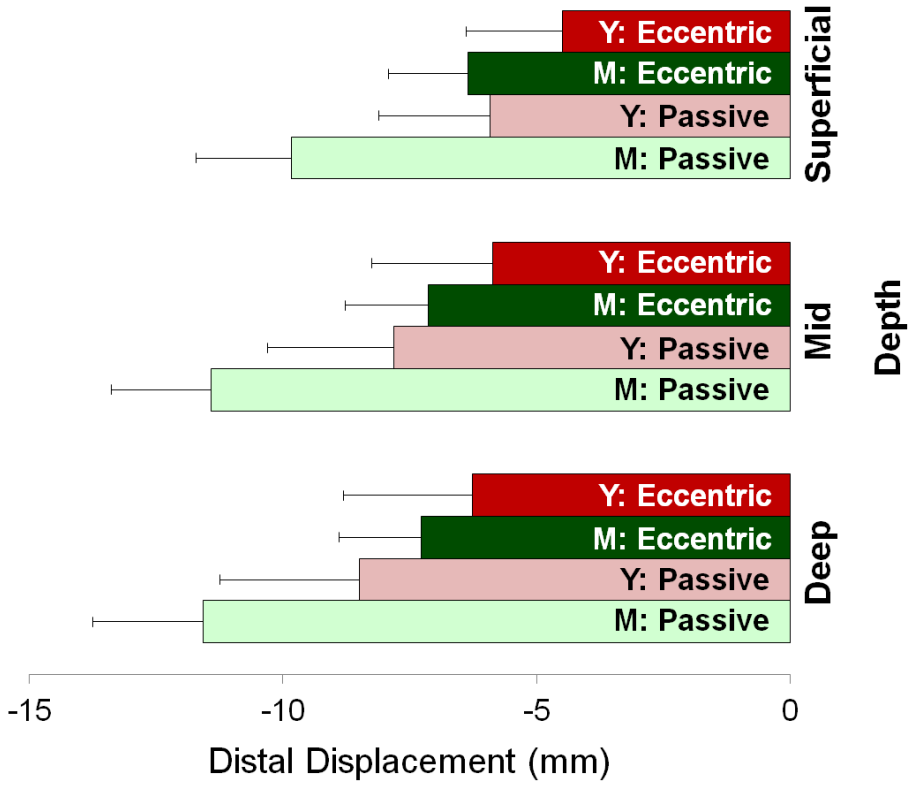

Figure 6.2 Average distal displacement (- standard deviation) in superficial, mid and deep regions for young (Y) and middle-aged (M) adults. Significant regional variation in tendon displacements in both passive and eccentric loading conditions. In all trials, the displacement of the superficial portion of the tendon was significantly lower than displacements in the mid and deep portions of the tendon ($p < 0.0002$).

6.3 Results

There were no significant differences between young and middle-aged adult populations in terms of height, tendon thickness or average hours of exercise per week (Table 6.1). Middle-aged adults underwent a significantly smaller range of motion in the passive trial ($p = 0.003$). For

eccentric loading conditions, there was no difference in the ankle excursion between age groups, or peak plantarflexor moment, though the frame of peak load occurred significantly ($p = 0.04$) closer to the frame of peak dorsiflexion in middle-aged adults.

In both age groups, and in both loading conditions, superficial tendon displacements were significantly lower than displacements in the mid and deep portions of the tendon (Figure 6.2; $p < 0.0002$). Average passive displacements were also significantly greater than eccentric displacements for young ($p = 0.049$) and middle-aged adults (Figure 6.1; $p = 0.0002$).

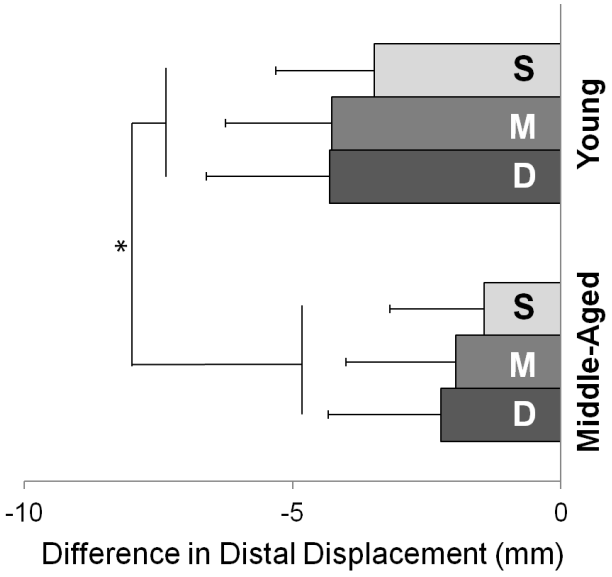

Figure 6.3 The difference between the average ROI displacement in passive and eccentric loading (- standard deviation) is plotted for young and middle-aged adults in the superficial (S), mid (M) and deep (D) regions. For both age groups, the average passive displacement was greater than the average eccentric displacement. The difference in distal displacement between the two loading conditions was significantly greater in middle-aged adults than young adults ($p = 0.03$), and significantly greater in in the mid and deep portions of the tendon than the superficial portion ($p = 0.000$), with no interaction between age group and tendon depth. *$p < 0.05$.

Aging effects were also observed. In the passive loading condition, average tendon displacements were significantly higher for middle-aged adults than young adults (Figure 6.1; $p = 0.0002$), with no aging effect on average tendon displacement observed in the eccentric loading

case. Likewise, the difference in distal displacement between passive and eccentric loading conditions was significantly greater in all regions of the tendon in middle-aged adults compared with young adults (Figure 6.3; $p = 0.03$). This difference was significantly higher in the mid and deep portions of the tendon ($p = 0.000$), with no interaction observed between age group and tendon depth.

The normalized displacement profile width was significantly lower in middle-aged adults (Figure 6.4; $p = 0.001$), with no observed effect of loading condition, and no interaction between age and loading condition.

6.4 Discussion

In this study, we observed non-uniform displacement patterns in passive and eccentric loading conditions in young and middle-aged adults, with a decrease in this non-uniformity observed with age. In both age groups, we measured significantly larger displacements in passive loading conditions than in eccentric loading conditions, with the magnitude of average passive displacement measured to be significantly higher in middle-aged adults. These results suggest that aging contributes to specific changes in tendon compliance and deformation patterns, which may have implications for the increase in injury incidence observed in middle-age.

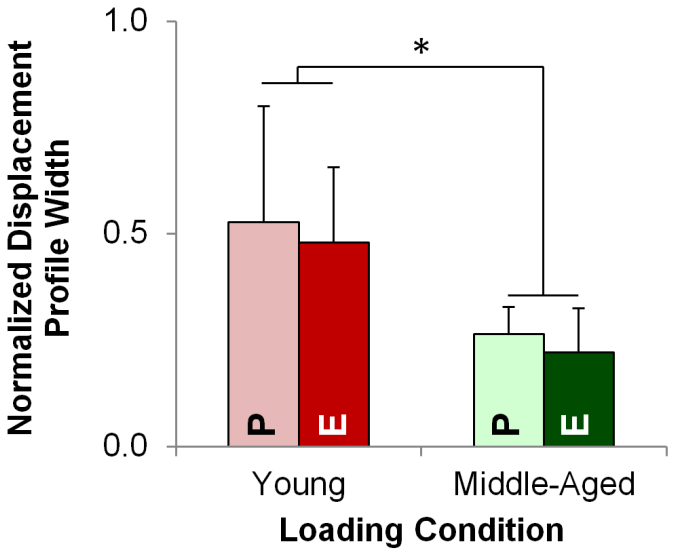

Figure 6.4 The difference between the average ROI displacement in passive and eccentric loading (- standard deviation) is plotted for young and middle-aged adults in the superficial (S), mid (M) and deep (D) regions. For both age groups, the average passive displacement was greater than the average eccentric displacement. The difference in distal displacement between the two loading conditions was significantly greater in middle-aged adults than young adults ($p = 0.03$), and significantly greater in in the mid and deep portions of the tendon than the superficial portion ($p = 0.000$), with no interaction between age group and tendon depth. *$p < 0.05$.

In all trials, we observed superficial tissue to undergo significantly less displacement than mid and deep tissue. This result is consistent with previous findings measured during passive (Arndt *et al.* 2012; Slane and Thelen 2014a) and eccentric (Slane and Thelen 2014a) loading conditions (Figure 6.1-2). The superficial-to-deep non-uniformity in displacements may reflect sliding between the tendon fascicles that comprise the Achilles tendon and arise separately from the soleus, medial gastrocnemius and lateral gastrocnemius muscles (Szaro *et al.* 2009), suggesting that different regions of the tendon may undergo different amounts of stretch.

Although significantly greater deep displacements than superficial displacements were observed in both populations, the relative magnitude of this non-uniformity was smaller in middle-aged adults. This observation is consistent with a recent *in vitro* study that showed

tendon fascicle sliding to be reduced with aging (Thorpe *et al.* 2013). It has been hypothesized that this reduction in fascicle sliding may result from an increase in collagen cross-linking with age (Couppe *et al.* 2009). These factors would be expected to contribute to an increase in relative tissue uniformity under both passive and eccentric loading conditions, as was observed here. In contrast, changes in muscle coordination patterns with age would be expected to produce an aging effect that presents only in active loading scenarios.

In both age groups, we observed larger tendon displacements under passive loading conditions compared with eccentric loading conditions, with a larger difference measured in middle-aged adults (Figure 6.3). This result is consistent with an age-related increase in tendon compliance. Previous *in vivo* studies have investigated alterations in tendon stiffness in young (typically aged 20-40), middle-aged (typically aged 41-60 years), and older adults (typically over 60 years), and have observed a significant increase in Achilles tendon compliance between young and middle-aged (Onambele *et al.* 2006), and young and older (Narici *et al.* 2005; Onambele *et al.* 2006; Stenroth *et al.* 2012) adults. A change in proximal tendon compliance (e.g. gastrocnemius aponeurosis) could also produce the results observed in this study. Prior studies have established that significant variations in tendon mechanical properties exist along the length of the tendon (DeWall *et al.* 2014; Finni *et al.* 2003; Magnusson *et al.* 2003). Thus, future studies investigatng the effects of aging on tendon deformations should consider regional variations both within the cross-section, as in this study, as well as along the tendon length.

For both age groups, larger differences between displacements in the two loading conditions were measured in the mid and deep portions of the tendon. These regions of the tendon likely comprise fascicles originating in the soleus muscle (Cummins *et al.* 1946; Szaro *et al.* 2009), suggesting that in the active loading condition the fascicles originating in the soleus muscle

stretch more than those originating in the gastrocnemius muscle. This differential stretch may reflect increased loading contribution of the soleus muscle during the eccentric loading condition, which could be evaluated by measuring the changes in relative displacements due to altering knee angle.

This study provides evidence that tendon undergoes complex deformation patterns that are affected by loading and change significantly with age. Middle-aged adults exhibited significantly less relative non-uniformity in displacements than young adults, with evidence of increased compliance in passive loading conditions. These results provide evidence of changes to tendon deformation patterns with age, that may be relevant to consider with respect to the increased injury incidence observed in middle-age.

.

Chapter 7: Spatial Variations in Shear Wave Speeds measured in the Achilles Tendons of Middle-Aged Adults[5]

7.1 Introduction

The incidence of gastrocnemius muscle strain and Achilles tendon injuries increases in middle-age. For example, a recent cross-sectional study (n = 2886) found that middle-aged runners (aged 40+ years) reported nearly twice as many Achilles tendon and plantarflexor muscle injuries than their younger (aged <40 years) counterparts (McKean *et al.* 2006). These soft tissue injuries can be challenging to treat and often have long-term consequences, with muscle strains linked with impaired performance and re-injury risk (Garrett 1990; Kannus *et al.* 1989; Orchard 2001). Thus, understanding the age-related changes to muscle-tendon tissue properties that may contribute to increased injury incidence is highly relevant clinically.

Prior studies have sought to understand the effects of aging on both the structure and tissue properties of the Achilles tendon. In comparative studies, aging has been shown to lead to specific changes in tendon, including decreased collagen fibril diameters (Nakagawa *et al.* 1994), decreased collagen crimp angle (Patterson-Kane *et al.* 1997; Tuite *et al.* 1997), and changes in collagen type III content (Birch *et al.* 1999), though effects may vary based on the tendon's primary function (Birch *et al.* 1999; Thorpe *et al.* 2012; Thorpe *et al.* 2013). It is generally believed that these effects lead to an increase in tendon compliance, which progress with age following maturation, resulting in altered tendinous tissue even as early as middle-age. Biomechanical studies on isolated tendon specimens have supported this supposition with a

[5] Slane LC, DeWall RJ, Martin JA, Lee KS, Thelen DG. Manuscript in preparation for submission to *Journal of Applied Physiology.*

variety of studies reporting an age-related decrease in the tendon elastic modulus following maturation (Blevins *et al.* 1994; Vogel 1980, 1983). However, *in vivo* studies have produced conflicting results, with some studies finding aging correlated with Achilles tendon compliance increasing (Narici *et al.* 2005; Onambele *et al.* 2006; Stenroth *et al.* 2012), decreasing (Kubo *et al.* 2007), or not changing (Karamanidis and Arampatzis 2005). This discrepancy could reflect limitations of prior methodological approaches. In the most common approach for measuring *in vivo* Achilles tendon stiffness, ultrasound images are collected while the subject performs a specific task, such as isometric plantarflexion. The motion of the muscle-tendon junction is then manually tracked and used to estimate tendon stretch over a large region that can include the Achilles free tendon, the soleus aponeurosis and, in some studies, the gastrocnemius aponeurosis (Child *et al.* 2010; Karamanidis and Arampatzis 2005; Kubo *et al.* 2003; Kubo *et al.* 2007; Rosager *et al.* 2002). Such landmark-tracking approaches may mask spatial variations in tendon deformations that can arise from variations in material properties and musculotendon architectural features (Arampatzis *et al.* 2005; DeWall *et al.* 2014; Finni *et al.* 2003; Maganaris and Paul 2000; Magnusson *et al.* 2001; Magnusson *et al.* 2003; Slane and Thelen 2014a). Thus, regional characterization of tendon tissue elasticity may be important for delineating age effects.

Supersonic Shear Imaging (SSI) or Shear Wave Elastography (SWE) is a quantitative ultrasound imaging technique for noninvasively inducing and tracking transient shear waves within tissues (Bercoff *et al.* 2004). SWE was first used in detecting pathological stiffness changes in a variety of soft tissues, including the breast (Athanasiou *et al.* 2010), liver (Bavu *et al.* 2011), and thyroid (Sebag *et al.* 2010), but has more recently been applied to characterize muscle and tendon (Arda *et al.* 2011; Aubry *et al.* 2013; Brum *et al.* 2014; Chen *et al.* 2013; DeWall *et al.* 2014; Hug *et al.* 2013). In transversely isotropic materials such as tendon, shear

wave speed is dependent on tissue shear elastic modulus (Brum *et al.* 2014). Prior studies on the Achilles tendon have shown that shear wave speed increases with passive stretch (Aubry *et al.* 2013; DeWall *et al.* 2014; Hug *et al.* 2013) and is diminished in previously ruptured tendons (Chen *et al.* 2013). A recent study involving 80 subjects from a wide range of ages (aged 20-83 years, mean: 45.4) found a significant decrease in Achilles free tendon shear wave speed with age when the ankle was in a plantarflexed posture, but no age effect when the ankle was in a dorsiflexed or resting posture (Aubry *et al.* 2013). However, a second study (aged 17-63 years, mean: 37.7) found that shear wave speeds in the free tendon in a relaxed (i.e. slightly plantarflexed) posture did not vary with age (Arda *et al.* 2011). Thus, it is important to consider ankle posture when assessing age-related changes in tendon shear wave speed.

We have recently used SWE to evaluate spatial variations in shear wave speed along the Achilles tendon length from the calcaneus to the gastrocnemius aponeurosis in young adults (DeWall *et al.* 2014). Tendon shear wave speeds consistently increased with passive stretch, reflecting the strain-stiffening behavior of the collagenous structures (Carlstedt 1987). We also observed significant variation in shear wave speed along the tendon length, with much lower speeds in the gastrocnemius aponeurosis than in the free tendon. This previous study indicates that even within individuals, shear wave speeds in the Achilles tendon vary significantly, and thus evaluating shear wave speeds from a single location may be insufficient for capturing age-related changes in shear wave speed.

The purpose of this study was to investigate spatial variations in shear wave speed in the relaxed and stretched Achilles tendons of middle-aged adults. We hypothesized that, relative to young adults, middle-aged adults would exhibit smaller stretch-induced increases in Achilles tendon shear wave speed, which would reflect a more compliant tendon. Further, we

hypothesized that aging would have the greatest effect on shear wave speed in the gastrocnemius aponeurosis, which is adjacent to the location where muscle strain injuries are often observed.

7.2 Materials and Methods

Ten healthy middle-aged adults (aged 49 ± 5 years, 5M, 5F), with no history of Achilles tendon injury, were recruited for this study. All subjects gave written consent to participate in this study as per the requirements of the University of Wisconsin-Madison institutional review board. Subjects completed a survey recording average weekly number of hours of participation in mild to strenuous exercise. Prior to testing, subjects walked for six minutes to precondition their muscle-tendon structures (Hawkins *et al.* 2009). Subjects were then positioned prone on an examination table, fully relaxed, with their knee extended and foot extended over the end of the table. The resting ankle angle of the right limb was measured with a plastic goniometer.

Ultrasound B-Mode and shear wave data were collected from the Achilles tendon using a 50 mm linear array transducer (L15-4, Aixplorer, Supersonic Imagine, Aix-en-Provence, France; software version: 5; preset: musculoskeletal; persist: high; smoothing: 7). The transducer was initially placed over the distal free tendon, with the inferior edge of the image approximately 10 mm distal to the superior edge of the calcaneus. Data were then collected sequentially in 10 mm increments along the Achilles tendon to the medial gastrocnemius aponeurosis, with the final region of interest (ROI) positioned, on average, 106 mm proximal to the muscle-tendon junction (Figure 7.1). The transducer was translated proximally every 50 mm, with external markers placed on the skin to mark transducer locations. A custom standoff pad (178 x 127 mm, 16 mm thick), remolded from a commercial pad (Aquaflex, Parker Laboratories, Fairfield, NJ), was used in the two most distal transducer positions. Data were collected from right limb in a random

order from the resting ankle angle (R; 27 ± 7 deg), a dorsiflexed angle (R - 15 deg) and a plantarflexed angle (R + 15 deg).

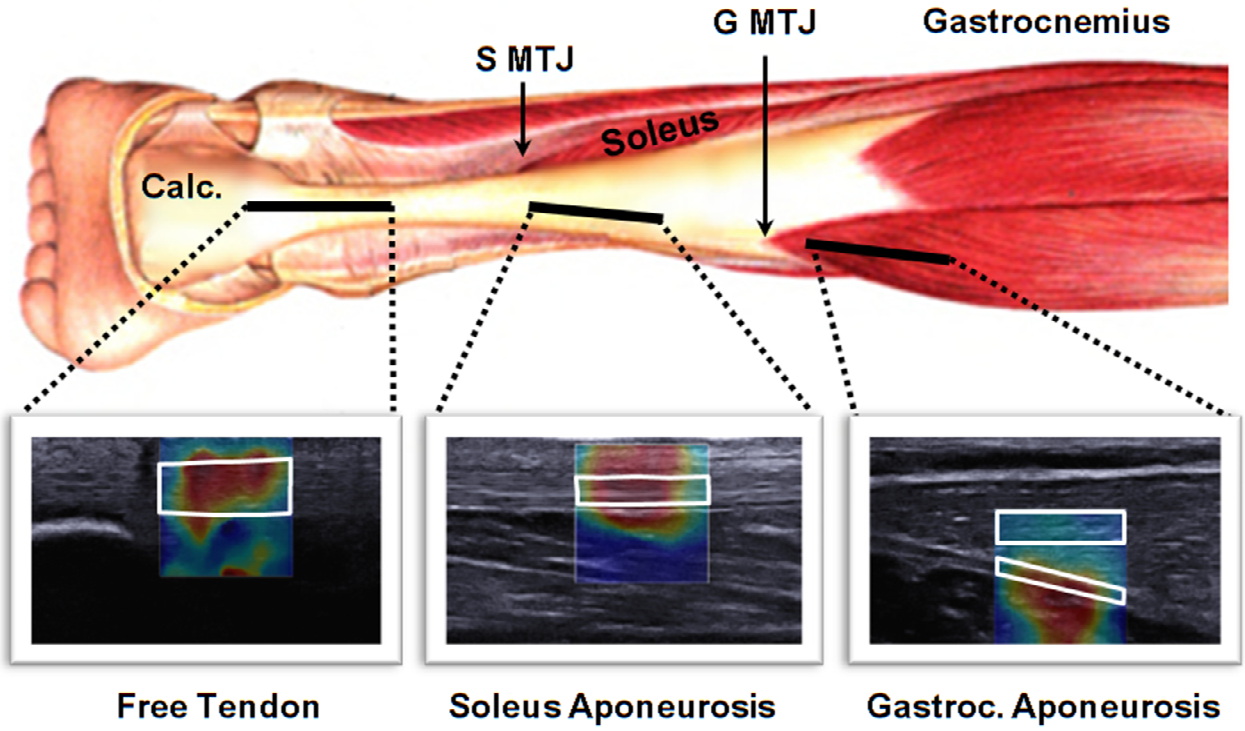

Figure 7.1 Ultrasound images and shear wave speed data were collected along the length of the Achilles tendon to the medial gastrocnemius aponeurosis. Distal images from the free tendon were collected with the calcaneus (Calc.) in view. The soleus aponeurosis was defined as the region from the soleus muscle-tendon junction (S MTJ) to the gastrocnemius muscle-tendon junction (G MTJ). The transducer was angled to enable collections along the tendon toward the medial G MTJ and into the gastrocnemius aponeurosis. Regions of interest (example outlined in white) were defined within the tendon boundaries. In the portion of the tendon proximal to the G MTJ, regions of interest were also defined from within the muscle tissue to enable comparison with gastrocnemius muscle shear wave speeds.

Shear wave speed data were evaluated post-hoc in a custom Matlab (Mathworks, Inc., Natick, MA) graphical user interface from DICOM images exported from the system. A single researcher manually defined regions of interest (ROIs) within the tendon boundaries visible in the B-mode images. In proximal regions of the leg, ROIs were also defined within the

gastrocnemius muscle. From these ROIs, shear wave speeds were obtained. Although some commercial systems enable the display of results in terms of Young's Modulus, we chose to report shear wave speed, as the assumption of isotropy necessary for the Young's Modulus computation is not valid in tendon (Kuo *et al.* 2001; Royer *et al.* 2011).

For each image set, the soleus muscle-tendon junction (S MTJ) and medial gastrocnemius muscle-tendon junction (G MTJ) were identified. The superior edge of the calcaneus (C) was defined as the most distal point for image analysis. To enable inter-subject comparisons, data were then interpolated into three regions: the free tendon (FT; from C to S MTJ), the soleus aponeurosis (SA; S MTJ to G MTJ) and the gastrocnemius aponeurosis (GA; G MTJ to end of collections). Data from the gastrocnemius muscle (GM) were also interpolated from the same regions as the data from the gastrocnemius aponeurosis. Tendon thickness was then measured by manually delineating the tendon boundaries in the region near the calcaneus. The maximum shear wave speed capacity of the machine is 16.3 m/s, a value which has been observed previously in loaded tendon (Aubry *et al.* 2013; DeWall *et al.* 2014). Thus, we also computed the percentage of pixels within each ROI that exhibited shear wave speed magnitudes equal to 16.3 m/s to evaluate potential saturation effects.

A two-way ANOVA was used to evaluate the effects of ankle posture (D, R, P) and region (FT, SA, GA, GM) on shear wave speed in middle-aged adults, with post-hoc Tukey comparisons used as follow-up ($p < 0.05$). To evaluate age-related differences, shear wave speed data were compared with measures from a healthy young adult population (aged 27 ± 4 years, 5M, 5F) who were tested similarly (DeWall *et al.* 2014). Linear regressions were used to evaluate age-related differences in shear wave speed within each region (FT, SA, GA, GM) for each posture (dorsiflexed, resting, plantarflexed) with significance set to $p < 0.0125$.

7.3 Results

Shear wave speed in the Achilles tendon varied significantly with imaging location (Figure 7.2), with greater speeds measured in the free tendon and lower speeds measured in the gastrocnemius aponeurosis (Figure 7.3). For example, in the resting posture, shear wave speed in the free tendon (12.3 ± 1.1 m/s) was significantly higher ($p < 0.001$) than the soleus aponeurosis (10.2 ± 1.3 m/s), the gastrocnemius aponeurosis (3.9 ± 0.6 m/s), and gastrocnemius muscle (2.8 ± 0.5 m/s).

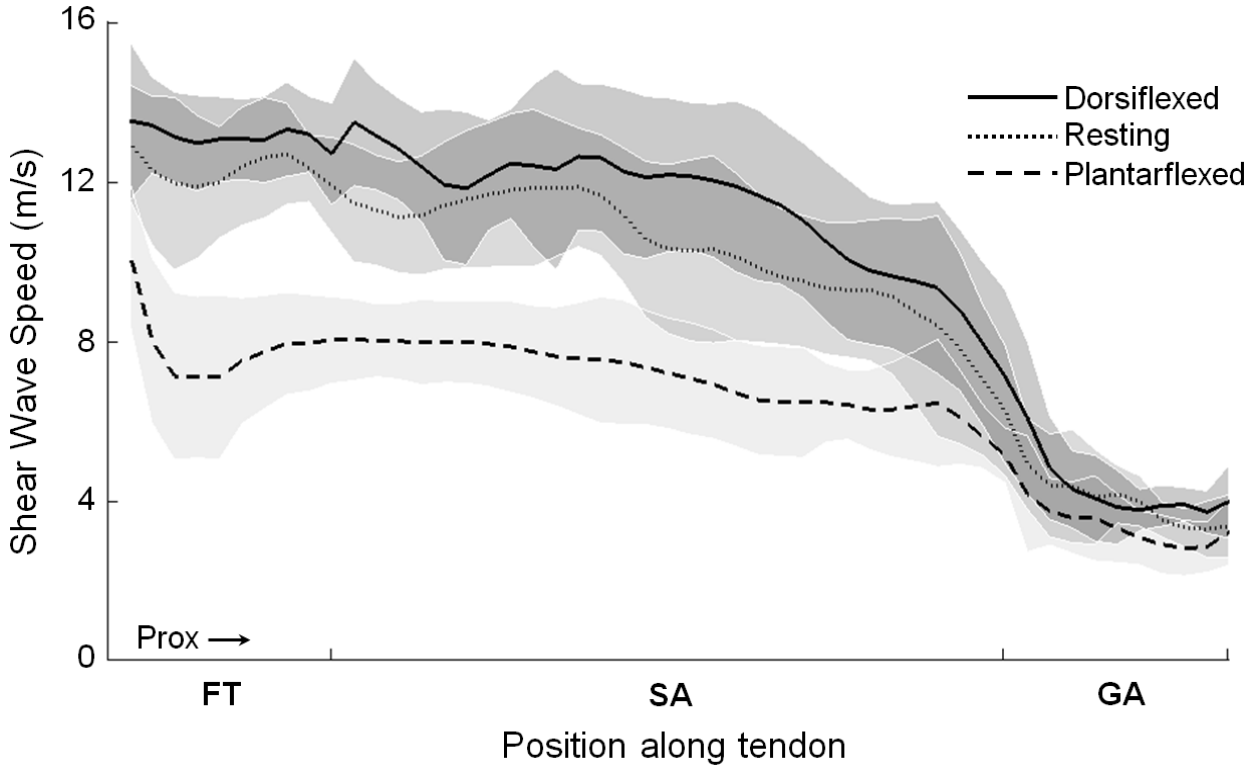

Figure 7.2 The average shear wave speed for ten middle-aged adults, is plotted along the length of the tendon for three ankle postures. Shear wave speed decreased proximally, with the highest shear wave speeds observed in the distal free tendon (FT), and the lowest in the proximal gastrocnemius aponeurosis (GA). Shear wave speed increased progressively from the plantarflexed posture to the resting and dorsiflexed postures. Data saturation in the free tendon was substantial in the resting (12% of data) and dorsiflexed (16%) postures.

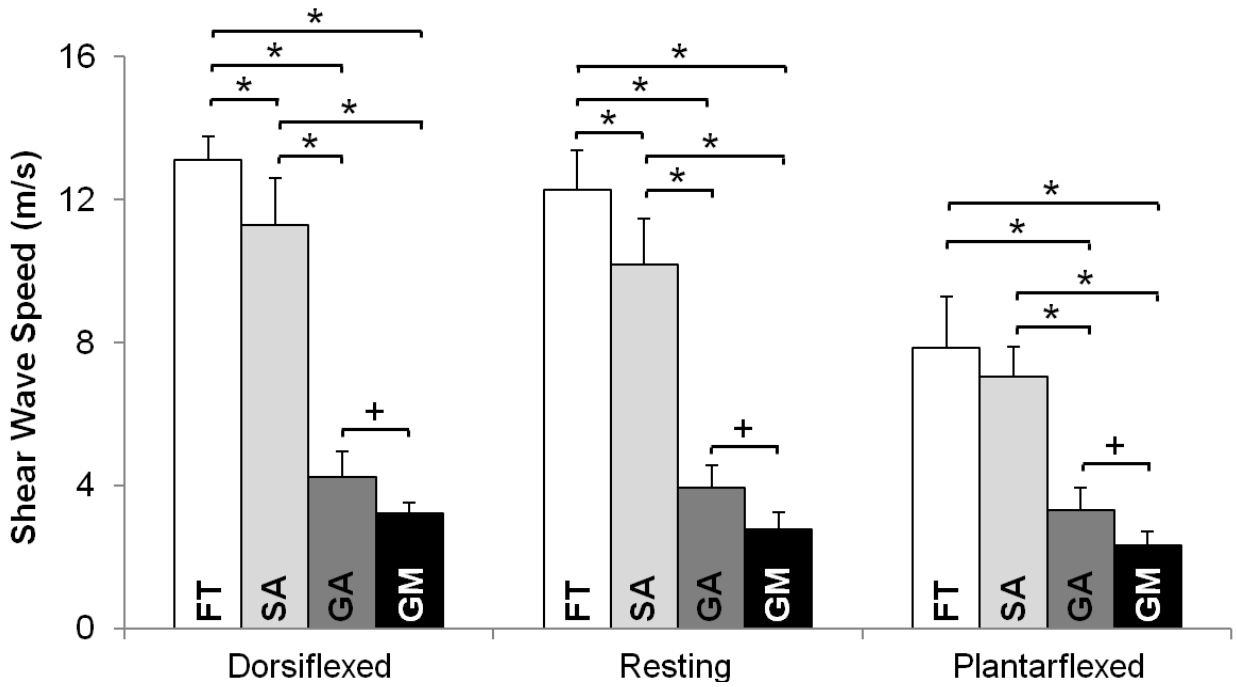

Figure 7.3 The average (+ standard deviation) shear wave speeds from ten middle-aged subjects for each ankle posture and each region: the Achilles free tendon (FT), soleus aponeurosis (SA), gastrocnemius aponeurosis (GA) and the gastrocnemius muscle (GM). Shear wave speed increased with dorsiflexion in all regions. *$p < 0.001$, $^{+}p < 0.05$.

Ankle posture had a significant effect on shear wave speed in all three regions of the tendon, with speed progressively increasing from a plantarflexed to resting posture, and from a resting to dorsiflexed posture. In the gastrocnemius muscle, there was a significant increase in shear wave speed between the dorsiflexed and plantarflexed postures. Portions of the Achilles free tendon reached the maximum shear wave speed of 16.3 m/s in both resting (12% saturation) and dorsiflexed (16%) postures.

There were no significant differences between middle-aged and young adult subjects in terms of height, tendon thickness, average weekly hours of exercise, or resting ankle angle (Table 7.1). Compared to the young subjects, middle-aged subjects exhibited no significant differences in shear wave speed in the free tendon, soleus aponeurosis or gastrocnemius muscle. When regressed against absolute age, there was a significant inverse relationship between resting

gastrocnemius aponeurosis shear wave speed and age (R^2 = 0.34, p = 0.007). A similar relationship was observed in the gastrocnemius aponeurosis in the dorsiflexed posture (R^2 = 0.55, p = 0.0002), but not the plantarflexed posture (p = 0.79; Figure 7.4).

Table 7.1 Comparison of subject populations**.** No significant differences between groups were observed. Resting ankle angle is defined in degrees of plantarflexion.

	Young adults	**Middle-aged adults**
Age:	27 ± 4 years	49 ± 4 years
Gender:	5 M, 5 F	5 M, 5 F
Height:	68 ± 3 inches	70 ± 5 inches
Tendon thickness:	4.4 ± 0.6 mm	4.7 ± 0.9 mm
Weekly exercise:	9.5 ± 5.4 hours	9.6 ± 4.7 hours
Resting ankle angle:	26 ± 5 deg.	25 ± 6 deg.

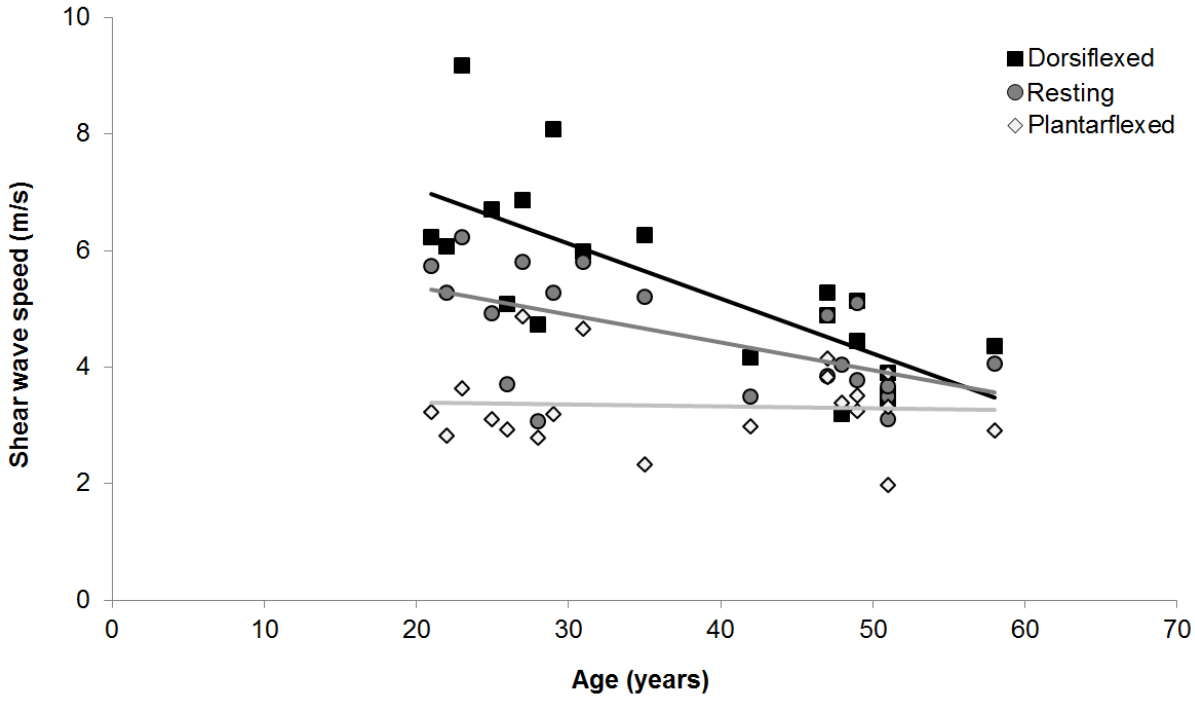

Figure 7.4 Shear wave speed in the gastrocnemius aponeurosis decreased with age in the resting (R^2 = 0.34, p = 0.007) and dorsiflexed posture (R^2 = 0.55, p = 0.0002), but not in the plantarflexed posture (p = 0.79).

7.4 Discussion

In this study, we compared spatial variations in Achilles tendon shear wave speed between young and middle-aged adults. We had hypothesized that middle-aged adults would exhibit lower shear wave speeds, reflecting more compliant tendinous tissue. However, this hypothesis was only supported for the gastrocnemius aponeurosis, with middle-aged adults exhibiting much smaller increases in aponeurosis shear wave speed in response to passive stretch. In contrast, the Achilles free tendon did not exhibit any significant age-related differences in shear wave speed. Thus, our results suggest that spatial variations in tendon tissue elasticity may be altered in middle-aged adults, which could affect localized tissue strain patterns.

Shear wave speeds were highly dependent on posture and imaging location along the tendon. For all imaging locations, shear wave speeds were lowest in a plantarflexed posture, in which the tendon is relatively slack and unloaded. Changing to a resting and then dorsiflexed posture progressively engages and stretches the tendon, resulting in a strain-stiffening effect (Carlstedt 1987) and hence an increase in shear wave speed. Similar postural effects have been observed previously (Aubry *et al.* 2013; DeWall *et al.* 2014; Hug *et al.* 2013), and are highly relevant when considering ways of standardizing SWE imaging for clinical use. Spatially, we observed significantly lower shear wave speeds in the proximal portions of the Achilles tendon (i.e. the gastrocnemius aponeurosis) than in the distal tendon (i.e. the free tendon). This result is consistent with prior *in vitro* (Lieber *et al.* 1991) and *in vivo* studies (Maganaris and Paul 2000) that have observed the aponeurosis to be more compliant than tendon.

Age-related changes in tendon shear wave speed were observed to be location dependent. We had hypothesized that middle-aged adults would exhibit a decrease in tendon compliance based on known structural changes with age (Birch *et al.* 1999; Nakagawa *et al.* 1994; Patterson-Kane

et al. 1997; Tuite *et al.* 1997), though prior biomechanical studies examining age-related changes in tendon stiffness have reported inconsistent results (Karamanidis and Arampatzis 2005; Kubo *et al.* 2007; Narici *et al.* 2005; Onambele *et al.* 2006; Stenroth *et al.* 2012). Interestingly, we did not see a change in the free tendon or soleus aponeurosis shear wave speed between age groups. To our knowledge, there are no prior studies that have specifically evaluated age-related changes in shear wave speed in the soleus or gastrocnemius aponeuroses, and two that have considered the Achilles free tendon. Similar to the results of this study, Arda *et al.* (2011) found no relationship between age and resting Achilles free tendon shear wave speed from a large sample (n = 127, aged 17-63 years, mean: 37.7). In contrast, Aubry *et al.* (2013) did measure an age-related decrease in free tendon shear wave speed (n = 80, aged 20-83 years, mean: 45.4), but only when the ankle was in plantarflexed postures. Methodologically, these two prior studies differ substantially from what described here, in that both evaluated shear wave speed from a single location within the Achilles tendon, rather than along the length of the free tendon. The second study also included an older population with a much larger age range than in our study (n = 20, aged 21-58 years, mean: 38.0). We also did not observe any age-related changes in shear wave speed in the gastrocnemius muscle. Although aging is linked with a variety of changes in skeletal muscle strength (Doherty 2001, 2003; Morse *et al.* 2005) and tissue properties (Kent-Braun *et al.* 2000; Morse *et al.* 2005; Porter *et al.* 1995; Sipila and Suominen 1991), these effects may be less pronounced in middle-aged (Beenakker *et al.* 2010; Doherty *et al.* 1993) and highly active populations (Kent-Braun *et al.* 2000; Sipila and Suominen 1991), like the subjects in this study. Thus, it is clear that future studies including older adult populations (aged 61+) are warranted to elucidate the relationship between aging and Achilles tendon shear wave speeds.

Gastrocnemius aponeurosis shear wave speeds in resting and dorsiflexed postures were significantly reduced in middle-aged adults (Figure 7.4). These results suggest the apparent strain-stiffening behavior of the gastrocnemius aponeurosis is fundamentally altered with aging. It is particularly intriguing that we observed this change in shear wave speed in the gastrocnemius aponeurosis without a concomitant change in the muscle tissue. As a result, differences in shear wave speed between muscle and tendon tissues were reduced in middle-aged adults. The apparent compliance of the gastrocnemius aponeurosis depends on a number of factors including aponeurosis material properties, muscle tissue composition and length, as well as muscle load transmission onto the aponeurosis (Abellaneda *et al.* 2009; Azizi *et al.* 2009; Azizi and Roberts 2009; Ettema and Huijing 1989; Scott and Loeb 1995). It has previously been shown through both experiments (Finni *et al.* 2003) and models (Epstein *et al.* 2006) that these factors can give rise to complex aponeurosis deformations, making it challenging to identify the specific underlying factors that gave rise to the observations in this study. However, the observed changes in tendon compliance with aging may be relevant to consider in the context of muscle strain injuries. Muscle strain injuries occur commonly in the gastrocnemius muscle (Garrett 1990; Orchard 2001; Speer *et al.* 1993), arise more frequently in middle-age (McKean *et al.* 2006) and have been observed to originate in the muscular tissue nearest the muscle-tendon junction (Garrett 1990; Kirkendall and Garrett 2002; Speer *et al.* 1993). In this study, we observed the age-related change in shear wave speed to occur in the portion of the tendon near where gastrocnemius muscle injuries are most often observed. Thus, it is possible that disruptions in localized tendon compliance affect nearby muscle tissue strain concentrations, giving rise to a potential for localized tissue strain injury. Given the complexity of the muscle-

tendon architecture and mechanics, further investigation is clearly needed to clarify muscle-tendon interactions and their effects on injury potential.

Data saturation was a limitation of this study. We measured significant saturation in the free tendon, with 16% and 12% of data saturating in dorsiflexed and resting postures. These saturation values were somewhat higher than what we observed in our young adult population (DeWall *et al.* 2014), which could potentially mask age-related changes in shear wave speed in the free tendon. These results further emphasize the importance of considering data saturation when using SWE to evaluate tendon shear wave speeds.

In summary, we observed spatial variations in Achilles tendon shear wave speed, with aging effects that were location dependent. Shear wave speeds decrease proximally, with the gastrocnemius aponeurosis of middle-aged adults exhibiting much smaller increases in shear wave speed in response to passive stretch than young adults. We did not observe any effects of aging on the free tendon or soleus aponeurosis. Our results suggest that spatial variations in tendon elasticity near the muscle-tendon junction may be altered in middle-aged adults, which may have implications for localized tissue strain patterns and injury.

Chapter 8: Length and Activation dependent Variations in Muscle Shear Wave Speed[6]

8.1 Introduction

Muscle mechanical properties are closely linked with neuromuscular health and disease. Abnormal muscle stiffness, for example, has been shown to be indicative of a variety of disease states including spasticity (Barrett, 2011), Duchenne muscular dystrophy (Cornu *et al*, 2001; Cornu *et al*, 1997) and hyperthyroidism (Bensamoun *et al*, 2007). However, it remains challenging to quantitatively assess *in vivo* muscle stiffness. Magnetic resonance (MR) elastography can be used to evaluate muscle stiffness from induced wave patterns, but is limited by the high imaging costs and availability of MR scanners. Ultrasonic shear wave elastography (SWE) is a new alternative approach for assessing spatial variations in tissue stiffness based on shear wave propagation speeds. Ultrasound SWE uses acoustic radiation force to induce transient shear waves within soft tissues, with wave speed then tracked using ultra-high frame rate ultrasonic imaging (Bercoff *et al*, 2004). Shear wave speed is related to the shear modulus of elasticity of the tissue and hence is considered to be a non-invasive, quantitative metric of tissue stiffness (D'Onofrio *et al*, 2010). Furthermore, ultrasonic motion tracking is sufficiently fast that it can be implemented on the scanner to provide real-time quantitative metrics of tissue stiffness.

[6] Chernak LA, DeWall RJ, Lee KS, Thelen DG (2013). *Physiological Measurement* 34: 713-721.

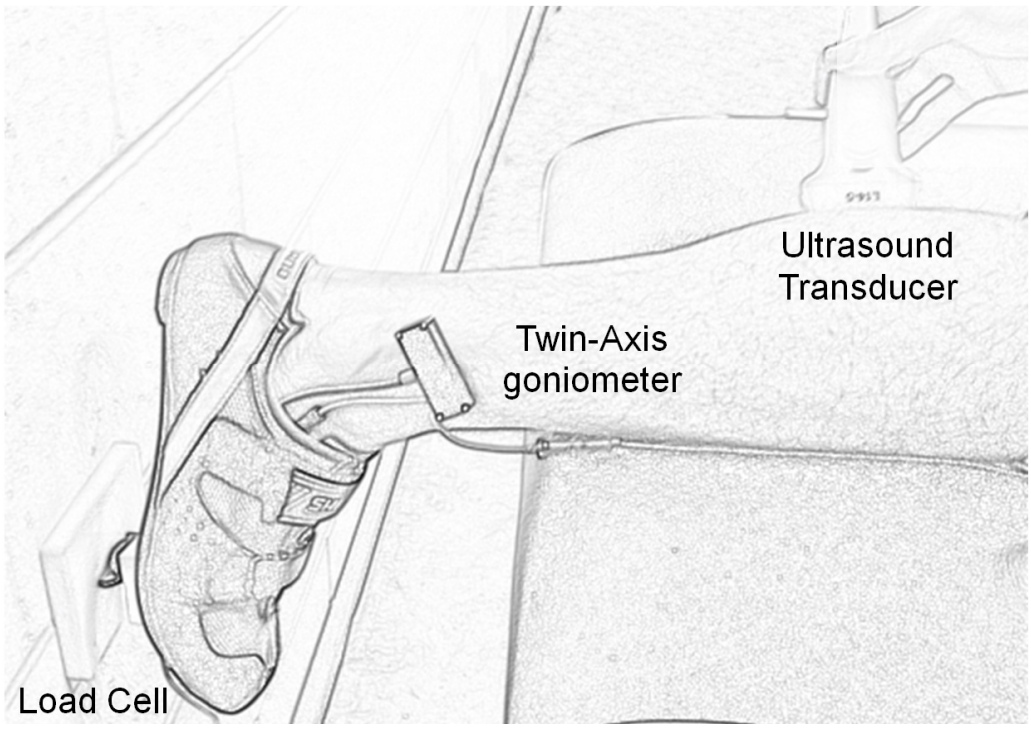

Figure 8.1 Experimental setup. Ultrasonic data were collected from the medial gastrocnemius muscle belly. Load information was collected from a load cell attached via a cycling shoe, and angle data were collected from a twin-axis electronic goniometer attached at the ankle joint. During active trials, the subject was instructed to push against the wall directly behind the foot as shown in the image. During passive trials, the foot was manually moved by a researcher to specific sagittal ankle angles.

Although SWE has proven successful in detecting pathological changes in stiffness in a variety of soft tissues (Sebag *et al*, 2010; Bavu *et al*, 2011; Athanasiou *et al*, 2010), its application to skeletal muscle tissue is complicated by the fibrous structure of muscle, and the capacity for muscle tissue stiffness to vary with muscle length and activation level. An early study by Levinson *et al* (1995) established the use of ultrasound in measuring wave propagation induced by external vibrators through skeletal muscle and demonstrated that wave speed increased with applied load. Gennisson *et al* then applied this methodology to measure the anisotropic shear moduli of muscle in both *in vitro* and *in vivo* test cases (Gennisson *et al*, 2003). More recent studies have provided further evidence of the capability of shear wave elastography

to characterize skeletal muscle properties. Most notably, prior studies have shown that muscle shear wave speed increases proportionally with muscle activity (Nordez and Hug, 2010; Gennisson *et al*, 2005; Gennisson *et al*, 2010), the anisotropy of muscle tissue can be characterized with SWE (Lee *et al*, 2012; Gennisson *et al*, 2010), and that ultrafast ultrasound imaging can be used to characterize muscle contractions, both in terms of transient properties (e.g. contraction time) as well as two and three dimensional spatial maps of contraction propagation (Deffieux *et al*, 2008; Deffieux *et al*, 2006). In 2010, Shinohara *et al* demonstrated that *in vivo* shear wave speeds can be modulated by altering gross body positioning, which changes muscle length, and a few recent publications have demonstrated SWE to be capable of capturing the inherent strain-stiffening behavior of passive muscle, by showing that shear wave speed increases in stretched muscle (Maisetti *et al*, 2012; Nordez *et al*, 2008; Gennisson *et al*, 2010).

Since muscle stiffness is known to increase monotonically with load (Durfee and Palmer, 1994), these previous observations suggest that SWE could potentially provide a tool by which to track functional variations in muscle force. Physiologically, net muscle force is generated from both muscle activation and intrinsic passive factors, such as the stretch of connective tissues within and surrounding the muscle. Thus, it is important to assess if shear wave speed responds similarly to force generated via active and passive processes. In the current study, we investigated the relative effect on shear wave speed of load induced via voluntary activation and postural manipulation. We hypothesized that shear wave speed would increase due to both muscle activation and passive stretch, and that in both cases the increase in shear wave speed would be proportional to the net load induced about the musculoskeletal joint.

8.2 Methods

Institutional Review Board approval and informed consent were obtained. Ten healthy young adults were recruited for this study (Table 8.1). Subjects were asked to walk at a comfortable pace for six minutes to pre-condition the muscle-tendon unit (Hawkins *et al*, 2009). All testing was then performed with the subject lying prone on an examination table. A twin-axis electronic goniometer (SG110/A, Biometrics Ltd, Newport, UK) was attached across the ankle to monitor sagittal ankle angle throughout testing. A load cell (LLB400, Futek Advanced Sensor Technology, Irvine, CA) was attached under the forefoot of a rigid-soled cycling shoe to measure the foot force (Figure 8.1).

Table 8.1 Subject information. Please note that positive angles denote plantarflexion.

			MVC	Range of Motion (deg)			
			Knee	Knee Extended		Knee Flexed	
Subject	Age	M/F		Max.	Max.	Max.	Max.
1	22	F	34	-8°	42°	-29°	47°
2	21	M	37	-12°	39°	-23°	41°
3	24	M	47	-12°	39°	-33°	28°
4	21	F	54	-8°	42°	-23°	31°
5	22	M	41	-11°	32°	-20°	29°
6	26	F	41	-23°	32°	-28°	30°
7	21	M	59	-12°	30°	-24°	29°
8	38	M	40	-7°	45°	-6°	50°
9	31	M	52	-14°	40°	-24°	38°
10	26	M	44	-15°	29°	-24°	38°

Imaging was performed using a linear array ultrasound transducer (L15-4, Supersonic Imagine, Aix-en-Provence, France) placed over the medial gastrocnemius muscle belly of the right limb. The transducer was centered 5 cm proximal to the distal muscle-tendon junction of the gastrocnemius. Care was taken during collections to move the probe such that data were collected from a similar location within the muscle belly for all collections. Ultrasonic B-Mode

images and shear wave data were collected using an Aixplorer clinical scanner (Supersonic Imagine, Aix-en-Provence, France), with software version 5. The musculoskeletal preset was used for collections with the persist and smoothing parameters set to high and 7 respectively.

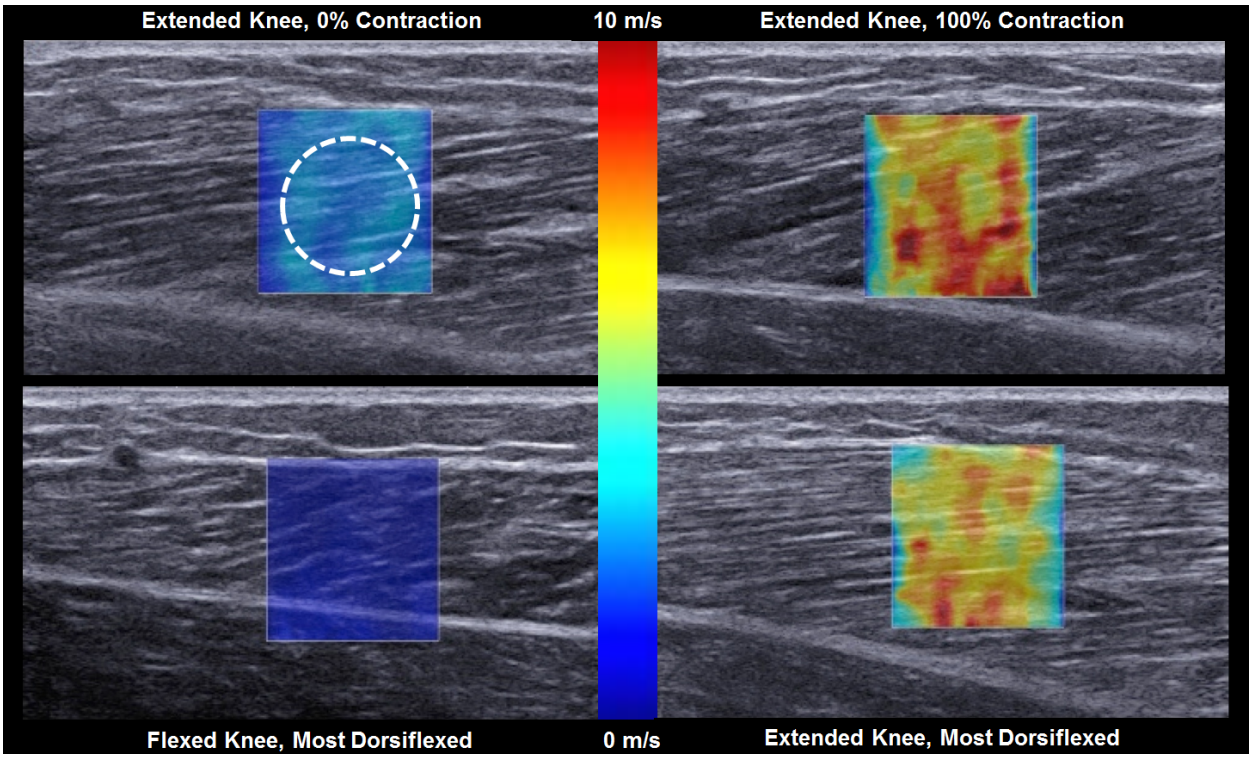

Figure 8.2 Data were collected in the medial gastrocnemius muscle belly. An increase in shear wave speed can be seen clearly when the subject is asked to apply a high load. When the ankle is dorsiflexed, the shear wave speed is noticeably higher in the extended knee posture. The data from subject 6 are shown. The image in the top left shows an example region of interest defined within the gastrocnemius muscle belly.

Ultrasound and shear wave data were collected while the ankle was statically held at ankle angles ranging from maximum dorsiflexion to maximum plantarflexion. The range of motion of each subject was established by passively moving the subjects' ankle through its range of motion first with the subjects' knee extended (0 deg knee flexion) and then with the knee flexed (90 deg). The flexed knee posture shortens the gastrocnemius considerably, such that the net force under the foot is primarily due to stretch of the soleus under that condition. Passive load data

were measured when the ankle was moved through its range of motion so that the passive moment could be compared to the moments generated from the maximum voluntary contraction of each subject. Shear wave images were collected with the subjects' ankle held in place by a researcher at set ankle angles ranging from maximum dorsiflexion to maximum plantarflexion, with 15 deg increments between postures. Specific angles (0 deg, 15 deg, 30 deg) were collected from all subjects, with -15 deg and 45 deg added if these fell within the subjects' range of motion. Data were collected in a random order with three trials of five images collected for each posture, leading to between 33 and 42 passive trials for each subject. For the flexed knee trials, subjects were instructed to leave their lower limb resting on the mat and to support themselves by bending at the knees and the waist.

Gastrocnemius shear wave speed, foot force and ankle angle data were also collected from a series of trials in which subjects were asked to actively generate ankle plantarflexor contractions. We first measured each subject's maximum voluntary contraction (MVC) by asking them to push as hard as they could against the wall located directly behind them. Subjects were then asked to sustain fixed contractions at six levels of effort (12.5%, 25%, 37.5%, 50%, 75%, and 100% of MVC) by again pushing against a fixed support. Ultrasound data were simultaneously collected from the medial gastrocnemius muscle belly, with three trials of five images for each activation level in a random order, for 18 total active trials per subject.

For each trial, shear wave speeds were averaged within a circular (~10mm diameter) region of interest (ROI) that was manually defined to lie within the medial gastrocnemius muscle belly (Figure 8.2). The ROI was defined using a plug-in for the DICOM reader OsiriX (OsiriX Foundation, Geneva, Switzerland). This process was independently repeated by a second rater, and intraclass correlation coefficient (ICC(2,1)) was used to assess inter-rater repeatability. We

separately determined the average foot force and ankle angle for each trial using custom MATLAB (Mathworks, Natick, MA) routines. Foot force data were multiplied by the perpendicular distance between the load cell and ankle joint center to ascertain the net internal ankle plantarflexion moment. Joint moments (M) were normalized to the moment achieved during the MVC (M_{MVC}) for each subject. Repeated measures analysis of variation (ANOVA) was used to evaluate the influence of activation level and posture on shear wave speeds. Any significant effects were followed up with post-hoc Tukey comparisons and a significance level of $p<0.05$ was used for all tests. All results are reported mean (standard deviation) across subjects unless otherwise noted.

8.3 Results

The relaxed gastrocnemius exhibited an average shear wave speed of 2.1 (0.3) m/s, as was observed with the knee flexed and the ankle in the most plantarflexed posture. Passive dorsiflexion of the ankle in a flexed knee posture did not induce a significant change in shear wave speed. However, passive dorsiflexion of the ankle with an extended knee resulted in the gastrocnemius muscle shear wave speed significantly increasing to 5.6 (1.5) m/s in the most dorsiflexed posture (Figure 8.3). For individual subjects, shear wave speeds were linearly correlated with the passive net ankle moment, with correlation coefficients averaging 0.8 (0.2).

During active contractions, shear wave speed monotonically varied with the normalized ankle moment generated (M/M_{MVC}), increasing from 3.6 (0.6) m/s in the 0% effort condition to 8.3 (1.0) m/s in the maximally contracted condition (Figure 5.4). The linear correlation between shear wave speed and active ankle moment averaged 0.9 (0.1) across the subjects tested.

However, the slope of this relationship was significantly ($p = 0.002$) lower in the active case (15.6 (m/s) / M/M_{MVC}) than in the passive case (5.1 (m/s)/$M/M_{MVC;}$ Table 5.2) .

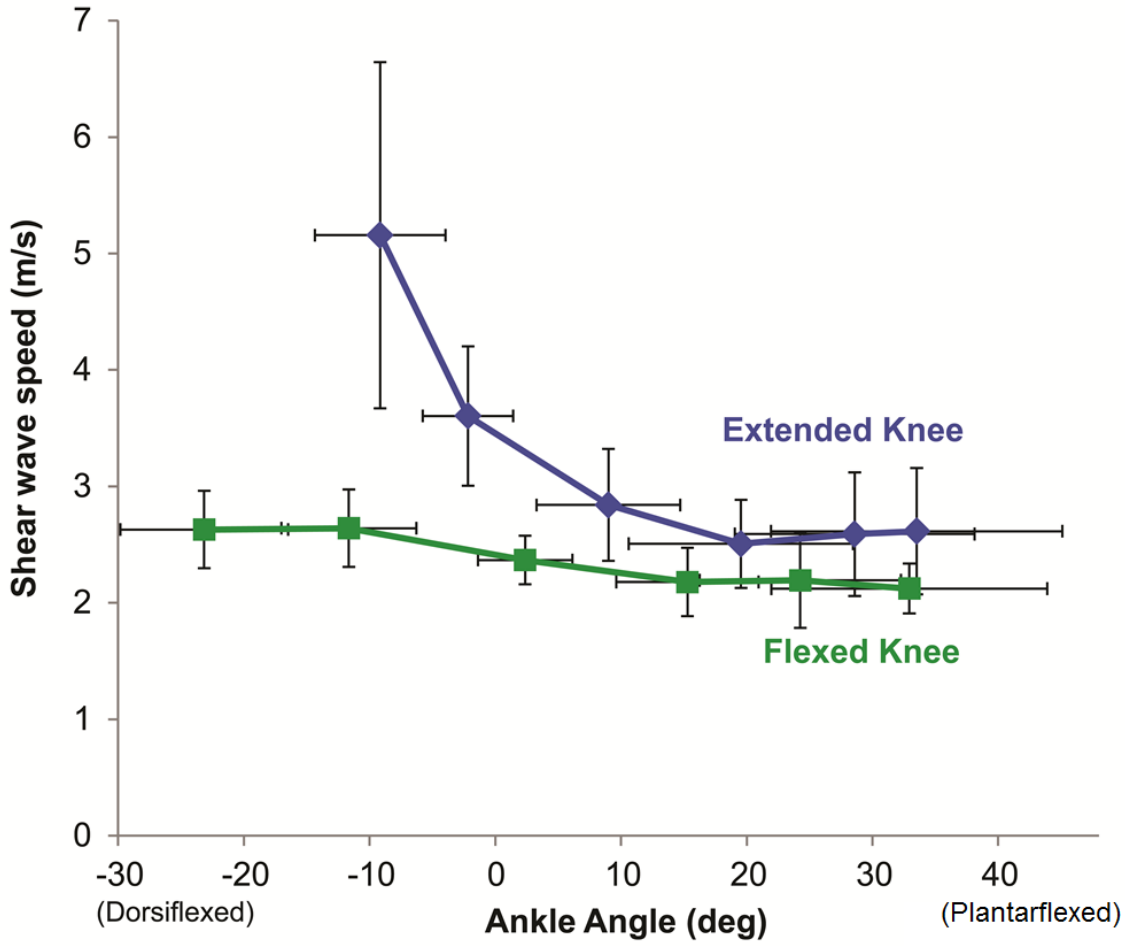

Figure 8.3 Passive ankle dorsiflexion induced a significant increase in shear wave speed when the knee was extended, but had little effect on shear wave speed when the knee was flexed. *$p<0.05$ in post-hoc comparisons.

Inter-rater repeatability for the shear speed measures obtained from the images was high, with the intraclass correlation coefficient (class 2) mean value of 0.999.

8.4 Discussion

The objective of this study was to determine if shear wave speed would track variations in ankle plantarflexor loads induced by either passive muscle stretch or active muscle contraction. We found that shear wave speed does correlate with variations in the net mechanical loading, but the nature of that relationship varies depending on whether the muscle force was actively or passively generated.

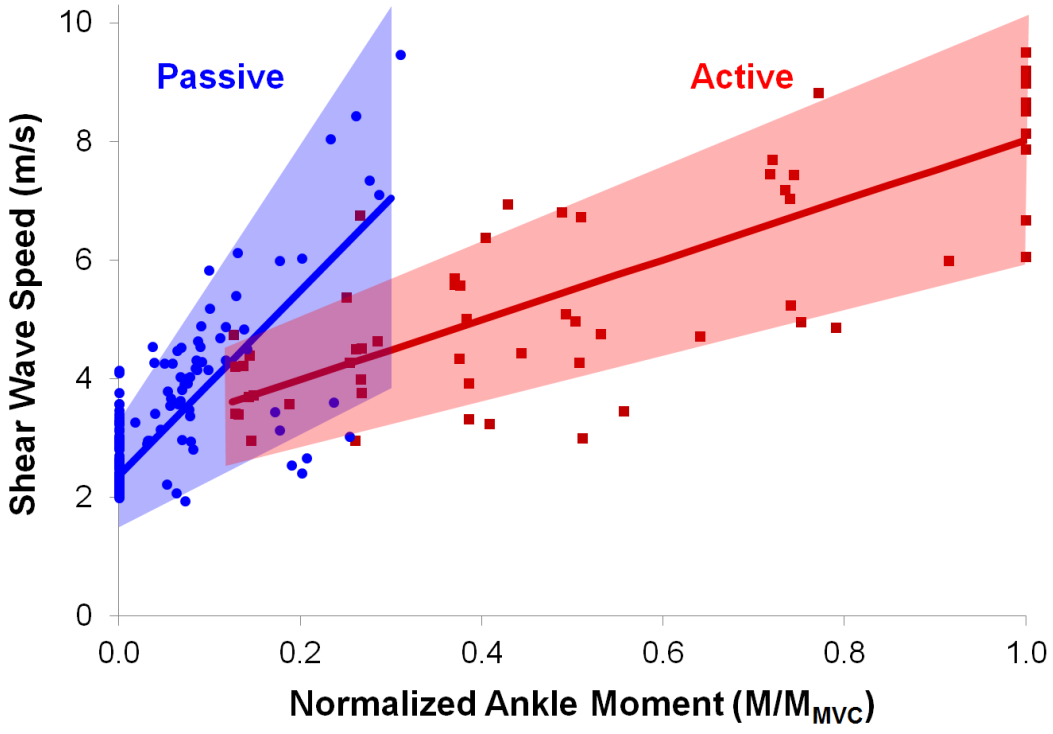

Figure 8.4 Shear wave speed was highly correlated to normalized ankle moment induced via passive stretch (extended knee) or active contraction. However, the slope of the best linear fit was significantly greater in the passive loading condition. The average (± 1 deviation) of trend lines across subjects is plotted, as well as data points from all trials.

Our passive experiments were designed to delineate the contribution of the gastrocnemius to the ankle joint moment generated. To achieve this aim, we stretched the plantarflexors with the knee in flexed and extended postures. The gastrocnemius is shortened in the flexed case such that the ankle moment primarily reflects passive loading of the soleus (Sale *et al*, 1982). As expected

in this case, we found that the gastrocnemius shear wave speeds did not significantly increase with dorsiflexion. However, in the extended knee posture, the gastrocnemius is more taut, such that dorsiflexion further stretches the muscle and induces a passive ankle moment at smaller dorsiflexion angles (Maisetti *et al*, 2012). Correspondingly, we observed an exponential increase in shear wave speed with ankle dorsiflexion in the extended knee condition (Akagi *et al*, 2012), which is consistent with prior results that have been reported (Shinohara *et al*, 2010; Akagi *et al*, 2012). Length dependent changes in passive muscle force are believed to arise from the stretch of titin (Horowits *et al*, 1986) and connective tissues within the muscle (Gajdosik, 2001). Hence, it was expected that passive stiffness would increase with muscle length, and would give rise to a monotonic increase in shear wave speed with force at stretched lengths.

Table 8.2 Active and passive trend lines for shear wave speed to normalized ankle moment for all subjects.

Active				**Passive**			
Subject	Slope	Intercept	R^2	Subject	Slope	Intercept	R^2
1	4.78	2.64	0.72	1	14.30	3.12	0.87
2	6.70	2.20	0.97	2	14.95	2.91	0.76
3	6.87	2.94	0.88	3	17.64	0.24	0.67
4	5.73	3.38	0.97	4	24.11	2.15	0.96
5	4.46	2.15	0.66	5	5.73	2.32	0.90
6	4.04	4.38	0.97	6	23.28	2.23	0.99
7	4.77	4.26	0.83	7	25.76	2.37	0.96
8	5.98	2.62	0.97	8	11.00	3.30	0.46
9	4.12	1.96	0.77	9	17.34	2.79	0.86
10	3.04	3.22	0.98	10	1.99	2.19	0.43
AVG	5.05	2.98	0.87	**AVG**	15.61	2.36	0.79
ST DEV	1.24	0.84	0.12	**ST DEV**	7.80	0.85	0.20

We also show that muscle shear wave speed can be modulated via active muscle contraction, which would represent a neurally modulated muscle stiffening effect. Prior biomechanical studies have found a linear relationship between net ankle stiffness and the moment generated by muscles about the joint (Agarwal and Gottlieb, 1977; Ochala *et al*, 2004; Sinkjaer *et al*, 1988). This muscle stiffening presumably arises from the increased number of activated cross-bridges (Ford *et al*, 1981). This effect is consistent with prior studies that showed that muscle shear wave speed is linearly related to muscle activation level, as assessed using surface electromyography (Nordez and Hug, 2010; Gennisson *et al*, 2005).

A major observation of the current study is that net loading-induced changes in shear wave speed appear to be different in active and passive conditions. In particular, we observed a larger change in shear wave speed with loading under the passive conditions. This result suggests that shear wave speed cannot be used as a surrogate measure of net ankle loading in situations where the muscles are both stretched and active, which would preclude a number of functional tasks that involve substantial ankle dorsiflexion. This result could arise from a couple of factors. First, we are only able to relate shear wave speed to the net ankle moment which is due to loading of the gastrocnemius and other soft tissues (e.g. the soleus) crossing the joint. Although it is generally believed that both the gastrocnemius and soleus contribute to the induced ankle moment in an extended knee posture (Sale *et al*, 1982), it is conceivable that the relative load sharing between the muscles differs between individuals and conditions. Specifically, if the gastrocnemius were to accommodate a relatively greater percentage of the ankle load in a passive condition than in the active condition, it could give rise to the steeper linear relationship between gastrocnemius shear wave speed and net ankle moment that we observed (Figure 8.4).

Unfortunately, it is not feasible to measure individual muscle loads *in vivo*, and an animal model may be necessary to investigate this factor more fully.

It is also possible that shear waves propagate differently through internal structures depending on whether the tissue is actively or passively loaded. In particular, shear wave propagation may be sensitive to anatomical features such as muscle thickness, fiber composition of tissue, the relative amount of connective tissue within the muscles and/or fascicle orientation. We performed a post-hoc analysis to assess whether variations in pennation angle or fascicle orientation with respect to the transducer may affect shear wave speed measures. To achieve this aim, we retrospectively measured the pennation angle in the B-Mode images. We found the average change in pennation angle to be 11.1 (± 7.0) deg with active contraction, and 6.8 (± 1.7) deg and 6.1 (± 2.3) change with passive stretch in the extended and flexed postures, which is similar to the changes in pennation angle that have been reported previously (Abellaneda *et al*, 2009). Perhaps more relevant to consider with respect to SWE, however, would be the change in orientation of the muscle fascicles with respect to the transducer, which would subsequently affect the angle at which the tissue is perturbed to induce shear wave speeds. We performed this analysis by measuring the fascicle angle with respect to the image plane in the data collected from passive trials. As expected, we found this angle to increase as the ankle was plantarflexed. In contrast, we found no relationship between shear wave speed and the angle measured, for either the extended knee or flexed knee cases, with the R^2 values of linear trend lines for these data of 0.0744 and 0.078 respectively.

There are some limitations to consider when interpreting the results to this study. Although shear wave speed in muscle has previously been shown to be sensitive to transducer position (Gennisson et al, 2010), this prior study focused on measuring the effects on shear wave speed of

rotating the probe in the coronal plane. In contrast, in our study, all data were collected from the sagittal plane. Likewise, prior studies have found that shear wave speed variations within muscle tissue are very low (Gennisson et al, 2010; Nordez and Hug, 2010), which is consistent with the high inter-rater repeatability that we measured for shear wave speeds. Secondly, although subjects initiated the active isometric contractions at a neutral ankle angle (0 deg), some ankle rotation (<10 deg at 50% MVC) did occur as they incremented up their contraction levels. Such motion can arise due to soft tissue deformation and compliance in the test device, effects which have been observed previously in similar setups (Maganaris et al, 2002; Maganaris, 2005; Muramatsu et al, 2001). The resulting shortening of the plantarflexors could affect the shear wave speeds within the tissue, as noted during the passive stretch trials. Based on our results from the passive trials (Figure 8.3), we would estimate that this change in angle would lead to a shear wave speed effect of less than 1 m/s on average, which would still result in a lower speed-force slope than observed in the passive loading case (Figure 8.4).

In conclusion, our results show that SWE is a promising approach for indirectly assessing muscle loading by tracking changes in shear wave speed. However, we did observe a differential effect of active and passive loading on shear wave speed which makes it important to carefully consider the relevant loading conditions when using SWE for both clinical and research studies.

Chapter 9: Conclusions and Future Directions

9.1 Contributions of this Dissertation

The purpose of this dissertation was to develop new ultrasound elastography tools to assess *in vivo* tendon tissue deformations (Chapters 3 and 4) and then use quantitative ultrasound techniques to investigate spatial variations in muscle-tendon deformations and elasticity in healthy young (Chapters 5 and 8) and middle-aged adults (Chapters 6 and 7). The major contributions of this work are summarized in the following sections.

9.1.1 Development of elastography approach for tracking tendon motion

The first accomplishment of this dissertation research has been the development of a quantitative ultrasound method for measuring high resolution regional displacements and strains within tendon. Inspired by early work in soft tissue elastography (Ophir 1991), the goal was to develop a 2D tracking algorithm capable of overcoming the technical challenges specific to tracking tendon motion with ultrasound. Thus, we customized our elastography approach using a variety of image processing methods including directly tracking ultrasound radiofrequency (RF) data (rather than the B-Mode images), adding quartic spline estimates of sub-pixel motion (Azar *et al.* 2010) and using a forward-backward cyclic tracking approach to reduce numerical drift (Pelc *et al.* 1995). We then performed a variety of phantom and *ex vivo* tendon studies to evaluate the fidelity and capabilities of this elastography method. The results showed excellent repeatability and high correlation between our tracking approach and digital image correlation in terms of displacements and strains for ultrasound phantoms and tendons. The results have also provided evidence of apparent Poisson's ratios in tendons that are greater than 0.5, a phenomenon that

theoretically arises from the tendon helical structure (Reese *et al.* 2010) and has recently been observed in rat tail tendons (Cheng and Screen 2007). These insights into the relationship between tendon microstructure and macro level properties enhance our understanding of the variation in tendinous tissue material properties that are often observed (LaCroix *et al.* 2013), and may prove relevant for understanding fundamental differences between energy-storing and positional tendons (Thorpe *et al.* 2012).

9.1.2. In vivo measurement of tendon deformation patterns

Using the 2D elastography approach, we have demonstrated evidence of significant non-uniformity in Achilles tendon displacements *in vivo* that may arise due to sliding between fascicles that originate in the different muscles of the triceps surae. For example, during passive and eccentric dorsiflexion, and in both flexed and extended knee postures, we have observed significantly larger displacements in deeper portions of the Achilles tendon when compared with the superficial portion of the Achilles tendon. These displacement patterns are load dependent, with significantly lower mid and deep tissue displacements in eccentric loading conditions (compared with passive loading conditions) when the knee was extended. Posture also significantly affected tissue displacement, with greater overall tissue displacements observed when the knee was in a more extended posture (Chapter 5). These observations may reflect the tendon undergoing shear deformation and stretch within its cross-section, and the findings highlight the complex interactions between posture and loading condition on tendon deformations.

9.1.3 Assessment of muscle elasticity using shear wave elastography

Muscle elasticity was evaluated in healthy young adults using ultrasound elastography. In this population, shear wave speed in the gastrocnemius muscle increased monotonically with stretch and with load, however, the nature of the increase is markedly different when loads were generated via active contraction or passive stretch. This result demonstrates the importance of controlling both posture and loading conditions when applying shear wave elastography in clinical use (Chapter 8).

9.1.4 Measurement of variations in tendon elasticity due to location and posture

Using shear wave elastography, we have also observed significant variation in Achilles tendon elasticity. Achilles tendon compliance was measured to increase in a distal-to-proximal fashion, with greater compliance at the muscle-tendon junction (Chapter 7). As expected, we also observed tendon elasticity to increase with dorsiflexion reflecting the strain-stiffening behavior of the collagenous structures (Carlstedt 1987).

9.1.5 The effects of aging on tendon deformation patterns and tendon elasticity

This dissertation work also shows evidence of significant aging effects on tendon elasticity and deformation patterns. Using shear wave elastography, we found age-related changes in tendon elasticity to be location dependent, with no aging effects measured in the free tendon, soleus aponeurosis or gastrocnemius muscle. In contract, compliance in the gastrocnemius aponeurosis was significantly increased with aging (Chapter 7). Using ultrasound elastography, we also found evidence of increased compliance of the Achilles tendon complex, with significantly higher tendon displacements measured in middle-aged adults during passive loading conditions (Chapter 6). Although it is often stated that tendon becomes more compliant with aging due to

micro-architectural changes (Blevins *et al.* 1994; Narici *et al.* 2008; Vogel 1980, 1983), the *in vivo* results on this topic are inconsistent (Karamanidis and Arampatzis 2005; Kubo *et al.* 2007; Onambele *et al.* 2006; Stenroth *et al.* 2012) and relatively little is known about changes that arise in middle-age. These discrepancies may arise, in part, due to methodological differences and the general approach of evaluating gross tissue motions and strains. The results from this dissertation suggest that spatial variation is significant, both along the Achilles tendon length, and within its cross-section, and further, that these regions are affected differently with aging. Thus, it is critical that future studies consider spatial regions when evaluating tendinous tissue, as these distinctions may prove relevant for understanding the propensity for localized tissue damage to occur.

We also observed an age-related change in tendon deformation patterns, with middle-aged adults found to exhibit greater uniformity of tendon displacements during eccentric loading conditions (Chapter 6). This result may arise due to changes in the collagen cross-linking in middle-aged tendon or alterations in muscle coordination patterns. These factors may affect the stretch of the tendon fascicles that arise in the different muscles, and could potentially lead to age-related changes in localized strain patterns.

9.2 Clinical Implications of Dissertation

The overall findings of this dissertation suggest that muscle-tendon mechanics are highly complex, load and posture dependent, and are altered with aging, even in middle-aged adults. The results presented here suggest that there are specific age-related changes to muscle and tendon deformation and elasticity in regions similar to those indicated in injuries that increase in

incidence in middle-age. Thus, there may be clinical implications of this work; however, these interpretations should be made cautiously.

For example, using ultrasound elastography, we consistently observed non-uniformity in tendon deformation under both passive stretch and active loading conditions. We hypothesized that this may relate to sliding between fascicles bundles that arise from the muscles of the triceps surae. This finding challenges the generally held assumption that tendon primarily undergoes axial deformations due to tensile loading, as commonly tested *ex vivo.* The complexities of the deformations presented in this dissertation are potentially relevant clinically for a few reasons:

First, these results suggest that interfascicle sliding may enable muscles to act independently while transmitting loads through a common tendinous structure. This could alter performance, in terms of energy storage and return, and as well as coordination.

The results also demonstrate the potential for tenocyte stimulation to arise from a complex array of sources that include stretch, lateral compression, and flow-induced shear. Understanding *in vivo* tenocyte deformation is important for translating fundamental tendon mechanobiological studies to rehabilitation recommendations, particularly with regards to the magnitude and type of exercises needed to enhance tendon healing. For both of these reasons, it is important to consider that we observed more uniform tendon motion in middle-aged adults, which could reflect a decrease in sliding between fascicles, as has been observed *in vitro* (Thorpe *et al.* 2013). Increased tendon uniformity could affect localized injury potential and mechanobiological responses.

Additionally, the variations in tendon deformation and elasticity observed here may provide new insights into the causes of localized muscle and tendon damage. For example, we observed an increase in compliance in the gastrocnemius aponeurosis with age. Interestingly, this region

corresponds with the location where gastrocnemius muscle strains are known to originate (Garrett 1990; Kirkendall and Garrett 2002; Speer *et al.* 1993), an injury that has specifically been observed to present more frequently in middle-age (McKean *et al.* 2006).

The results from this dissertation highlight the need for additional evaluation of high resolution tendon elasticity and deformation to inform our understanding of injury and rehabilitation.

9.3 Ongoing Work and Next Steps

The results from this dissertation set the stage for the pursuit of a variety of additional research studies, to both broaden our understanding of complex muscle-tendon deformations and elasticity, and to deepen our interpretation of these results. In the following sections, I propose future directions to be pursued.

9.3.1 Investigation of tendon deformation and elasticity in additional populations

Clear follow-up work to the studies presented here includes the recruitment and testing of additional subject populations using the described methods. Older adult populations (61+) are of particular interest to elucidate if the aging effects observed in this dissertation work (e.g. increase in gastrocnemius aponeurosis compliance) progress linearly with age.

The results from this dissertation will also serve effectively as a baseline for healthy tendon deformations and elasticity in subjects of various ages. These data will enable the evaluation of a variety of additional populations suffering from injury or disease. Subjects with a history of Achilles tendinopathy are of particular interest, and it is hypothesized that the tendon degradation will lead to decreased shear wave speeds in the free tendon, and increased displacement uniformity.

9.3.2 Additional validation and refinement of ultrasound methods

Ongoing validation of the ultrasound tools presented here are critical as we expand our research interests and applications. Although we have previously demonstrated the ability of the elastography approach to sufficiently measure average tendon displacements and strains (Chapters 3 and 4), we have recently begun pilot work to verify its accuracy in measuring non-uniform displacement patterns. In this pilot work, custom phantoms, designed to induce non-uniform deformations, were loaded in a mechanical testing setup. A finite element model was then developed to mimic the phantom and loading setup (FEBio, University of Utah) such that displacements and strains measured with elastography could be compared with those predicted in the model. These pilot data have shown promising results (Ehlers *et al.* 2014), and work is ongoing.

A second goal is to evaluate the effects of transducer alignment on tracking capabilities, to evaluate the sensitivity of this approach. It has previously been shown that transducer tilt can significantly alter tendon B-Mode image grayscale quality (van Schie *et al.* 1999), however it is unclear how sensitive the elastography tracking approach is to alterations in transducer alignment or tilt. To evaluate this sensitivity, we have developed a custom transducer grip that enables controlled adjustment of transducer positioning and incidence angle. This project will involve the collection of ultrasound data during the mechanical loading of *ex vivo* tendons, at various degrees of transducer tilt. This future study will enable us to better understand the sensitivity of the tracking approach to misalignment, and thus, the potential limitations of applying this technique *in vivo*.

9.3.3 Twitch-induced wave propagations

The ultra-high frame rate capabilities of the Supersonic Imagine Machine (Aixplorer, Supersonic Imagine; Aix-en-Provence, France) can be used to collect ultrasound RF data with very high temporal resolution. These ultra-high frame rate data can be tracked using our elastography approach, enabling the evaluation of deformations at a very small time scale. I have recently begun collaborating with Dr. Antoine Nordez from the Université de Nantes to investigate the capability of applying this approach to track the propagation of a muscle twitch along the tendon. During a recent research visit we collected pilot ultrasound data from the Achilles tendon while muscle twitches were induced by stimulating electrodes placed over the medial gastrocnemius muscle. Following collections, I used the elastography tracking approach to measure the propagation of the wave down the length of the tendon, and found wave speeds to increase with ankle dorsiflexion. These pilot data show the promise of this approach, and the aim is to continue collaboration on this project.

9.3.4 Musculoskeletal models

In order to better understand the implications of the results described here, we have developed a collaboration with researchers at the University of Virginia who are experts in the development of advanced musculoskeletal models. This collaboration has many benefits, including that it enables us to test the effects of specific alterations in tendon mechanics that we are observing *in vivo*. For example, an early model created by the group evaluated the effects of restraining fascicle-sliding in the Achilles tendon to mimic the increased uniformity we observed in middle-aged adults (Handsfield *et al.* 2013). Continued collaboration will provide important insight into the findings presented here.

9.3.5 In vitro experiments

Another valuable tool for providing context for the results in this dissertation is advanced *in vitro* testing. Exciting work at Queen Mary University of London has used this approach to evaluate interfascicular sliding (Screen *et al.* 2004), in different types of tendons (Thorpe *et al.* 2012), and of different specimen age (Thorpe *et al.* 2013). These results have provided context to the *in vivo* findings presented in this dissertation. Future collaboration with this lab group will enable the development of multi-scale approaches to measuring complex tendon deformation patterns.

9.4 Conclusions

The results of this dissertation show evidence that muscle-tendon mechanics are highly non-uniform, and change significantly with age. These results are important steps to understanding muscle-tendon mechanics, but additional experimental work, both *in vitro* and *in vivo,* paired with technical advances and the use of musculoskeletal models will be critical to advancing our understanding of muscle-tendon injuries and rehabilitation.

Appendix A. Maximum Measureable Shear Wave Speed

To better understand the physical limitations on maximum measureable shear wave speeds in our tissue of interest, tendon, we can compute the physical frame rate limitations in this application. First, we can compute the minimum amount of time that it takes a sound wave to return to the transducer using equation A.1, an estimate of the average speed of sound, v, in soft tissue of 1540 m/s (Shin *et al.* 2010), and a distance, d, of 40 mm (the wave must travel twice the distance of the depth of the tissue). With these values, we compute that the time for the sound wave to return to the transducer to be 0.026 ms (Figure A.1). Thus, the maximum frame rate that could be used to measure tissue at a depth of 20 mm would be 38,500 frames/second.

$$v = d/t \tag{A.1}$$

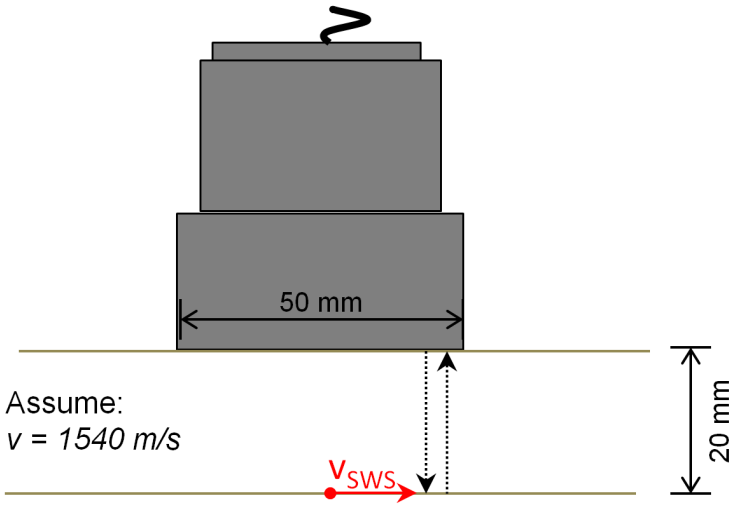

Figure A.1 Schematic of ultrasound wave propagation

In the shear wave tracking approach, we must be capable of collecting ultrasound data at a high enough frame rate to capture the wave propagating within the transducer window, without exceeding the maximum frame rate to limitation computed above. The necessary frame rate to

measure wave travel speed, v_{SWS}, can be computed using equation A.1. With a standard transducer width of 50 mm, and the assumption that the shear wave is induced in the center of the transducer, the distance, *d*, over which wave travel speed can be computed in 25 mm. Due to the attenuation of the waves as they travel over the tissue, smaller measurement distances will enhance the tracking. The maximum frame rate necessary to measure shear wave propagation was then computed for various frame rates and measurement distances (Figure A.2).

The maximum necessary frame rate varies based on the measurement distance and wave propagation speed. With smaller increments between measurements, such at 0.5 mm, we can observe that even wave speeds (e.g. 20 m/s) similar to what we have measured in tendon (>16.3 m/s) exceed the highest frame rate possible for measuring ultrasound information at a depth of 20 mm. Thus, it is clear that at the shear wave speeds we measure in tendon, we are approaching the physical limitations of ultrasound for this approach. This further emphasizes the relevance of considering slack postures of the Achilles tendon when using the SSI approach.

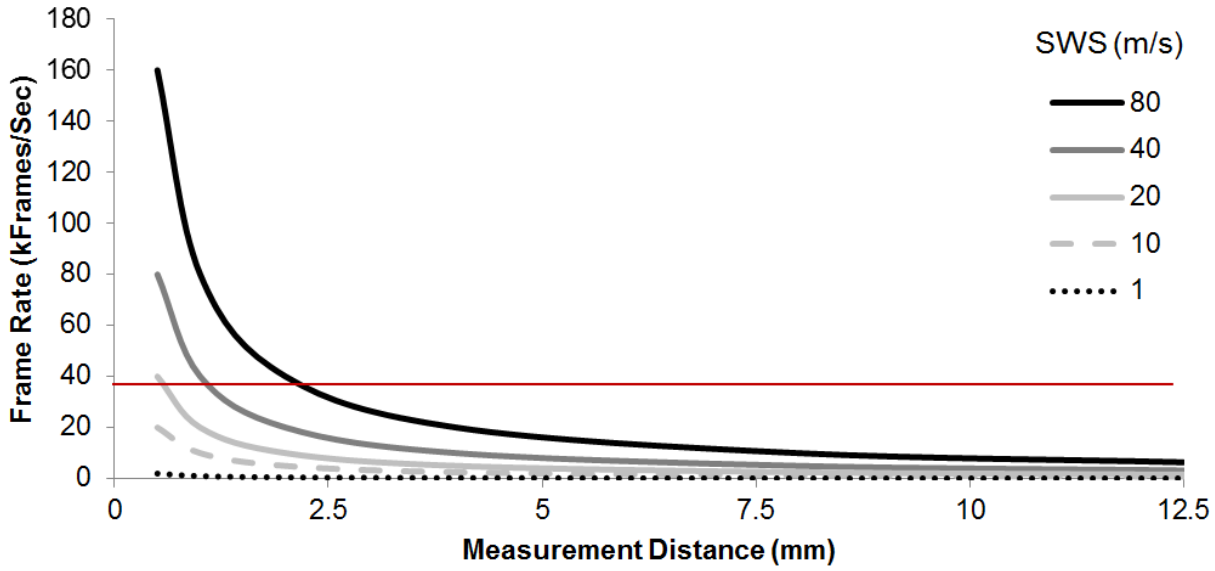

Figure A.2 The frame rate (in kFrames/sec or 1000*frames/sec) necessary to compute shear wave speed (SWS) varies based on the tissue wave speed and the distance between subsequent measurement points. The red line indicates the maximum frame rate that can be used for our

hypothetical tissue at 20 mm of depth.

Appendix B. Overview of Eccentric Loading Device

To create a functional loading condition from which to collect ultrasound data, an eccentric loading device for the plantarflexor muscles and Achilles tendon was designed and built (Bunger 2012). The plantarflexor moment undergone by the subjects was computed based measurements from load cells in the belt (Figure B.1). The moment from the loading assembly, $M_{loading}$, could be computed based on the force in the load cells, $F_{loadcells}$, and the moment arm of the pulley, r_{pulley}, via Equation B.1. In the current device design, as of April 2014, r_{pulley}, is equal to 0.0631 m.

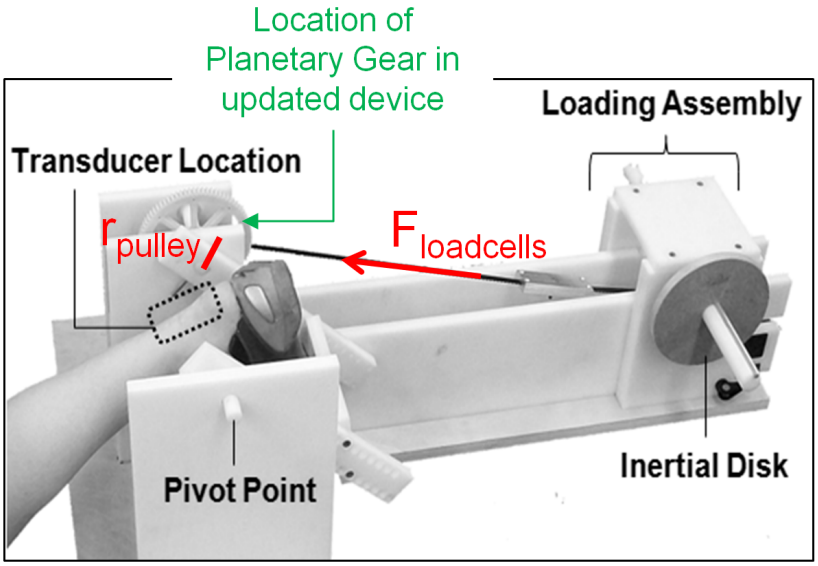

Figure B.1. Updates to inertial loading device.

$$M_{loading} = F_{loadcells} \times r_{pulley} \quad \text{(B.1)}$$

The moment from the loading assembly, $M_{loading}$, can then be related to the plantarflexor moment, $M_{plantarflexors}$, by the gear ratio of the planetary gear, $N_{planetary}$ via equation B.2. $N_{planetary}$ is equal to 0.1428.

$$\frac{M_{loading}}{M_{plantarflexors}} = N_{planetary} \tag{B.2}$$

Thus, the plantarflexor moment, $M_{plantarflexors}$, can be computed directly from the force in the load cells via equation B.3.

$$M_{plantarflexors} = \frac{M_{loading}}{0.1428} = \frac{F_{loadcells} \times 0.0631m}{0.1428} \tag{B.3}$$

References

Abellaneda, S., Guissard, N., Duchateau, J., 2009. The relative lengthening of the myotendinous structures in the medial gastrocnemius during passive stretching differs among individuals. Journal of Applied Physiology 106, 169-177.

Alfredson, H., 2003. Chronic midportion Achilles tendinopathy: an update on research and treatment. Clin Sports Med 22, 727-741.

Alfredson, H., Lorentzon, R., 2000. Chronic Achilles tendinosis: recommendations for treatment and prevention. Sports Medicine 29, 135-146.

Alfredson, H., Pietila, T., Jonsson, P., Lorentzon, R., 1998. Heavy-load eccentric calf muscle training for the treatment of chronic Achilles tendinosis. Am. J. Sports Med. 26, 360-366.

Almeida, S.A., Williams, K.M., Shaffer, R.A., Brodine, S.K., 1999. Epidemiological patterns of musculoskeletal injuries and physical training. Med Sci Sport Exer 31, 1176-1182.

Arampatzis, A., Stafilidis, S., DeMonte, G., Karamanidis, K., Morey-Klapsing, G., Bruggenmann, G.P., 2005. Strain and elongation of the human gastrocnemius tendon and aponeurosis during maximal plantarflexion effort. Journal of Biomechanics 38, 833-841.

Arda, K., Ciledag, N., Aktas, E., Aribas, B.K., Kose, K., 2011. Quantitative assessment of normal soft-tissue elasticity using shear-wave ultrasound elastography. American Journal of Roentgenology 197, 532-536.

Arndt, A., Bengtsson, A.S., Peolsson, M., Thorstensson, A., Movin, T., 2012. Non-uniform displacement within the Achilles tendon during passive ankle joint motion. Knee surgery, sports traumatology, arthroscopy: official journal of the ESSKA 20, 1868-1874.

Arndt, A., Tomatis, L., Ryberg, A., Kleman, D., Peolsson, M., Thorstensson, A., 2006. In vivo sonometry measurement of strain in the human achilles tendon. Journal of Biomechanics 39, S495.

Arndt, A.N., Komi, P.V., Bruggemann, G.P., Lukkariniemi, J., 1998. Individual muscle contributions to the in vivo achilles tendon force. Clinical Biomechanics 13, 532-541.

Arnoczky, S.P., Lavagnino, M., Egerbacher, M., 2007. The mechanobiological aetiopathogenesis of tendinopathy: is it the over-stimulation or the under-stimulation of tendon cells? Int J Exp Pathol 88, 217-226.

Arruda, E.M., Calve, S., Dennis, R.G., Mundy, K., Baar, K., 2006. Regional variation of tibialis anterior tendon mechanics is lost following denervation. Journal of Applied Physiology 101, 1113-1117.

Astrom, M., Rausing, A., 1995. Chronic Achilles tendinopathy. A survey of surgical and histopathologic findings. Clin Orthop Relat R, 151-164.

Athanasiou, A., Tardivon, A., Tanter, M., Sigal-Zafrani, B., Bercoff, J., Deffieux, T., Gennisson, J.L., Fink, M., Neuenschwander, S., 2010. Breast lesions: quantitative elastography with supersonic shear imaging--preliminary results. Radiology 256, 297-303.

Aubry, S., Risson, J.R., Kastler, A., Barbier-Brion, B., Siliman, G., Runge, M., Kastler, B., 2013. Biomechanical properties of the calcaneal tendon in vivo assessed by transient shear wave elastography. Skeletal Radiol 42, 1143-1150.

Azar, R.Z., Goksel, O., Salcudean, S.E., 2010. Sub-Sample Displacement Estimation From Digitized Ultrasound RF Signals Using Multi-Dimensional Polynomial Fitting of the Cross-Correlation Function. IEEE Transactions on Ultrasonics, Ferroelectrics, and Frequency Control 57, 2403-2420.

Azizi, E., Halenda, G.M., Roberts, T.J., 2009. Mechanical properties of the gastrocnemius aponeurosis in wild turkeys. Integr Comp Biol 49, 51-58.

Azizi, E., Roberts, T.J., 2009. Biaxial strain and variable stiffness in aponeuroses. The Journal of Physiology 587, 4309-4318.

Bavu, E., Gennisson, J.L., Couade, M., Bercoff, J., Mallet, V., Fink, M., Badel, A., Vallet-Pichard, A., Nalpas, B., Tanter, M., Pol, S., 2011. Noninvasive in vivo liver fibrosis evaluation using supersonic shear imaging: a clinical study on 113 hepatitis C virus patients. Ultrasound in Medicine & Biology 37, 1361-1373.

Beenakker, K.G., Ling, C.H., Meskers, C.G., de Craen, A.J., Stijnen, T., Westendorp, R.G., Maier, A.B., 2010. Patterns of muscle strength loss with age in the general population and patients with a chronic inflammatory state. Ageing Res Rev 9, 431-436.

Bercoff, J., Tanter, M., Fink, M., 2004. Supersonic shear imaging: a new technique for soft tissue elasticity mapping. IEEE Trans Ultrason Ferroelectr Freq Control 51, 396-409.

Birch, H.L., Bailey, J.V., Bailey, A.J., Goodship, A.E., 1999. Age-related changes to the molecular and cellular components of equine flexor tendons. Equine Vet J 31, 391-396.

Blevins, F.T., Hecker, A.T., Bigler, G.T., Boland, A.L., Hayes, W.C., 1994. The effects of donor age and strain rate on the biomechanical properties of bone-patellar tendon-bone allografts. Am. J. Sports Med. 22, 328-333.

Blitz, N.M., Eliot, D.J., 2007. Anatomical aspects of the gastrocnemius aponeurosis and its insertion: a cadaveric study. J Foot Ankle Surg 46, 101-108.

Bohs, L.N., Trahey, G.E., 1991. A Novel Method for Angle Independent Ultrasonic-Imaging of Blood-Flow and Tissue Motion. IEEE Transactions on Biomedical Engineering 38, 280-286.

Brum, J., Bernal, M., Gennisson, J.L., Tanter, M., 2014. In vivo evaluation of the elastic anisotropy of the human Achilles tendon using shear wave dispersion analysis. Phys Med Biol 59, 505-523.

Bunger, D., 2012. Dynamic Loading Device for Imaging of Plantarflexor and Achilles Tendon Tissue Deformation. University of Wisconsin-Madison.

Carlstedt, C.A., 1987. Mechanical and chemical factors in tendon healing. Effects of indomethacin and surgery in the rabbit. Acta Orthop Scand Suppl 224, 1-75.

Chamberlain, C.S., Duenwald-Kuehl, S.E., Okotie, G., Brounts, S.H., Baer, G.S., Vanderby, R., 2013. Temporal healing in rat achilles tendon: ultrasound correlations. Annals of Biomedical Engineering 41, 477-487.

Chen, X.C., Zohdy, M.J., Emelianov, S.Y., O'Donnell, M., 2004. Lateral speckle tracking using synthetic lateral phase. IEEE Transactions on Ultrasonics, Ferroelectrics, and Frequency Control 51, 540-550.

Chen, X.M., Cui, L.G., He, P., Shen, W.W., Qian, Y.J., Wang, J.R., 2013. Shear wave elastographic characterization of normal and torn achilles tendons: a pilot study. J Ultrasound Med 32, 449-455.

Cheng, V.W.T., Screen, H.R.C., 2007. The micro-structural strain response of tendon. J Mater Sci 42, 8957-8965.

Chernak, L.A., Thelen, D.G., 2012. Tendon motion and strain patterns evaluated with two-dimensional ultrasound elastography. Journal of Biomechanics 45, 2618-2623.

Child, S., Bryant, A.L., Clark, R.A., Crossley, K.M., 2010. Mechanical Properties of the Achilles Tendon Aponeurosis Are Altered in Athletes With Achilles Tendinopathy. Am J Sports Med.

Couppe, C., Hansen, P., Kongsgaard, M., Kovanen, V., Suetta, C., Aagaard, P., Kjaer, M., Magnusson, S.P., 2009. Mechanical properties and collagen cross-linking of the patellar tendon in old and young men. Journal of Applied Physiology 107, 880-886.

Cummins, E.J., Anson, B.J., et al., 1946. The structure of the calcaneal tendon (of Achilles) in relation to orthopedic surgery, with additional observations on the plantaris muscle. Surg Gynecol Obstet 83, 107-116.

De Zordo, T., Lill, S.R., Fink, C., Feuchtner, G.M., Jaschke, W., Bellmann-Weiler, R., Klauser, A.S., 2009. Real-time sonoelastography of lateral epicondylitis: comparison of findings between patients and healthy volunteers. American Journal of Roentgenology 193, 180-185.

DeWall, R.J., Slane, L.C., Lee, K.S., Thelen, D.G., 2014. Spatial variations in Achilles shear wave speed. Journal of Biomechanics, in press.

Doherty, T.J., 2001. The influence of aging and sex on skeletal muscle mass and strength. Curr Opin Clin Nutr Metab Care 4, 503-508.

Doherty, T.J., 2003. Invited review: Aging and sarcopenia. Journal of Applied Physiology 95, 1717-1727.

Doherty, T.J., Vandervoort, A.A., Brown, W.F., 1993. Effects of Aging on the Motor Unit - a Brief Review. Canadian Journal of Applied Physiology-Revue Canadienne De Physiologie Appliquee 18, 331-358.

Drakonaki, E., Allen, G., Wilson, D., 2009. Real-time ultrasound elastography of the normal Achilles tendon: reproducibility and pattern description. Clinical Radiology 64, 1196-1202.

Duenwald-Kuehl, S., Kobayashi, H., Lakes, R., Vanderby, R., Jr., 2012a. Time-dependent ultrasound echo changes occur in tendon during viscoelastic testing. Journal of Biomechanical Engineering 134, 111006.

Duenwald-Kuehl, S., Lakes, R., Vanderby, R., 2012b. Strain-induced damage reduces echo intensity changes in tendon during loading. Journal of Biomechanics 45, 1607-1611.

Duenwald, S., Kobayashi, H., Frisch, K., Lakes, R., Vanderby, R., Jr., 2011. Ultrasound echo is related to stress and strain in tendon. Journal of Biomechanics 44, 424-429.

Ebbini, E.S., 2006. Phase-coupled two-dimensional speckle tracking algorithm. IEEE Transactions on Ultrasonics, Ferroelectrics, and Frequency Control 53, 972-990.

Ehlers, A., Slane, L.C., Thelen, D.G., 2014. Evaluation of 2D ultrasound elastography for the measurement of non-uniform displacements and strains. 2014 World Congress of Biomechanics.

Ellison, M., Kobayashi, H., Delaney, F., Danielson, K., Vanderby, R., Jr., Muir, P., Forrest, L.J., 2013. Feasibility and repeatability for in vivo measurements of stiffness gradients in the canine gastrocnemius tendon using an acoustoelastic strain gauge. Veterinary radiology & ultrasound : the official journal of the American College of Veterinary Radiology and the International Veterinary Radiology Association 54, 548-554.

Epstein, M., Wong, M., Herzog, W., 2006. Should tendon and aponeurosis be considered in series? Journal of Biomechanics 39, 2020-2025.

Ettema, G.J., Huijing, P.A., 1989. Properties of the tendinous structures and series elastic component of EDL muscle-tendon complex of the rat. Journal of Biomechanics 22, 1209-1215.

Fahlstrom, M., Jonsson, P., Lorentzon, R., Alfredson, H., 2003. Chronic Achilles tendon pain treated with eccentric calf-muscle training. Knee Surg Sports Traumatol Arthrosc 11, 327-333.

Farron, J., Varghese, T., Thelen, D.G., 2009. Measurement of tendon strain during muscle twitch contractions using ultrasound elastography. IEEE Transactions on Ultrasonics, Ferroelectrics, and Frequency Control 56, 27-35.

Finni, T., Hodgson, J.A., Lai, A.M., Edgerton, V.R., Sinha, S., 2003. Nonuniform strain of human soleus aponeurosis-tendon complex during submaximal voluntary contractions in vivo. Journal of Applied Physiology 95, 829-837.

Fleming, B.C., Beynnon, B.D., 2004. In vivo measurement of ligament/tendon strains and forces: a review. Annals of Biomedical Engineering 32, 318-328.

Fong, K.D., Trindade, M.C., Wang, Z., Nacamuli, R.P., Pham, H., Fang, T.D., Song, H.M., Smith, R.L., Longaker, M.T., Chang, J., 2005. Microarray analysis of mechanical shear effects on flexor tendon cells. Plast Reconstr Surg 116, 1393-1404; discussion 1405-1396.

Fukunaga, T., Kawakami, Y., Kubo, K., Kanehisa, H., 2002. Muscle and tendon interaction during human movements. Exerc Sport Sci Rev 30, 106-110.

Garrett, W.E., 1990. Muscle Strain Injuries - Clinical and Basic Aspects. Med Sci Sport Exer 22, 436-443.

Gennisson, J.L., Cornu, C., Catheline, S., Fink, M., Portero, P., 2005. Human muscle hardness assessment during incremental isometric contraction using transient elastography. Journal of Biomechanics 38, 1543-1550.

Gennisson, J.L., Deffieux, T., Mace, E., Montaldo, G., Fink, M., Tanter, M., 2010. Viscoelastic and anisotropic mechanical properties of in vivo muscle tissue assessed by supersonic shear imaging. Ultrasound in Medicine & Biology 36, 789-801.

Handsfield, G., Chernak, L.A., Thelen, D.G., Blemker, S.S., 2013. A finite element model of the triceps surae to explore Achilles tendon sliding and adhesion during eccentric contractions. Computer Methods in Biomechanics and Biomedical Engineering, 11th International Symposium, Salt Lake City, UT.

Haraldsson, B.T., Aagaard, P., Qvortrup, K., Bojsen-Moller, J., Krogsgaard, M., Koskinen, S., Kjaer, M., Magnusson, S.P., 2008. Lateral force transmission between human tendon fascicles. Matrix Biol 27, 86-95.

Hawkins, D., Lum, C., Gaydos, D., Dunning, R., 2009. Dynamic creep and pre-conditioning of the Achilles tendon in-vivo. Journal of Biomechanics 42, 2813-2817.

Houshian, S., Tscherning, T., Riegels-Nielsen, P., 1998. The epidemiology of Achilles tendon rupture in a Danish county. Injury 29, 651-654.

Huang, L., O'Donnell, M., 2010 A synthetic lateral phase (SLP) displacement estimator using complex FIR filters. In Ultrasonics Symposium (IUS), 2010 IEEE.

Hug, F., Lacourpaille, L., Maisetti, O., Nordez, A., 2013. Slack length of gastrocnemius medialis and Achilles tendon occurs at different ankle angles. Journal of Biomechanics.

Hughes, D.S., Kelly, J.L., 1953. Second-order elastic deformation of solids. Physical Review 92, 1145-1149.

Inoue, Y., Takahashi, M., Arita, J., Aoki, T., Hasegawa, K., Beck, Y., Makuuchi, M., Kokudo, N., 2010. Intra-operative freehand real-time elastography for small focal liver lesions: "visual palpation" for non-palpable tumors. Surgery 148, 1000-1011.

Itoh, A., Ueno, E., Tohno, E., Kamma, H., Takahashi, H., Shiina, T., Yamakawa, M., Matsumura, T., 2006. Breast disease: clinical application of US elastography for diagnosis. Radiology 239, 341-350.

Ivanenko, Y.P., Poppele, R.E., Lacquaniti, F., 2004. Five basic muscle activation patterns account for muscle activity during human locomotion. The Journal of Physiology 556, 267-282.

Iwanuma, S., Akagi, R., Kurihara, T., Ikegawa, S., Kanehisa, H., Fukunaga, T., Kawakami, Y., 2011. Longitudinal and transverse deformation of human Achilles tendon induced by isometric plantar flexion at different intensities. Journal of Applied Physiology 110, 1615-1621.

Jiang, J., Hall, T.J., 2009. A Generalized Speckle Tracking Algorithm for Ultrasonic Strain Imaging Using Dynamic Programming. Ultrasound in Medicine & Biology 35, 1863-1879.

Jung, H.J., Vangipuram, G., Fisher, M.B., Yang, G., Hsu, S., Bianchi, J., Ronholdt, C., Woo, S.L., 2011. The effects of multiple freeze-thaw cycles on the biomechanical properties of the human bone-patellar tendon-bone allograft. Journal of orthopaedic research : official publication of the Orthopaedic Research Society 29, 1193-1198.

Kaluzynski, K., Chen, X.C., Emelianov, S.Y., Skovoroda, A.R., O'Donnell, M., 2001. Strain rate imaging using two-dimensional speckle tracking. IEEE Transactions on Ultrasonics, Ferroelectrics, and Frequency Control 48, 1111-1123.

Kannus, P., Niittymaki, S., Jarvinen, M., Lehto, M., 1989. Sports injuries in elderly athletes: a three-year prospective, controlled study. Age Ageing 18, 263-270.

Karamanidis, K., Arampatzis, A., 2005. Mechanical and morphological properties of different muscle-tendon units in the lower extremity and running mechanics: effect of aging and physical activity. The Journal of Experimental Biology 208, 3907-3923.

Kent-Braun, J.A., Ng, A.V., Young, K., 2000. Skeletal muscle contractile and noncontractile components in young and older women and men. Journal of Applied Physiology 88, 662-668.

Kim, P.J., Martin, E., Ballehr, L., Richey, J.M., Steinberg, J.S., 2011. Variability of insertion of the Achilles tendon on the calcaneus: an MRI study of younger subjects. J Foot Ankle Surg 50, 41-43.

Kirkendall, D.T., Garrett, W.E., 2002. Clinical perspectives regarding eccentric muscle injury. Clin Orthop Relat R, S81-S89.

Knobloch, K., 2007. Eccentric training in Achilles tendinopathy: is it harmful to tendon microcirculation? Brit J Sport Med 41, e2; discussion e2.

Knobloch, K., Yoon, U., Vogt, P.M., 2008. Acute and overuse injuries correlated to hours of training in master running athletes. Foot & ankle international. / American Orthopaedic Foot and Ankle Society [and] Swiss Foot and Ankle Society 29, 671-676.

Kobayashi, H., Vanderby, R., 2005. New strain energy function for acoustoelastic analysis of dilatational waves in nearly incompressible, hyper-elastic materials. Journal of Applied Mechanics 72, 843-851.

Kobayashi, H., Vanderby, R., 2006. Acoustoelastic analysis of reflected waves in nearly incompressible, hyper-elastic materials: Forward and inverse problems. Journal of the Acoustical Society of America 121, 879-887.

Komolafe, O.A., Doehring, T.C., 2010. Fascicle-scale loading and failure behavior of the Achilles tendon. Journal of Biomechanical Engineering 132, 021004.

Kongsgaard, M., Nielsen, C.H., Hegnsvad, S., Aagaard, P., Magnusson, S.P., 2011. Mechanical properties of the human Achilles tendon, in vivo. Clinical Biomechanics 26, 772-777.

Konofagou, E., Ophir, J., 1998. A new elastographic method for estimation and imaging of lateral displacements, lateral strains, corrected axial strains and Poisson's ratios in tissues. Ultrasound in Medicine & Biology 24, 1183-1199.

Korstanje, J., Selles, R., Henk, S., Hovius, S., Bosch, J., 2009. Dedicated ultrasound speckle tracking to study tendon displacement. In:conference proceedings of SPIE Medical Imaging 2009: Ultrasonic Imaging and Signal Processing. Lake Buena Vista, FL, USA.

Korstanje, J.W., Selles, R.W., Stam, H.J., Hovius, S.E., Bosch, J.G., 2010. Development and validation of ultrasound speckle tracking to quantify tendon displacement. Journal of Biomechanics 43, 1373-1379.

Kubo, K., Kanehisa, H., Fukunaga, T., 2002. Effect of stretching training on the viscoelastic properties of human tendon structures in vivo. J Appl Physiol 92, 595-601.

Kubo, K., Kanehisa, H., Fukunaga, T., 2003. Gender differences in the viscoelastic properties of tendon structures. Eur J Appl Physiol 88, 520-526.

Kubo, K., Morimoto, M., Komuro, T., Tsunoda, N., Kanehisa, H., Fukunaga, T., 2007. Age-related differences in the properties of the plantar flexor muscles and tendons. Med Sci Sport Exer 39, 541-547.

Kujala, U.M., Sarna, S., Kaprio, J., 2005. Cumulative incidence of achilles tendon rupture and tendinopathy in male former elite athletes. Clinical journal of sport medicine: official journal of the Canadian Academy of Sport Medicine 15, 133-135.

Kuo, P.-L., Li, P.-C., Li, M.-L., 2001. Elastic properties of tendon measured by two different approaches. Ultrasound in Medicine & Biology 27, 1275-1284.

Kvist, M., 1991. Achilles tendon injuries in athletes. Annales chirurgiae et gynaecologiae 80, 188-201.

LaCroix, A.S., Duenwald-Kuehl, S.E., Lakes, R.S., Vanderby, R., 2013. Relationship between tendon stiffness and failure: a metaanalysis. Journal of Applied Physiology 115, 43-51.

Lanir, Y., Salant, E.L., Foux, A., 1988. Physico-chemical and microstructural changes in collagen fiber bundles following stretch in-vitro. Biorheology 25, 591-603.

Lempriere, B.M., 1968. Poissons Ratio in Orthotropic Materials. American Institute of Aeronautics and Astronautics Journal 6, 2226-2227.

Lerner, R.M., Huang, S.R., Parker, K.J., 1990. Sonoelasticity Images Derived from Ultrasound Signals in Mechanically Vibrated Tissues. Ultrasound in Medicine and Biology 16, 231-239.

Lieber, R.L., Leonard, M.E., Brown, C.G., Trestik, C.L., 1991. Frog semitendinosis tendon load-strain and stress-strain properties during passive loading. American Journal of Physiology 261, C86-92.

Lopata, R., Nillesen, M., Hansen, H., Gerrits, I., Thijssen, J., de Korte, C., 2009. Performance evaluation of methods for two-dimensional displacement and strain estimation using ultrasound radio frequency data. Ultrasound in Medicine & Biology 35, 796-812.

Lubinski, M.A., Emelianov, S.Y., O'Donnell, M., 1999. Speckle tracking methods for ultrasonic elasticity imaging using short-time correlation. IEEE Transactions on Ultrasonics, Ferroelectrics, and Frequency Control 46, 82-96.

Lubinski, M.A., Emelianov, S.Y., Raghavan, K.R., Yagle, A.E., Skovoroda, A.R., ODonnell, M., 1996. Lateral displacement estimation using tissue incompressibility. IEEE Transactions on Ultrasonics, Ferroelectrics, and Frequency Control 43, 247-256.

Lynch, H.A., Johannessen, W., Wu, J.P., Jawa, A., Elliott, D.M., 2003. Effect of fiber orientation and strain rate on the nonlinear uniaxial tensile material properties of tendon. Journal of Biomechanical Engineering 125, 726-731.

Lyshchik, A., Higashi, T., Asato, R., Tanaka, S., Ito, J., Mai, J.J., Pellot-Barakat, C., Insana, M.F., Brill, A.B., Saga, T., Hiraoka, M., Togashi, K., 2005. Thyroid gland tumor diagnosis at US elastography. Radiology 237, 202-211.

Maeda, T., Sakabe, T., Sunaga, A., Sakai, K., Rivera, A.L., Keene, D.R., Sasaki, T., Stavnezer, E., Iannotti, J., Schweitzer, R., Ilic, D., Baskaran, H., Sakai, T., 2011. Conversion of mechanical force into TGF-beta-mediated biochemical signals. Current Biology 21, 933-941.

Maffulli, N., Longo, U.G., 2008. Conservative management for tendinopathy: is there enough scientific evidence? Rheumatology (Oxford) 47, 390-391.

Maffulli, N., Wong, J., Almekinders, L.C., 2003. Types and epidemiology of tendinopathy. Clin Sports Med 22, 675-692.

Maganaris, C.N., 2003. Tendon conditioning: artefact or property? Proceedings of the Royal Society - Biological Sciences 270 Suppl 1, S39-42.

Maganaris, C.N., 2005. Validity of procedures involved in ultrasound-based measurement of human plantarflexor tendon elongation on contraction. Journal of Biomechanics 38, 9-13.

Maganaris, C.N., Narici, M.V., Almekinders, L.C., Maffulli, N., 2004. Biomechanics and pathophysiology of overuse tendon injuries: ideas on insertional tendinopathy. Sports Medicine 34, 1005-1017.

Maganaris, C.N., Paul, J.P., 1999. In vivo human tendon mechanical properties. The Journal of Physiology 521 Pt 1, 307-313.

Maganaris, C.N., Paul, J.P., 2000. Load-elongation characteristics of in vivo human tendon and aponeurosis. J Exp Biol 203, 751-756.

Maganaris, C.N., Paul, J.P., 2002. Tensile properties of the in vivo human gastrocnemius tendon. Journal of Biomechanics 35, 1639-1646.

Magnusson, S.P., Aagaard, P., Dyhre-Poulsen, P., Kjaer, M., 2001. Load-displacement properties of the human triceps surae aponeurosis in vivo. J Physiol 531, 277-288.

Magnusson, S.P., Hansen, P., Aagaard, P., Brond, J., Dyhre-Poulsen, P., Bojsen-Moller, J., Kjaer, M., 2003. Differential strain patterns of the human gastrocnemius aponeurosis and free tendon, in vivo. Acta Physiologica Scandinavica 177, 185-195.

McKean, K.A., Manson, N.A., Stanish, W.D., 2006. Musculoskeletal injury in the masters runners. Clinical journal of sport medicine : official journal of the Canadian Academy of Sport Medicine 16, 149-154.

Morse, C.I., Thom, J.M., Birch, K.M., Narici, M.V., 2005. Changes in triceps surae muscle architecture with sarcopenia. Acta Physiologica Scandinavica 183, 291-298.

Muramatsu, T., Muraoka, T., Kawakami, Y., Fukunaga, T., 2002. Superficial aponeurosis of human gastrocnemius is elongated during contraction: implications for modeling muscle-tendon unit. Journal of Biomechanics 35, 217-223.

Muramatsu, T., Muraoka, T., Takeshita, D., Kawakami, Y., Hirano, Y., Fukunaga, T., 2001. Mechanical properties of tendon and aponeurosis of human gastrocnemius muscle in vivo. Journal of Applied Physiology 90, 1671-1678.

Nakagawa, Y., Majima, T., Nagashima, K., 1994. Effect of ageing on ultrastructure of slow and fast skeletal muscle tendon in rabbit Achilles tendons. Acta Physiologica Scandinavica 152, 307-313.

Narici, M.V., Maffulli, N., Maganaris, C.N., 2008. Ageing of human muscles and tendons. Disabil. Rehabil. 30, 1548-1554.

Narici, M.V., Maganaris, C., Reeves, N., 2005. Myotendinous alterations and effects of resistive loading in old age. Scandinavian journal of medicine & science in sports 15, 392-401.

Narici, M.V., Maganaris, C.N., 2006. Adaptability of elderly human muscles and tendons to increased loading. J Anat 208, 433-443.

Nightingale, K., Soo, M.S., Nightingale, R., Trahey, G., 2002. Acoustic radiation force impulse imaging: In vivo demonstration of clinical feasibility. Ultrasound in Medicine and Biology 28, 227-235.

Nillius, S.A., Nilsson, B.E., Westlin, N.E., 1976. The incidence of Achilles tendon rupture. Acta orthopaedica Scandinavica 47, 118-121.

Nordez, A., Hug, F., 2010. Muscle shear elastic modulus measured using supersonic shear imaging is highly related to muscle activity level. Journal of Applied Physiology 108, 1389-1394.

O'Brien, T., 1984. The needle test for complete rupture of the Achilles tendon. J. Bone Joint Surg. Am. 66, 1099-1101.

O'Donnell, M., Skovoroda, A.R., Shapo, B.M., Emelianov, S.Y., 1994. Internal Displacement and Strain Imaging Using Ultrasonic Speckle Tracking. IEEE Transactions on Ultrasonics, Ferroelectrics, and Frequency Control 41, 314-325.

Onambele, G.L., Narici, M.V., Maganaris, C.N., 2006. Calf muscle-tendon properties and postural balance in old age. Journal of Applied Physiology 100, 2048-2056.

Ophir, J., Alam, S.K., Garra, B., Kallel, F., Konofagou, E., Krouskop, T., Varghese, T., 1999. Elastography: ultrasonic estimation and imaging of the elastic properties of tissues. Proceedings of the Institution of Mechanical Engineers. Part H, Journal of Engineering in Medicine 213, 203-233.

Ophir, J., Céspedes, I., Ponnekanti, H., Yazdi, Y., Li, X., 1991. Elastography: A quantitative method for imaging the elasticity of biological tissues. Ultrasonic Imaging 13, 111-134.

Orchard, J.W., 2001. Intrinsic and extrinsic risk factors for muscle strains in Australian football. Am. J. Sports Med. 29, 300-303.

Parker, J., Kenyon, R.V., Troxel, D.E., 1983. Comparison of interpolating methods for image resampling. IEEE Transactions on Medical Imaging 2, 31-39.

Patterson-Kane, J.C., Firth, E.C., Goodship, A.E., Parry, D.A., 1997. Age-related differences in collagen crimp patterns in the superficial digital flexor tendon core region of untrained horses. Aust Vet J 75, 39-44.

Peixinho, C.C., Alves, D.S., Lacerda, R.G., Vieira, T.M.M., Oliveira, L.F., 2008. Strain and slackness of achilles tendon during passive joint mobilization via imaging ultrasonography. Rev Bras Fisioter 12, 366-372.

Pelc, N.J., Drangova, M., Pelc, L.R., Zhu, Y., Noll, D.C., Bowman, B.S., Herfkens, R.J., 1995. Tracking of cyclic motion with phase-contrast cine MR velocity data. Journal of Magnetic Resonance Imaging : JMRI 5, 339-345.

Porter, M.M., Vandervoort, A.A., Lexell, J., 1995. Aging of human muscle: structure, function and adaptability. Scandinavian journal of medicine & science in sports 5, 129-142.

Reese, S.P., Maas, S.A., Weiss, J.A., 2010. Micromechanical models of helical superstructures in ligament and tendon fibers predict large Poisson's ratios. Journal of Biomechanics 43, 1394-1400.

Righetti, R., Srinivasan, S., Ophir, J., 2003. Lateral resolution in elastography. Ultrasound in Medicine & Biology 29, 695-704.

Rosager, S., Aagaard, P., Dyhre-Poulsen, P., Neergaard, K., Kjaer, M., Magnusson, S.P., 2002. Load-displacement properties of the human triceps surae aponeurosis and tendon in runners and non-runners. Scand J Med Sci Sports 12, 90-98.

Royer, D., Gennisson, J.L., Deffieux, T., Tanter, M., 2011. On the elasticity of transverse isotropic soft tissues. Journal of the Acoustical Society of America 129, 2757-2760.

Sarvazyan, A.P., Rudenko, O.V., Swanson, S.D., Fowlkes, J.B., Emelianov, S.Y., 1998. Shear wave elasticity imaging: A new ultrasonic technology of medical diagnostics. Ultrasound in Medicine and Biology 24, 1419-1435.

Scott, S.H., Loeb, G.E., 1995. Mechanical properties of aponeurosis and tendon of the cat soleus muscle during whole-muscle isometric contractions. J Morphol 224, 73-86.

Screen, H.R.C., Bader, D.L., Lee, D.A., Shelton, J.C., 2004. Local strain measurement within tendon. Strain 40, 157-163.

Sebag, F., Vaillant-Lombard, J., Berbis, J., Griset, V., Henry, J.F., Petit, P., Oliver, C., 2010. Shear wave elastography: a new ultrasound imaging mode for the differential diagnosis of benign and malignant thyroid nodules. J Clin Endocrinol Metab 95, 5281-5288.

Sharma, P., Maffulli, N., 2005. Tendon injury and tendinopathy: healing and repair. Journal of Bone and Joint Surgery 87, 187-202.

Shin, H.C., Prager, R., Gomersall, H., Kingsbury, N., Treece, G., Gee, A., 2010. Estimation of Average Speed of Sound Using Deconvolution of Medical Ultrasound Data. Ultrasound in Medicine and Biology 36, 623-636.

Sipila, S., Suominen, H., 1991. Ultrasound Imaging of the Quadriceps Muscle in Elderly Athletes and Untrained Men. Muscle & Nerve 14, 527-533.

Slane, L.C., Thelen, D., 2014a. Non-Uniform Displacements within the Achilles Tendon observed during Passive and Eccentric Loading. Submitted to Journal of Biomechanics.

Slane, L.C., Thelen, D.G., 2014b. The Use of 2D Ultrasound Elastography for Measuring Tendon Motion and Strain. Journal of Biomechanics 47, 750-754.

Smith, C.W., Wootton, R.J., Evans, K.E., 1999. Interpretation of experimental data for Poisson's ratio of highly nonlinear materials. Exp Mech 39, 356-362.

Sobotta, J., 1909. Sobotta"s Atlas and Text-book of Human Anatomy.

Speer, K.P., Lohnes, J., Garrett, W.E., Jr., 1993. Radiographic imaging of muscle strain injury. Am. J. Sports Med. 21, 89-95; discussion 96.

Stenroth, L., Peltonen, J., Cronin, N.J., Sipila, S., Finni, T., 2012. Age-related differences in Achilles tendon properties and triceps surae muscle architecture in vivo. Journal of Applied Physiology 113, 1537-1544.

Szaro, P., Witkowski, G., Smigielski, R., Krajewski, P., Ciszek, B., 2009. Fascicles of the adult human Achilles tendon - an anatomical study. Ann Anat 191, 586-593.

Thitaikumar, A., Mobbs, L.M., Kraemer-Chant, C.M., Garra, B.S., Ophir, J., 2008. Breast tumor classification using axial shear strain elastography: a feasibility study. Phys Med Biol 53, 4809-4823.

Thorpe, C.T., Udeze, C.P., Birch, H.L., Clegg, P.D., Screen, H.R., 2012. Specialization of tendon mechanical properties results from interfascicular differences. J R Soc Interface 9, 3108-3117.

Thorpe, C.T., Udeze, C.P., Birch, H.L., Clegg, P.D., Screen, H.R.C., 2013. Capacity for Sliding between Tendon Fascicles Decreases with Ageing in Injury Prone Equine Tendons: A Possible Mechanism for Age-Related Tendinopathy? Eur Cells Mater 25, 48-60.

Trahey, G.E., Allison, J.W., Vonramm, O.T., 1987. Angle Independent Ultrasonic-Detection of Blood-Flow. IEEE Transactions on Biomedical Engineering 34, 965-967.

Tuite, D.J., Renstrom, P.A., O'Brien, M., 1997. The aging tendon. Scandinavian journal of medicine & science in sports 7, 72-77.

Ultrasonix, 2010. Static Elastography.

van Schie, J.T., Bakker, E.M., van Weeren, P.R., 1999. Ultrasonographic evaluation of equine tendons: a quantitative in vitro study of the effects of amplifier gain level, transducer-tilt, and transducer-displacement. Vet Radiol Ultrasound 40, 151-160.

Varghese, T., 2009. Quasi-Static Ultrasound Elastography. Ultrasound Clinics 4, 323-338.

Varghese, T., Ophir, J., 1997. Enhancement of echo-signal correlation in elastography using temporal stretching. Ieee T Ultrason Ferr 44, 173-180.

Vergari, C., Pourcelot, P., Holden, L., Ravary-Plumioen, B., Gerard, G., Laugier, P., Mitton, D., Crevier-Denoix, N., 2011. True stress and Poisson's ratio of tendons during loading. Journal of Biomechanics 44, 719-724.

Vogel, H.G., 1980. Influence of maturation and aging on mechanical and biochemical properties of connective tissue in rats. Mech Ageing Dev 14, 283-292.

Vogel, H.G., 1983. Age dependence of mechanical properties of rat tail tendons (hysteresis experiments). Aktuelle Gerontol 13, 22-27.

Wells, P.N.T., Liang, H.D., 2011. Medical ultrasound: imaging of soft tissue strain and elasticity. Journal of the Royal Society Interface 8, 1521-1549.

White, J.W., 1943. Torsion of the Achilles tendon: its surgical significance. Archives of Surgery 46, 784-787.

Winter, D.A., Yack, H.J., 1987. EMG profiles during normal human walking: stride-to-stride and inter-subject variability. Electroen Clin Neuro 67, 402-411.

Zafar, M.S., Mahmood, A., Maffulli, N., 2009. Basic science and clinical aspects of achilles tendinopathy. Sports Med Arthrosc 17, 190-197.

Zajac, F., 1989. Muscle and tendon: properties, models, scaling, and application to biomechanics and motor control. Critical Reviews in Biomedical Engineering 17, 359-411.

Zhi, H., Ou, B., Luo, B.M., Feng, X., Wen, Y.L., Yang, H.Y., 2007. Comparison of ultrasound elastography, mammography, and sonography in the diagnosis of solid breast lesions. Journal of Ultrasound in Medicine: Official journal of the American Institute of Ultrasound in Medicine 26, 807-815.